VILNIUS UNIVERSITY
CENTRE FOR PHYSICAL SCIENCES AND TECHNOLOGY

Eglė
GRAŽĖNAITĖ

Inorganic green pigments: investigation of historical and synthesis of novel pigments by sol-gel method

DOCTORAL DISSERTATION

Physical Sciences,
Chemistry 03P

VILNIUS 2018

This dissertation was written between 2013 and 2017 at Vilnius University.

Scientific supervisors:
Prof. dr. Aldona Beganskienė (Vilnius University, Physical Sciences, Chemistry – 03P) (2013.10.01 – 2016.10.18)
Prof. habil. dr. Aivaras Kareiva (Vilnius University, Physical Sciences, Chemistry – 03P) (2016.10.19 – 2017.09.30)

Scientific consultant:
Prof. RNDr. Jiří Pinkas (Masaryk University, Physical Sciences, Chemistry – 03P) (2013.10.01 – 2017.09.30)

VILNIAUS UNIVERSITETAS
FIZINIŲ IR TECHNOLOGIJOS MOKSLŲ CENTRAS

Eglė
GRAŽĖNAITĖ

Žalieji neorganiniai pigmentai: istorinių tyrimas ir naujų sintezė zolių-gelių metodu

DAKTARO DISERTACIJA

Fiziniai mokslai,
Chemija 03P

VILNIUS 2018

Disertacija rengta 2013 – 2017 metais Vilniaus universitete.

Moksliniai vadovai:
Prof. dr. Aldona Beganskienė (Vilniaus universitetas, fiziniai mokslai, chemija – 03P) (2013.10.01 – 2016.10.18)
Prof. habil. dr. Aivaras Kareiva (Vilniaus universitetas, fiziniai mokslai, chemija – 03P) (2016.10.19 – 2017.09.30)

Mokslinis konsultantas:
Prof. dr. Jiří Pinkas (Masaryko universitetas, fiziniai mokslai, chemija – 03P) (2013.10.01 – 2017.09.30)

CONTENTS

LIST OF ABBREVIATIONS

at%	atomic percent;
a.u.	arbitrary units;
CIELab	colour characterisation method, recommended by Commission Internationale de l'Eclairage by measuring parameters L^*, a^*, and b^*.
CMYK	colour model used in colour printing (cyan, magenta, yellow, and key – black);
DR-UV	Diffuse reflectance UV/Vis spectroscopy;
DTG	Derivative thermogravimetry;
EDTA	Ethylenediaminetetraacetic acid;
EDX	Energy-dispersive X-ray spectroscopy;
FTIR	Fourier-transform infrared spectroscopy;
FWHM	Full width at half maximum;
ICP-OES	Inductively coupled plasma optical emission spectrometry;
NIR	Near-infrared region;
OM	Optical microscopy;
PR	pigment, derived by coprecipitation synthesis method;
SEM	Scanning electron microscopy;
SG	pigment, derived by sol-gel synthesis method;
SN	pigment, derived by sonochemical synthesis method;
TG	Thermogravimetry;
UV/Vis	Ultraviolet/Visible region;
wt%	weight percent;
XPS	X-ray photoelectron spectroscopy;
XRD	X-ray powder diffraction.

INTRODUCTION

The historical artefacts are witnesses and educators of our history, culture and mastership of foretime handicraftsmen. The interest in investigation of the heritage objects is gradually growing since the end of 19th century. Luckily, versatile (from humanitarian to fundamental) examination of the artefacts is finally a common knowledge. The first thing we usually notice on the object is colours, and therefore the pigments excite great attraction of the researchers.

Pigments and dyes are used since prehistoric times and are developed in these days for various techniques from paints (oil, tempera, lime, watercolour, gouache, acrylics, etc.) for canvas, wood, fresco, body art, and others to colouring agents of more delicate ceramics and ceramic glazes. The colouring of the glazes is generally achieved by adding colouring oxides, which are transition metal oxides. The colouring of ceramic glazes is often unpredictable due to the dependence on the firing conditions (atmosphere, temperature) and the glaze matrix itself, since some transition metals can form different oxides at different oxidation states [1]. In other words, the colour performance of pigments depends notably on their thermal stability, chemical reactivity towards the glaze components and also on the coordination state of the transition metal ions [2, 3]. However, reaction with and/or dissolution of the pigment in the glaze cannot be effectively anticipated and prevented. As a result, the same pigment can produce different colours in different glazes [3]. Fortunately, the most beautiful and resistant colours can be attained by using oxides of spinel crystal structure, because spinels tend less to change molecularly during firing, especially at high temperatures [4-12].

However, the majority of inorganic pigments with vital colours contain toxic metals, such as Pb, Hg, Cu, Co, etc. It is necessary to develop new and safe pigments with the same or even better properties. In this study, the main investigations were focused on green inorganic pigments, since until now there was no thorough and classified research in this field to the best of our knowledge. Green pigments can be based on copper, iron, chromium, cobalt, and other metals, which emphasize the originality, uniqueness and complexity of the investigation. The main scientific novelty of this doctoral dissertation is the development of pigments and corresponding ceramic glazes having different shade of bluish-green colours by variation of transition or lanthanide metal and its concentration. The second scientific novelty is the case of $CoGa_2O_4$ employment as a ceramic pigment for the first time to our knowledge.

The aim of this PhD thesis was to investigate the analogous pigments to historical green pigments and to develop novel cobalt chromite based pigments and compare their abilities to colour corresponding ceramic glazes. For this reason, the tasks of the present thesis were formulated as follows:

1. Investigation of analogous to historical green pigments and their lead-based glazes using XRD analysis and FTIR spectroscopy.
2. Investigation and comparison of properties of new cobalt chromite based pigments $Co_{1-x}M_xCr_2O_4$ ($M = Ni^{2+}$, Cu^{2+}, Zn^{2+}) ($x = 0–1$) synthesised by sol-gel and sonochemical methods.
3. Synthesis and characterisation of lead-based and lead-free glazes with sol-gel derived $Co_{1-x}M_xCr_2O_4$ ($M = Ni^{2+}$, Cu^{2+}, Zn^{2+}) pigments.
4. Sol-gel synthesis and investigation of new lanthanide-doped cobalt chromite based pigments $CoCr_{2-x}Ln_xO_4$ ($Ln = Tm^{3+}$ and Yb^{3+}) ($x = 0–0.5$).
5. Synthesis and characterisation of lead-free glazes with obtained $CoCr_{2-x}Ln_xO_4$ ($Ln = Tm^{3+}$ and Yb^{3+}) pigments.
6. Sol-gel synthesis and investigation of new gallium-doped cobalt chromite based pigments $CoCr_{2-x}Ga_xO_4$ ($x = 0–2$).
7. Synthesis and characterisation of lead-free glazes with obtained $CoCr_{2-x}Ga_xO_4$ ($x = 0–2$) pigments.

1. LITERATURE SURVEY

1.1. Brief review of inorganic historical pigments

Pigments and dyes are used since the prehistoric times. Naturally, the colours of nature were used either from minerals in the earth (inorganic) or from the plants and animals (organic). The majority of inorganic pigments are brighter and last longer than organic ones. The earliest employments of the pigments are found as prehistoric paintings in the caves. Mostly used pigments were earth pigments (red, yellow, brown ochres – iron oxides in various states of hydration; green earths, having a complex silicate structure containing aluminium, iron, magnesium and potassium ions, were used less frequently due to its relative rarity) and carbon blacks (soot, charcoal). The other used black pigment was manganese oxide MnO_2. In the era of great Egypt, Mesopotamia and China civilisations (circa 4000 BCE), the variety of more vivid colours was introduced, causing the rise of the first manufactured pigments. Natural pigments included green malachite ($CuCO_3 \cdot Cu(OH)_2$), blue azurite ($2CuCO_3 \cdot Cu(OH)_2$) and lapis lazuli ($Na_8[Al_6Si_6O_{24}]S_n$), red cinnabar (HgS), reddish yellow to orange realgar (As_4S_4), and yellow orpiment (As_2S_3). The most famous and probably the oldest of synthesised pigments was Egyptian blue ($CaCuSi_4O_{10}$) – first produced circa 3000 BCE. The Chinese discovered a similar product Han purple ($BaCuSi_2O_6$) and Han blue ($BaCuSi_4O_{10}$). Vermilion, the pigment made from the powdered mineral cinnabar, alternatively was produced by the Chinese by mixing mercury with molten sulphur and heating the mixture to produce the compound [13-17].

The influence of the Egyptians was significant in the arts and the Greeks inherited from them the painting palette. However, soon they started to create a new group of artificial pigments, such as white lead ($2Pb(CO_3)_2 \cdot Pb(OH)_2$), red lead ($Pb_3O_4$), and yellow lead massicot (PbO). The Romans used inorganic pigments employed by the Egyptians and Greeks and later it spread throughout the whole Europe [15, 16]. In the Middle Ages (500–1000 CE) the preparation of relatively pure natural pigments was improved, however, the traces of impurities still remained. Fortunately, it helps to identify the minerals from which pigments were made and to ascertain roughly their geographical origin [13]. In the early Renaissance, the technique of purification of lapis lazuli and the extraction of resultant ultramarine was developed. Natural ultramarine is very expensive, yet still produced in small quantities for artists today by a very similar method to that used in the Renaissance. Other main pigments discovered in the Renaissance were lead tin yellow ($SnO \cdot SiO_2 \cdot PbO$) [15],

Naples yellow ($Pb(SbO_3)_2$ or $PbSbO_4$), and brown umbers (hydrated iron and manganese oxides) [16].

The biggest breakthrough in production of artificial and synthetic pigments came with the 18th and 19th centuries and industrial manufactory. The artists' palette became richer with more brilliant colours than ever before. Invented pigments of new blue, green, yellow, and other shades partly took the place of pigments with not so expressive colours and in some cases the harmful ones. However, the desire for original colours introduced even more deadly pigments. Prussian, or Berlin blue ($Fe_4[Fe(CN)_6]_3 \cdot (14\text{-}16)H_2O$) was accidentally synthesised by Diesbach in 1704. Poisonous Scheele's green ($CuHAsO_3$ or $Cu(AsO_2)_2 \cdot nCu(OH)_2 \cdot mH_2O$) was introduced in 1775, cobalt green ($CoO \cdot nZnO$) was developed by Rinmann in 1780. Cobalt blue ($CoAl_2O_4$) oxides were first obtained by Leithner in 1775. Thenard introduced the manufactory of this pigment in 1802 and only in 5 years the production of it started in France followed shortly by Germany and Norway. It partially replaced another blue cobalt pigment smalt (cobalt containing potassium glass), which was popular in Europe since the 14th century. Ceruleum ($CoO \cdot nSnO_2$), a sky blue pigment, firstly synthesised by Hoepfner in 1789, was seemingly forgotten, until the 1850s–60s, when it was reintroduced and marketed by Rowney & Co. Other developed cobalt pigments, such as cobalt yellow aureolin ($K_3Co(NO_2)_6 \cdot nH_2O$, by Fisher, 1831) and cobalt violet ($Co_3(AsO_4)_2$ first mentioned in 1855; $Co_3(PO_4)_2$ by Salvetat in 1859; $CoNH_4PO_4 \cdot H_2O$), despite their beautiful colours, never gained the importance of cobalt blue. Another alluring green pigment called Schweinfurt green, also known as emerald green or Paris green ($Cu(CH_3COO)_2 \cdot 3Cu(AsO_2)_2$), was introduced in 1814 by Russ and Sattler from Schweinfurt, Germany. Moreover, in the earlier 19th century, the alternate materials for lead white were invented. Synthetic barium sulfate $BaSO_4$, *blanc fixe*, was used since 1830, especially as extender, and zinc white ZnO was introduced slightly later, which became the main replacement. In 1828, the tremendous invention was independently made by two chemists, Guime and Gmelin, giving slightly different synthesis routes for reasonably low-priced synthetic ultramarine. Next greatly significant group of the pigments is chromium pigments. Most significant among these are the various chromates, which vary in colour from yellow, orange, red and purple to brown and green, and the green oxide and oxide hydrate. The most notable ones from this family are chrome yellow ($PbCrO_4$, or $PbCrO_4 \cdot nPbSO_4$, from light yellow to orange-yellow), zinc yellow ($K_2O \cdot 4ZnCrO_4 \cdot 3H_2O$), barium yellow ($BaCrO_4$), strontium yellow ($SrCrO_4$), chrome orange ($PbCrO_4 \cdot Pb(OH)_2$), chrome red ($nPbCrO_4 \cdot mPbO$), and green

chromium oxide (Cr_2O_3) first described by Vauquelin in 1809. Viridian ($Cr_2O_3 \cdot 2H_2O$), having remarkably transparent and brighter green colour than chromium oxide, was developed by Pannetier about 1838 and quickly superseded green copper pigments. More yellow and red hues were obtained by discovering cadmium yellows by Stromeyer in 1819. The colours ranged from lemon yellow (CdS) to orange. The entrance of synthetic iron oxides, so-called mars pigments, into pigmentary world from the 18th–19th centuries had very important role, since the sources of natural earths were diminishing. The mars colours differed in a wide range of hues, from yellows, reds, violets, browns and black, giving the name for the pigment (eg., Mars violet). Another violet pigment manganese phosphate ($(NH_4)_2Mn_2(P_2O_7)_2$) was known since 1868(?) and historically named misleading as permanent mauve [15-18].

The invention and production of new inorganic pigments has never stopped. During 20th century, there were developed advanced pigments, such as titanium white (TiO_2, 1908), cadmium red ($CdS \cdot nCdSe$, 1910), molybdate orange or red ($PbCrO_4 \cdot PbMoO_4 \cdot PbSO_4$, 1933), manganese blue ($n BaSO_4 \cdot m BaMnO_4$, 1935), greenish yellow bismuth vanadate ($BiVO_4$, 1970), nickel rutile yellow ($(Ti_{0.85}Sb_{0.10}Ni_{0.05})O_2$, in the end of the 20th century) [15-18] and many others.

In modern times, the majority of new inorganic pigments are created by improving already existing pigments. Substitution of one or few elements in the chemical structure allows achieving desirable and better properties, such as superior colour [19], solar absorbing [20, 21] or reflecting [22-24] characteristics, decreased production cost [19, 25], etc. For the last few decades, the great attention and effort were put into the reduction of toxicity of traditional pigments. To accomplish this intention, more common, such as zinc [25] and aluminium [24], or innovative substitution elements, such as rare earth elements, could be used. By using lanthanides as dopants vast gamut of colours could be achieved: various shades of red [26-28], brown [29, 30], various shades of yellow [31-34], blue [35, 36] and various shades of violet [37, 38], from yellow to green [39], from yellow to orange red [40]. Naturally, many of created pigments could be used to colour ceramic glazes.

1.2. The history and application of ceramic glazes

Glazes are thin layers of glassy substance fused onto a ceramic surface. In physical and chemical nature, they are hard, impermeable to gases and liquids and slightly or entirely insoluble, excepting in strong acids or bases. Glazes may be transparent, translucent, opaque, colourless or coloured. In

many cases, glazes are formed from three main components: (1) silica (SiO_2), a glass former; (2) a flux, a reducer of the melting temperature of the silica, such as feldspar (aluminosilicate minerals with the general formula AT_4O_8, where A = K, Na or Ca; T = Al and Si), whiting ($CaCO_3$), talc, zinc, ashes, lead, boron, etc., used in their oxide or carbonate forms. The latter two are used in low-temperature glazes; (3) alumina (Al_2O_3), a stiffener, used to increase the viscosity and stability of the glaze. It is more used in the form of kaolin ($Al_2O_3 \cdot 2SiO \cdot 2H_2O$), feldspar or ball clay, rather than oxide.

To colour the glaze, colouring oxide or other form of the pigment is used. The most typical metal oxides are of Fe, Cu, Co, Cr, Ni, Mn, Sn and Ti; not so common oxides are of Sb, V, Cd, Se, Au and U [1, 4, 41]. Glazes may be classified into these groups:

1. Raw glazes, containing lead: a) with no alumina, where lead is the only base or with other bases; b) containing Al_2O_3 and various bases, with different amounts of lead; containing boron trioxide with or without alkalis (Na, K, Li).

2. Raw lead-free glazes, containing Al_2O_3 with various bases: a) containing alkaline earths (Ca, Sr, Mg, Ba), but no alkalis; b) containing alkaline earths and alkalis (natural clay slips or synthetic mixtures of minerals); c) with alkaline earths, alkalis and ZnO; d) with B_2O_3; e) salt-glazes, which are the results of the action of the fumes of common white salt.

3. Fritted glazes, containing lead in addition to other bases: a) without Al_2O_3 or B_2O_3; b) with Al_2O_3 and B_2O_3 and with or without alkalis.

4. Fritted lead-free glazes: a) without B_2O_3; b) with B_2O_3, where alkalis are the only bases, or alkalis and alkaline earths are present with or without zinc; c) containing significant amounts of barium [4].

Stoneware, earthenware and other ceramics have been decorated by glazes since the ancient times. Remained items and archaeological findings witness the excellence of the craftsmanship in the use of glazes for both large and small objects [4]. The famous Ishtar Gate and Processional Road of Babylon is a great example of grand objects (see Fig. 1). Small items usually were various amulets, beads and other. Fig. 2 demonstrates faience beads from Ya'er cemetery in Xinjiang, China (1050–300 BCE) [42].

It is believed that the origin of glazing is attributed to the Egyptians as early as 5th millennium BCE. They created so-called Egyptian paste by mixing sand with natron, natural mixture of Na salts. As the paste dried, the salts migrated to the surface and, upon firing, melted and formed glass. Similar compositions of glazes could be traced in Mesopotamia and India back to the 3rd millennium BCE. During the same millennium, the

knowledge of glazing art spread from Egypt to the eastern Mediterranean, where the Greeks and the Romans eventually developed their own glaze technique terra sigillata. Later the glazing craft reached West Europe, while Lithuania – only since the first ages of Common Era [1, 4, 17].

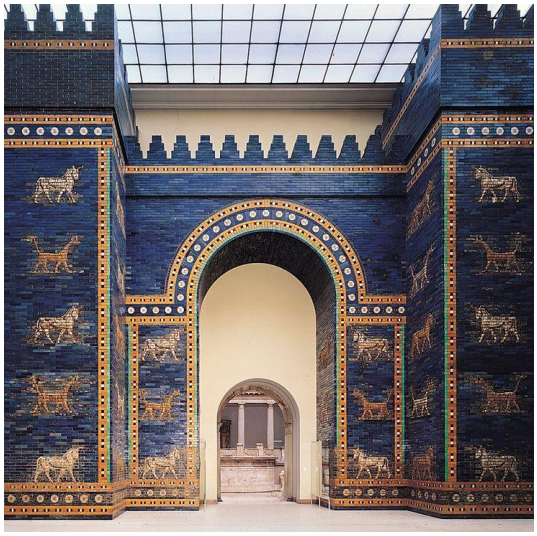

Figure 1. Ishtar Gate, neo babylonian art of glazing, 630–562 BCE. Pergamon museum, Berlin [43]

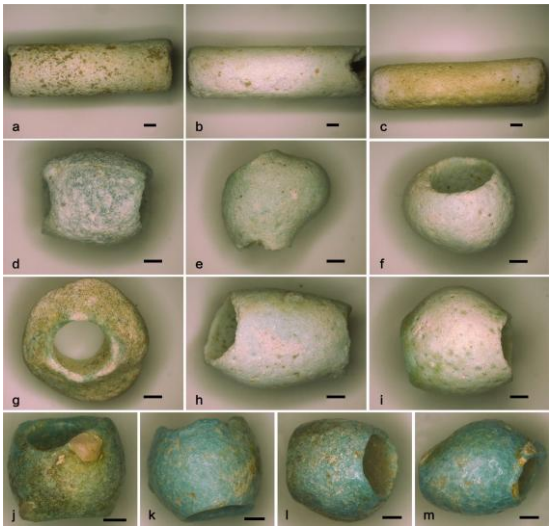

Figure 2. Digital photographs of glazed faience beads from Ya'er cemetery in Xinjiang, China (1050–300 BCE). The scale bar is 1 mm [42]

By the end of the 1st millennium BCE, Pb-based glazes appeared in China and in the eastern Roman Empire, although there are records of detection of

it back to 5^{th}–4^{th} millennium BCE in Egypt. [4]. The use of glazes containing lead spread widely to the Middle East and Europe. This type of glazes continued to be the most generally used in Europe until about 15^{th} century. However, it is logical to presume that application of lead compounds in glazes originated not in just one country, since lead ores are widely distributed geographically and the metallurgy of lead was developed ages before Current Era [1, 4].

Various pigments were used to colour ceramic glazes. The wonderful turquoise amulets, scarabs, beads and statuettes of the Egyptians were coloured by Egyptian blue ($CaCuSi_4O_{10}$). In Mesopotamia Cu, Fe, Co, Mn and other oxides were employed for glazed bricks of the Ishtar Gate in Babylon (see Fig. 1). During the Chinese Tang dynasty (618–907 CE), three main colours were applied: white, green (Cu) and yellow-brown (Fe) [1]. Few Chinese dynasties developed celadon glazes having light blue (sky-green), olive-green or even black colours, which depended on the ratios of base glaze components, iron as Fe_2O_3 content and its reducing/oxidizing state [44, 45]. In the Ming dynasty (1368–1644), blue (Co) and white porcelain was developed, and many other colours (e.g., Cu red, Fe yellow) were created. The production of porcelain in Europe began only in 18^{th} century. In the Middle East, earthenware was decorated with tin-opacified glazes (in France and Italy called faience) with metal oxides, giving different colours: Co – blue, Cu – green, Mn – purple, Fe – orange, and Pb-Sb (Naples yellow) – bright yellow. In the late 18^{th} century, Cr_2O_3 was used to make green and yellow glazes. During the late 19^{th} century and early 20^{th} century, uranium oxides were used to achieve bright yellow colours [1].

The search for new ceramic pigments and the improvement of the existing ones is an everlasting practice. For instance, the interest in synthesis of nanoscaled pigments for industrial ceramic ink-jet printing is evolving drastically. The main challenges of this glazing technique are the accessibility of the suitable colours and the size of pigment particles used to prepare the inks. Pigment particles are required to be micro- (usually 200–600 nm) or nanoscaled (usually 10–50 nm) and spherical to avoid the clogging of nozzles, used for printing, and to provide excellent dispersion in the ink. Due to the influence of the great surface energies, the micro sized pigment particles tend to agglomerate, though [46, 47]. Various shades of blue could be obtained with shell/core structured $CoAl_2O_4/Al_2O_3$ [46], bright red (scarlet) – $CdS_{0.75}Se_{0.25}$ [48], orange – $Ti_{0.97}Cr_{0.015}Sb_{0.015}O_2$ [49], various shades of green by using $CoCr_2O_4$, Cr_2O_3 or $ZnCo_2O_4$, and many other pigments. Typical CMYK colours could be obtained employing different metal oxides: blue with $CoAl_2O_4$ or Co_2SiO_4, black – $CoFe_2O_4$, magenta –

Au or Cu and yellow – Ti(Cr, Sb)O_2, $(Ti_{0.85}Ni_{0.05}Nb_{0.10})O_2$, Pr-$ZrSiO_4$ [47, 50], and many others. Naturally, all these pigments could be applied for classical glazing techniques. Novel ceramic pigments are evolved to improve colour, less toxicity, environmental friendliness, lower production cost and other features. In most cases obtained pigments characterise few of mentioned properties, for instance, brighter or more diverse colours and lower toxicity, greater colours and lower cost, etc. Due to the low toxicity and their unique optical properties, lanthanides are promising elements for the preparation of less poisonous pigments. New improved environment friendly $Y_{2-x}M_xZr_{2-y}Fe_yO_{7-\delta}$ pigment series of red-orange (M = Pr) and red (M = Tb) shade were prepared by polymeric sol-gel method, which could be applied for ceramic tiles, cool roofing materials and other production [51, 52]. New environmental friendly lanthanide-iron-based oxide reddish brown pigments $Tb_3Fe_5O_{12}$ and $PrFeO_3$ were prepared by sol-gel processing [53]. Environmentally friendly ceramic yellow pigments having the general formula $Y_{1.86-x}M_xTb_{0.14}O_{3-x/2x}$ (M = Ca and/or Zn; x = 0.06–0.64) were prepared by a modification of Pechini method [31]. Recently, a natural magnesium aluminium silicate attapulgite (APT) is employed to produce low-cost pigments with improved colour properties. G. Tian et al. have prepared hybrid red pigments APT/Fe_2O_3 by one-pot hydrothermal synthesis [54], and X. Wang's research group have produced hybrid yellow APT/$BiVO_4$ pigments by sol-gel method [19].

1.3. Historical and novel inorganic green pigments

Very wide and interesting area of the pigments is green inorganic pigments. As it was mentioned before, they can be based on Fe, Cu, Cr, Co, and other metals. Fe-based pigments usually are earth pigments and are named by their provenance. These pigments are used since the ancient times and can be applied in all kinds of art. The main colouring agents are the green clay minerals celadonite and glauconite [18]. Celadonite is bluish green dioctahedral mica. Its theoretical composition is $KFe^{3+}(Mg,Fe^{2+})[Si_4O_{10}](OH)_2$. Glauconite is grass green dioctahedral mica with a yellow hue, having less crystalline structure with theoretical composition of $(K,Na)(Fe^{3+},Al,Mg)_2(Si,Al)_4O_{10}(OH)_2$ [55, 56]. Naturally, the colour of the pigments varies in hues depending on the ratio of components in each provenance. However, these two pigments are hard to distinguish optically after they are ground, because both appear as pale, slightly greyish green powders. Moreover, analytical characterisation is difficult likewise due to similarity in the structure and composition [18, 56]. Earth pigments

are characterised by a low covering power and intensity, but good resistance to alkalis, light and atmospheric effects. Besides, they are non-toxic. Green Cu-based pigments were widely used since the ancient Egypt times for various art techniques, such as mural-painting, painting and ceramics until the 19th century. Due to their disadvantages (low hiding power and intensity, bad resistance to atmospheric effects, toxicity) later they were almost completely replaced by other green pigments [16, 17]. Besides previously mentioned green Cu-based pigments (malachite, Scheele's and Schweinfurt green), other pigments were used. Apart from Egyptian blue, the Egyptians also synthesised Egyptian green, which often is called green frit. Egyptian green was produced similarly to Egyptian blue, only varying ratios of the same starting materials (quartz, lime, a copper compound and natural soda (natron)) and firing at higher temperatures. The colour can range from green through turquoise to pale blue [18, 57]. Natural mineral chrysocolla with chemical composition $(Cu,Al)_2H_2Si_2O_5(OH)_4{\cdot}nH_2O$ is found in association with azurite, malachite, cuprite and other minerals and was used as pigment since the ancient times until circa 17th century. It is commonly bluish green in colour and the name of it historically was used mistakenly as a term for malachite in classical and mediaeval literature. Another natural mineral brochantite ($Cu_4SO_4(OH)_6$), varying in hues from emerald green to greenish black, has been identified less commonly in artefacts from the 14th–17th centuries. In the artefacts of 18th–19th centuries, detected brochantite was considered as synthetic [18]. Synthetic copper acetate group pigments, called verdigris and many other names, were used from the ancient times to the early 20th century. There are several known salts: deep bluish green neutral hydrous and anhydrous verdigris ($Cu(CH_3COO)_2{\cdot}H_2O$, $Cu(CH_3COO)_2$, respectively), bluish green basic verdigris $Cu(CH_3COO)_2{\cdot}Cu(OH)_2{\cdot}5H_2O$, green basic verdigris $Cu(CH_3COO)_2{\cdot}[Cu(OH)_2]_2$ and other forms. Verdigris dissolved in colophony produced copper resinate. Cu-based pigments were replaced generally by Cr-based pigments [17, 18]. Synthetic chromium oxides, mentioned previously, were discovered in 19th century. Another beautiful green chromium pigment, lighter than eskolaite Cr_2O_3, is Victoria green, which is stated to be the mixture of viridian, zinc yellow and Prussian blue or barium sulphate or other white pigment [18]. In other reference the pigment named as Victoria green is a mixture of calcium compound, chromium oxide and silica [58]. Interestingly, in some literature the pigment identified with the structure of uvarovite $Ca_3Cr_2(SiO_4)_3$ is named as Victoria green too [59, 60]. The synthetic uvarovite synthesised in the 19th century is still used as ceramic pigment until these days [61, 62]. The natural mineral uvarovite, on the other hand, was not detected as a pigment to the best of our

knowledge. However, natural clay mineral volkonskoite ($Ca(Cr,Mg,Fe)_2(Si,Al)_4O_{10}(OH)_2 \cdot 4H_2O$) is detected as a green pigment in Russian icons from 11th century. Cr-based pigments find applications in all art techniques and have a good resistance to light, atmospheric effects, alkalis and acids and aggressive gas. Formerly noticed cobalt, Rinamann's or zinc green ($CoO \cdot nZnO$) was not very popular among the artists despite its chemical stability, since it created relatively weak colours and its production was too expensive [17, 18].

Modern green pigments, besides Fe, Cu, Co and Cr, can contain Ni, Ti and many other elements. For the most part scientists are searching new synthesis routes to produce and/or improve already existing pigments, as it was mentioned before. For instance, H. Onoda and K. Sugimoto prepared green phosphate pigments imitating natural ores xenophillite ($Na_4Fe_7(PO_4)_6$) and vivianite ($Fe_3(PO_4)_2$) by hydrothermal synthesis method [63]. Naturally, copper containing pigments are still being produced, which would be less toxic than their predecessors and which ones' colours would be superior to commercial Cr-based pigments. A bright green pigment Y_2BaCuO_5 with great NIR reflectance was synthesised using the nano-emulsion method [64]. Novel pigments $Sc_2(Cu_{1-x}Zn_x)_2O_5$ (x = 0–0.1), having brilliant green colours and high resistance to the UV irradiation, were developed using conventional solid state method [65]. For economical and environmental reasons, scientists are developing methods to use industrial wastes as Cr_2O_3 precursor for the synthesis of Cr-based pigments. F. Andreola prepared green powder with the main phase of uvarovite by solid state reaction [62], and W. Hajjaji et al. developed Cr-doped titanite $CaTiSiO_5$ using the ceramic route and obtained variations of colours in transparent glazes from green to brown [66]. D. Esteves et al. used industrial waste as starting materials for the preparation of Ni-olivine (Ni_2SiO_4) by the solid state reaction method. The application of Cr/Ni galvanic sludge improved the formation of Ni_2SiO_4 at lower temperatures and stronger and darker green hue, comparing to pigments, prepared from pure/commercial reagents [60]. Another spinels $CoCr_{2-2x}Al_{2x}O_4$ (x = 0–1 in steps of 0.2) were prepared by solid combustion synthesis, varying the colour from the green shades in Cr-rich to blue shades in Al-rich pigments [67]. (Co,Zn)-$MgTi_2O_5$ karrooite-hosted pigments, prepared using solid state reaction, exhibited a gamut of yellowish green colours, which became less yellowish and more saturated or darker the higher the Co content was [68]. Inverse spinel Co_2TiO_4, due to its reliable chemical stability and corrosion resistance, is often used as a green pigment, although it contains poisonous, limited and expensive cobalt. To reduce the cost and toxicity, Co can be replaced by cheaper and less toxic elements, the

pigment can be mixed with light pigments, or coated on mica, leading by all these methods to the loss of the intensity of the colour. J. Zou et al. introduced new $CoTiO_3/TiO_2$ complex shell/core structured pigments with ranging green hues [69].

Scientists around the globe have been preparing many and various green pigments, which is impossible here to review them all. Worth to mention that quite significant section of ceramic green and other colour pigments is spinel structured pigments.

1.4. The chemical structure of spinels

Different metal oxides and mixed-metal oxides are employed as ceramic pigments. For various applications pigments have specific requirements such as chemical and thermal stability, particle size, hiding and tinting power, etc. Mixed-metal oxides, displaying general spinel formula AB_2O_4, are characteristic for their high mechanical resistance, high thermal and chemical stability. The cubic spinel unit cell consists of 56 atoms (32 oxygen anions, and 24 cations, 8 of them occupying tetrahedral sites and the other 16 being located at the octahedral sites). The cations A and B ordinarily are divalent and trivalent, respectively, although other combinations are possible too. The schematic view of conventional face-centred cubic spinel structure is shown in Fig. 3. The main factors controlling the preference of the individual ions for the two crystallographic sites are the ionic radii and coordination chemistry of the ions. There are two ideal types of spinel structure: the first one known as normal spinel is characterised by cations A^{2+} occupying tetrahedral positions and cations B^{3+} occupying octahedral positions. The second possible structure is inverse spinel, in which all tetrahedral sites are occupied by cations B^{3+}, while octahedral sites are situated by equal number of cations A^{2+} and B^{3+}, and therefore can be formulated as $B(AB)O_4$. Besides these two ideal spinel structures, spinels can be partially inverted; if the inversion is incomplete, the distribution of cations may become random [25, 70, 71]. The formation of inverse spinel can be influenced by synthesis temperature and pressure as-well [72]. Owing to easy incorporation of various metal ions into the spinel lattice, the properties of spinel type materials are remarkable, which lead to wide applications as magnetic compounds [73], catalysts and sensors for toxic gases [73-76], refractories, materials for information storage [77-79], pigments [20, 22, 25, 80], and many others.

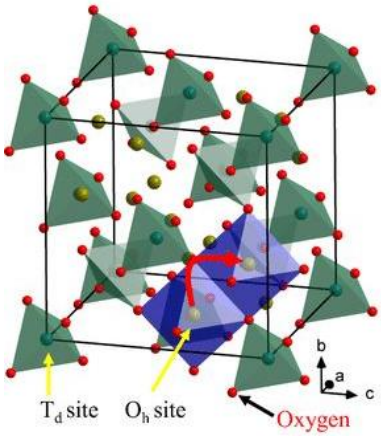

Figure 3. The cubic unit cell of spinel structure. Octahedral (O_h) and tetrahedral (T_d) sites are represented in blue and green shaded polyhedrons, respectively. The red curved arrow indicates the nearest-neighbour electron hopping process in inverse spinel [81]

As it was mentioned before, spinel structure is very attractive in pigmentary field. The nature of tetrahedral or octahedral cations and potential of different types of doping give diversity in colours and properties. For example, thermal and chemical stability is necessary for ceramic pigments to obtain high quality glazes [3], $CuCr_2O_4$ is effective for solar-absorbing paints [82] and, conversely, cobalt chromite doped by zinc and aluminium is impressive due to high solar reflectance and could be used for cool coatings of the buildings [22]. Spinels as pigments can be produced by conventional solid-state reactions [80, 83], combustion or sol-gel combustion method [76, 82], coprecipitation [84], hydrothermal synthesis [85], thermolysis of organic precursors [86, 87], air plasma spray-drying technique [88], microemulsion [75], polymer precursor method [25, 89], sonochemical synthesis [90-92] and sol-gel [22, 93-96] method. The latter two procedures are effective for preparing materials of high purity in nanoscale size and good control of stoichiometry and chemical homogeneity.

1.5. Sol-gel processing

Historical pigments were produced by grinding natural minerals, firing the mixtures of starting materials (solid-state reaction), coprecipitation reaction method and other techniques. However, these synthesis routes are characteristic for several drawbacks, such as poor control of stoichiometry and homogeneity, non-uniformity of particle size and shape, lack of reproducibility and other factors, related to the synthesis specifics [97]. For

instance, one of the advantages of sol-gel synthesis is that this method requires much lower temperatures and shorter calcination times to obtain the desired product, comparing to conventional solid-state method [96, 98]. The overview of this process with steps, possible routes and various products is given in Fig. 4.

The first sol-gel synthesis of an inorganic material (silica) from a metal organic molecular precursor was described in the middle of 19th century by M. Ebelmen, a French chemist, who noticed that silicic esters hydrolyse slowly in the presence of moisture to give hydrated silica. It then took more than a century before sol-gel technology began to attract both academic and industrial interest and since the end of 20th century the sol-gel chemistry has become tremendously popular and opened new opportunities in the field of materials science. The principle of the sol-gel technology is that a solution of molecular precursors is converted by a chemical reaction into a sol or a gel, which on drying and densification gives a solid material [99].

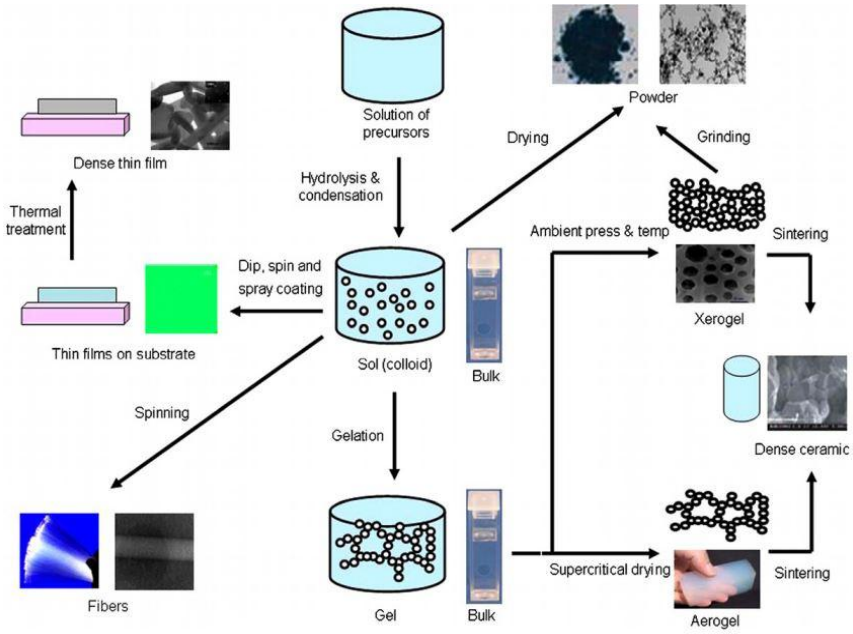

Figure 4. Schematic diagram depicting the sol-gel processing stages and routes [100]

The precursors used for the preparation of colloid (sol) are usually metal organic compounds (such as metal alkoxides $M(OR)_n$, where M represents a network-forming element such as Si, Al, B, Ti, Zr, etc, and R is typically an alkyl group) or inorganic metal salts (e. g., nitrates) [100, 101]. Independently of the type of precursors, the production of sol and then gel

proceeds several main consecutive reactions – hydrolysis, condensation and polymerisation. Only the basic principles and specifications of both synthesis types, depending on the precursor origin, are further reviewed concisely.

Synthesis with metal alkoxides as starting materials. The hydrolysis reaction of metal alkoxide initiates very easily when mixing with water, since metal alkoxides are very reactive in general due to the highly electronegative OR groups, that stabilise M in its highest oxidation state and causing thus the great sensitivity of metal ion to nucleophilic attack. Moreover, both the hydrolysis and condensation reactions usually occur simultaneously. The hydrolysis reaction could be represented as Eq. (1):

$$M(OR)_n + xH_2O \rightarrow M(OH)_x(OR)_{n-x} + x\text{ROH} \quad (1)$$

Hydrolysis is followed by condensation to form –M–O–M– bonds via either dehydration (see Eq. (2)) or dealcoholation (Eq. (3)):

(a) dehydration:

$$\text{–M–OH + HO–M–} \rightarrow \text{–M–O–M–} + H_2O \quad (2)$$

(b) dealcoholation:

$$\text{–M–OH + RO–M–} \rightarrow \text{–M–O–M–} + \text{ROH} \quad (3)$$

When adequate number of interconnected –M–O–M– bonds are assembled (polycondensation), a sol or colloidal particles are formed. The whole system is affected by significant factors, which are temperature of the synthesis, molar ratio of water to alkoxide, nature and concentration of catalyst (acidic or basic), type of solvent (water or alcohol-water) and alkoxide precursor and pressure. All these parameters but the latter one are variable. By appropriate adjustment of these factors, either linear polymeric gel or more crosslinked polymeric gel can be formed [97, 100-102]. However, the sol-gel synthesis via metal alkoxides distinguishes major disadvantages, such as high sensibility to the moist environment and unavailability of commercial precursors especially for the mixed-metal oxides. The sol-gel synthesis of mixed oxides from alkoxide mixture usually suffers from the different hydrolysis susceptibilities of the individual components. Thus, during the hydrolysis of the alkoxides, the benefits of improved homogeneity can be lost, which may ultimately lead to mixed phases in the final materials [96].

Synthesis with inorganic metal salts as starting materials. Metal ions M^{z+}, dissolved in water in a form of metal salt, are solvated by water molecules $[M(H_2O)_n]^{z+}$. The solvated cations show a great tendency to release the protons due to the occurrence of charge transfer from water molecule to the metal. Depending on the degree of charge transfer and resultant water acidity increase, hydrolysis proceeds, which could be defined as following equilibria (Eq. 4):

$$[M(OH_2)]^{z+} \rightleftharpoons [M–OH]^{(z–1)+} + H^+ \rightleftharpoons [M=O]^{(z–2)+} + 2H^+ \quad (4)$$

In addition, Equation (4) describes the ligands forming during the hydrolysis reaction: aqua ($M–OH_2$), hydroxo (M–OH), and oxo (M=O). Two main factors determining the degree of the hydrolysis are the formal charge z of the cation M^{z+} and pH of the solution. The rough diagram of the origin of the possibly formed complexes depending on these two parameters is given in Fig. 5. For instance, lower-valent cations ($z < +4$) may form aqua, hydroxo, or aqua-hydroxo complexes over the complete pH scale, whereas higher-valent cations ($z > +5$) yield oxo or oxo-hydroxo complexes over the same range of pH. Tetravalent cations ($z = +4$) are on the borderline and give rise to any kind of possible complexes depending upon pH of the solution.

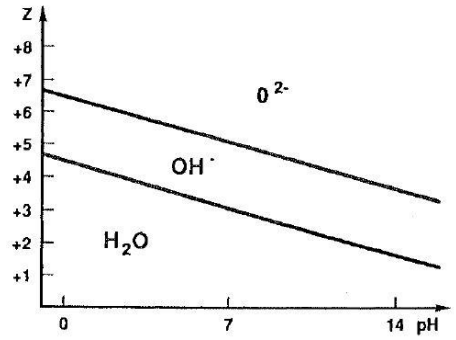

Figure 5. The dependence of possible water related ligands (aqua, hydroxo and oxo) existence on the metal cation charge z and solution pH [101]

However, the precise nature of the complexes depends not only on the z and pH of aqueous solution, but on the coordination number and the electronegativity of the metal too. To predict chemical reactions happening in the solution and the resulting ligands, the partial charge model can be successfully applied. This model declares that when the two atoms combine, charge transfer occurs causing each atom to gain a partial positive or partial negative charge. The charge transfer would proceed until the

electronegativities of all the atoms become equal to the mean electronegativity.

However, the concentration of the solutions of the simple inorganic salts is not capable attaining a good homogeneity at atomic scale. As a resulting product heterogeneous mixture of precipitates as the original salt form or as colloidal hydroxides is generally obtained by evaporating the solvent. The precipitates tend to deposit on condition of unequal reaction rates of hydrolysis and condensation or increased pH values. To bypass that, suitable organic ligands, such as citric acid, EDTA, etc., are engaged, creating stable mixture of precursor solutions. Introduced chelating agent thus weakens the hydrolysis of coordinated water molecules.

Condensation of the hydrolysed species proceeds via olation or oxolation. Olation occurs commonly with hydroxo-aqua complexes $[M(OH)_x(H_2O)_{n-x}]^{(z-x)+}$, ($x < n$), leading to the formation of a hydroxo bridge M–OH–M, whereas oxolation happens typically with oxo-hydroxo complexes $[MO_x(OH)_{n-x}]^{n+x-z}$, ($x < n$), causing the formation of an oxo bridge M–O–M [97, 101].

The hydrolysis and condensation processes of metal salts avoid the disadvantage of alkoxide sol-gel process (high sensitivity to moisture), however, have still the drawback of different hydrolysis susceptibilities of the individual components. [96].

Further processing of the sol or gel enables one to make sol-gel materials in different configurations (see Fig. 4). Thin films can be produced on a piece of substrate by spin, dip and spray coating of the sol solution. With further drying and heat treatment of the gel, it can be transformed into dense ceramic or glass particles. During the drying process at ambient pressure, the solvent is removed and substantial shrinkage occurs, resulting xerogel. When solvent removal occurs under hypercritical (supercritical) conditions, the network does not shrink and a highly porous, low-density material aerogel is produced. Heat treatment of a xerogel at elevated temperature produces viscous sintering (shrinkage of the xerogel due to a small amount of viscous flow) and effectively transforms the porous gel into a dense glass. As the viscosity of the sol is adjusted into a proper viscosity range, ceramic fibers can be drawn from the sol. Ultra-fine and uniform ceramic powders are formed by emulsion, spray pyrolysis or precipitation techniques [100].

1.6. Basics of the sonochemical synthesis

Sonochemistry is the research area in which molecules undergo a chemical reaction due to the application of powerful ultrasound radiation

(20 kHz to 10 MHz). It is noteworthy, however, that no direct interaction between the ultrasound molecules can be responsible for the chemical reactions. Instead, the chemical effects of the ultrasound arise from temporary "hot-spots", formed during acoustic cavitation (the creation, growth and collapse of bubbles in a liquid). This acoustic cavitation leads to the rapid release of energy with heating and cooling rates of about milliard $°C \cdot s^{-1}$, temperatures of few thousand °C and pressures of few thousand atmospheres. Under such extreme conditions the solvent molecules experience homolytic bond cleavage and generate radicals, which may interact in many ways chemically and physically. In general, different properties of the final product, such as particle size, shape and its purity would be under the control of following series of factors: sonication output power, frequency of irradiation, time, temperature, origin of the solvent, and chemical species and their concentrations in the reaction mixture. Appropriate choice of sonochemical reactors is necessary for a specific demand of sonochemical synthesis. The choices available are ultrasonic horn, bath, longitudinal horn and multiple transducers. The most popular reactor is ultrasonic horn (see Fig. 6), which is suitable for focusing the energy on particular sample zone.

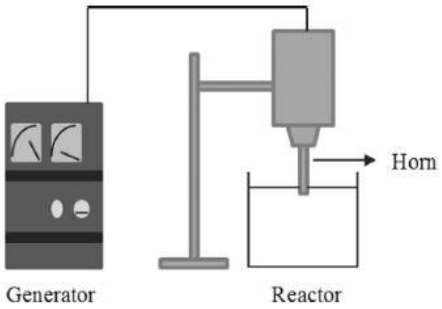

Figure 6. Simplified scheme of ultrasonic horn reactor [103]

The sonochemical method has some advantages, including uniformity of mixing, morphological control and reduction of crystal growth. Ultrasound can also fracture agglomerates to produce a uniform composition of products. One of the main disadvantages is the possible difficulties occurring by applying sonochemistry for industry. Unfortunately, there is not enough available information about features and performance of sonochemical reactors [91, 103-105].

2. EXPERIMENTAL SECTION

2.1. Chemicals and materials

Nine analogous to historical green pigments were purchased from Kremer Pigmente. In this study, all the pigments were called according to manufacturer's catalogue: malachite ($CuCO_3{\cdot}Cu(OH)_2$), verdigris ($Cu(CH_3COO)_2{\cdot}[Cu(OH)_2]_3{\cdot}2H_2O$), Egyptian green (Cu silicate), cobalt green (Co, Al, Ti, Ni, Zn oxides), cobalt bottle green ($CoCr_2O_4$), chrome oxide green (Cr_2O_3), Victoria green ($Ca_3Cr_2(SiO_4)_3$), Florentine green and green jasper. The chemical formulas given in the brackets are as the producer stated. Florentine green and green jasper were bought with the unknown chemical compositions.

For the synthesis of green pigments, bluish-green spinel-type cobalt chromite was chosen as the base structure. All reagents were of analytical grade or high purity and used as received from commercial sources without further purification. Chromium(III) nitrate nonahydrate ($Cr(NO_3)_3{\cdot}9H_2O$, 99%, Sigma-Aldrich and p.a., Pliva-Lachema), cobalt(II) nitrate hexahydrate ($Co(NO_3)_2{\cdot}6H_2O$, ≥97.7%, Alfa Aesar and p.a., Lach-Ner), copper(II) acetate monohydrate ($Cu(CH_3COO)_2{\cdot}H_2O$, 99%, Sigma-Aldrich and p.a., Riedel-de Haen AG), nickel(II) acetate tetrahydrate ($Ni(CH_3COO)_2{\cdot}4H_2O$, 98%, Sigma-Aldrich), nickel(II) nitrate hexahydrate ($Ni(NO_3)_2{\cdot}6H_2O$, p.a., Pliva-Lachema), zinc acetate dihydrate ($Zn(CH_3COO)_2{\cdot}2H_2O$, p.a., Roth, and p.a., Pliva-Lachema), thulium(III) oxide (Tm_2O_3, 99.99%, Alfa Aesar), ytterbium(III) oxide (Yb_2O_3, 99.9%, Merck), and gallium(III) oxide (Ga_2O_3, 99.99%, Alfa Aesar), were used as starting materials. Metal oxides were dissolved in concentrated nitric acid (HNO_3, 67%, Eurochemicals). 1,2-ethanediol ($C_2H_6O_2$, 99.5%, Sigma-Aldrich) as complexing agent and ammonia solution (NH_4OH, 26%, Mikrochem) were used for sol-gel and sonochemical syntheses, respectively. Acetone (C_3H_6O, p.a., Mikrochem) and pure argon were used in the sonochemical processing.

For the preparation of lead-based ceramic glazes, red lead (Pb_3O_4) and silica (SiO_2) were purchased from Kremer Pigmente. For the preparation of lead-free ceramic glazes the Czech transparent colourless base glaze (commercial ID P074 10) was used.

2.2. Synthesis methods

All $CoCr_2O_4$ based compounds were prepared initially by sol-gel and sonochemical synthesis routes.

2.2.1. Sol-gel synthesis

For the preparation of $Co_{1-x}M_xCr_2O_4$ (M = Ni^{2+}, Cu^{2+}, and Zn^{2+}; x = 0; 0.25; 0.5; 0.75; and 1) pigments, stoichiometric amounts of metal nitrates or acetates were dissolved in deionised water and mixed together. After stirring the solutions at 40–50 °C for 20 min, 1,2-ethanediol (2 mL) was added with continuous stirring at the same temperature for 1 h. The solutions were concentrated by continuous stirring and evaporation at 60–70 °C. Prepared gels were dried in a furnace at 105 °C in air. Dried gels were ground in an agate mortar and calcined at 600, 700, and 800 °C in air for 3 h with a heating rate of 10 °C/min. The powders calcined at 700 °C were ground again and additionally annealed at 1000 °C in air for 5 h with the heating rate of 10 °C/min and later were used for the preparation of ceramic glazes.

For the preparation of $CoCr_{2-x}Ln_xO_4$ (Ln = Tm^{3+} and Yb^{3+}; x = 0; 0.01; 0.02; 0.03; 0.04; 0.05; 0.1; 0.2; 0.3; 0.4 and 0.5; and $CoCr_{2-x}Ga_xO_4$ (x = 0; 0.5; 1; 1.5; and 2) compounds, metal oxides were dissolved in required amounts of hot diluted HNO_3 with continuous stirring and covered glass beaker by a watch glass, until the clear solutions were obtained. The stoichiometric amounts of $Cr(NO_3)_3{\cdot}9H_2O$ and $Co(NO_3)_2{\cdot}6H_2O$ were dissolved in deionised water and mixed together with respective metal oxide solution. After mixing, the solutions were stirred at 40–50 °C for 20 min and then 2 mL of 1,2-ethandiol was added with continuous stirring at the same temperature for 1 h. The solutions were concentrated by continuous stirring and evaporation at 60–70 °C. Prepared gels were dried in a furnace at 105–110 °C in air, carefully ground in the agate mortar and annealed at 700 °C in air for 3 h with a heating rate of 5 °C/min. The obtained powders were ground once again and additionally heated at 800, 900, and 1000 °C in air for 5 h with the heating rate of 10 °C/min. After the calcination at 700 °C, $CoCr_{2-x}Ga_xO_4$ powders were exceptionally annealed only at 1000 °C.

2.2.2. Sonochemical synthesis

For the sonochemical reactions, the mixtures of Co-M-Cr-O (M = Ni, Cu, Zn) gel precursors were prepared in identical manner as for the sol-gel synthesis, except that after 20 min of stirring ammonia instead of 1,2-ethanediol was added, until the pH of the solution reached values of 9–10. After stirring for 10 min, the flask with the solution was purged with pure argon for 15 min and irradiated with ultrasound radiation under argon for 2.5 h by employing a direct immersion horn. The reaction cell was cooled during the sonication process. After sonication was completed, the

precipitate was separated from the solution by centrifugation, washed once with distilled water and once with acetone and finally dried in air. As-prepared products were ground in agate mortar and calcined at 600, 700, and 800 °C for 3 h in air with a heating rate of 10 °C/min. Sonication was performed using a Sonics and Materials VCX130 reactor with a titanium 13 mm diameter horn operating at 20 kHz at a power of 20 W/cm^2.

Since the ammonia caused spontaneous precipitation, for comparison a coprecipitation reaction to obtain $Co_{1-x}M_xCr_2O_4$ (M = Ni^{2+}, Cu^{2+}, and Zn^{2+}; x = 0 and 0.5) powders was performed as-well. The processing route was as a sonochemical synthesis except involving the ultrasound treatment.

2.2.3. Synthesis of ceramic glazes

For the preparation of the Pb-based ceramic glazes with the commercial pigments, in all cases the same molar ratio of ingredients has been selected: Pb_3O_4 : SiO_2 : pigment = 2.85 : 1.9 : 0.25 [106]. The samples with evaluated weight percentages of the pigments are described in Table 1. The amount of unknown composition pigments (No. 8 and No. 9) was picked to be 1.40 wt%. 0.5 g of each mixture was mingled with a small amount of water and carefully plastered onto terracotta tiles (3 x 4 cm). After drying in air, the prepared terracotta samples were fired in an oxidising atmosphere at 900 and 1000 °C for 1 h with a heating rate of 5 °C/min.

Table 1. The information about commercial analogous to historical green pigments (Kremer Pigmente) and their weight percentages in the lead-based glazes

Sample No.	Catalogue No.	Pigment (formula according to producer)	wt%
1.	10300	Malachite ($CuCO_3 \cdot Cu(OH)_2$)	2.60
2.	44450	Verdigris ($Cu(CH_3COO)_2 \cdot [Cu(OH)_2]_3 \cdot 2H_2O$)	5.81
3.	44100	Cobalt green (Co, Al, Ti, Ni, Zn oxides)	5.74
4.	44130	Cobalt bottle green ($CoCr_2O_4$, Li, Ti, Zn oxides)	2.67
5.	44200	Chrome oxide green (Cr_2O_3)	1.80
6.	10064	Egyptian green (Cu silicate)	1.47
7.	44190	Victoria green ($3CaO : Cr_2O_3 : 3SiO_2$)	5.70
8.	11152	Florentine green (?)	1.40
9.	11200	Green jasper (?)	1.40

For the preparation of the glazes with $Co_{1-x}M_xCr_2O_4$ (M = Ni^{2+}, Cu^{2+}, and Zn^{2+}; x = 0; 0.25; 0.5; 0.75; and 1) pigments obtained by sol-gel processing, the same molar ratio of glass-forming ingredients has been selected: Pb_3O_4 : SiO_2 = 1.5 : 1. The amounts of pigments (x = 0 and 1) have been

chosen to be 3, 5 and 7 wt%. The percentage of pigments with the other substitution ratios (x = 0.25; 0.5; 0.75) has been set to 5 wt%. The mixtures of the components and drops of water were thoroughly plastered onto terracotta tiles and after drying in air fired in oxidising atmosphere at 1000 °C for 1 h with a heating rate of 5 °C/min.

For the preparation of Pb-free ceramic glazes, 5 wt% of the pigment was applied for the majority types of the base glazes according to the glaze manufacturer's recommendations. Prepared wet mixtures were carefully plastered on terracotta tiles, and after drying in air fired in oxidising atmosphere at 1000 °C for 1 h with a heating rate of 5 °C/min. For the preparation of the ceramic glazes with the commercial pigments, 0.5 g, 0.6 g or 1 g of each mixture was used. For the preparation of the glazes with synthesised pigments, 1 g of each mixture was used.

2.3. Characterisation techniques

X-ray powder diffraction (XRD). The XRD analysis of the samples was performed using a Rigaku MiniFlex II diffractometer, operated at 30 kV and 10 mA with a scanning speed of 10°/min, in a scanning range of 2θ = 10–80°, using Cu Kα radiation (λ = 1.540562 Å). The unit-cell lattice parameters for the chromites, substituted by lanthanides, were obtained by Rietveld refinement of the powder XRD data using the FULLPROF software. The tentative crystallite sizes of synthesised pigments were determined by the Scherrer equation (Eq. 5):

$$\tau = \frac{0.9\lambda}{B\cos\theta} \tag{5}$$

where τ is the mean crystallite size, λ is the X-ray wavelength, B is the line broadening at half maximum intensity (FWHM) (in radians) and θ is the Bragg angle.

SEM-EDX. The morphological features of commercial and synthesised pigments were investigated using a scanning electron microscope Hitachi SU-70 at different magnifications. The images of morphology of fired glazes were obtained employing Hitachi TM3000, using 15.0 kV accelerating voltage for EDX measurements of commercial pigments and lead-free base glaze powder.

Fourier-transform infrared spectroscopy (FTIR). For FTIR studies a Perkin Elmer Spectrum BX spectrometer with ATR accessory was used. Transmittance (%) was taken in the range of 4000–600 cm^{-1} by the co-addition of 10 scans with a resolution of 2 cm^{-1}. For some samples the FTIR

spectra were recorded in the same range by a Bruker Tensor 27 equipment with a resolution 4 cm^{-1} for each spectrum, which consisted of 32 scans. For latter measurements the KBr pellet technique was applied.

Raman spectroscopy. Raman spectroscopy was carried out using a Horiba Scientific LabRam HR Evolution spectrometer with the Olympus microscope (objective magnification 50) in the spectral range of 80–1000 cm^{-1} at 532 nm.

Inductively coupled plasma optical emission spectrometry (ICP-OES). For the determination of element ratio in the sol-gel synthesised pigments with initial calculations, Thermo iCAP 6500 Duo technique was employed. $Co_{1-x}M_xCr_2O_4$ and $CoCr_{2-x}Ln_xO_4$ samples were dissolved in concentrated HCl and H_3PO_4, respectively, and $CoCr_{2-x}Ga_xO_4$ powders were dissolved in the mixture of concentrated H_2SO_4, HF, and $HClO_4$ (2 : 1 : 1.25, by volume, respectively). The samples were decomposed in microwave system Ethos One from Milestone.

Thermal analysis. The thermal behaviour of the Co-M-Cr-O gel precursors was investigated through thermogravimetry and derivative thermogravimetry (TG/DTG) with Perkin Elmer STA6000 apparatus. Dried samples were placed in an open corundum crucible and heated from room temperature up to 950 °C with a heating rate of 10 °C/min under dried air flow of 20 mL/min. The precursors obtained by sonochemical and coprecipitation methods were analysed by Netzsch STA 449C apparatus, using Pt crucible and a heating rate of 5 °C/min from room temperature up to 950 °C under an air flow of 70 mL/min air and 10 mL/min of nitrogen.

Diffuse reflectance UV/Vis spectroscopy (DR-UV). The diffuse reflectance spectra of sol-gel and sonochemically derived pigments were determined on an Agilent Technologies Cary 5000 spectrophotometer from 200 to 800 nm, using a $BaCO_3$ pellet as white reference.

CIELab colour characterisation. The colour of the synthesised pigments and their ceramic glazes was evaluated by the CIELab colourimetric method, which is recommended by the Commission Internationale de l'Eclairage. The L^*, a^*, and b^* parameters were measured on a Perkin Elmer Lambda 950 spectrophotometer in the 780–380 nm range, employing an illuminant D65 and a 10° standard observer. In the CIELab system, the coordinate L^* represents the lightness of the colour ($L^* = 0$ and $L^* = 100$ represents black and white, respectively). The negative/positive values of coordinate a^* represent green/red hue, respectively, and the parameter b^* corresponds to blue/yellow hue, where negative values are for blue and positive – for yellow.

X-ray photoelectron spectroscopy (XPS). XPS analysis of samples was carried out on the upgraded Vacuum Generator (VG) ESCALAB MKII spectrometer fitted with a XR4 twin anode. The non-monochromatic Al Kα X-ray source was used (hν = 1486.6 eV) and the spectra were acquired with electron analyser pass energy of 20 eV for narrow scans. All spectra were recorded at a 90° take-off angle and calibrated from the hydrocarbon contamination using the C1s peak at 284.6 eV. Core level peaks of Co2p, Cr2p, C1s, N1s, O1s, Tm4d and Yb4d were analysed using a nonlinear Shirley-type background. All XPS measurements were performed without any pre-etching of the samples.

Optical microscopy (OM). The ceramic glazes were investigated using a Motic SMZ-171 optical microscope at different magnifications. Digital photographs were taken by Moticam 10.0MP digital camera accessory and processed with a Motic Images Plus 3.0 ML software.

The digital images of both the pigment and ceramic glaze samples were taken using a Canon PowerShot S110 digital camera. The photographs were processed with Photoshop CC and CorelDraw softwares.

3. RESULTS AND DISCUSSION

3.1. Characterisation of analogous to historical green pigments, their glaze mixtures and ceramic glazes

In this part of dissertation the applicability of XRD analysis and FTIR spectroscopy to investigate commercial analogous to historical green pigments and their glaze mixtures was evaluated.

3.1.1. EDX analysis

The first aim was to determine the composition of green inorganic pigments with unknown constitution. For this purpose the EDX analysis was performed foremost. The results are given in Table 2.

Table 2. The EDX analysis results of commercial pigments

Pigment	Element (at%)					
Malachite	Cu (9.93)					
Verdigris	Cu (6.55)					
Cobalt green	Ba (5.81)	Ni (5.71)	S (4.45)	Ti (4.10)	Co (3.17)	Zn (2.20)
Cobalt bottle green	Cr (19.66)	Mg (5.81)	Co (2.18)	Zn (1.57)		
Chrome oxide green	Cr (17.62)					
Egyptian green	Si (16.15)	Cu (2.34)	Na (1.03)			
Victoria green	Si (13.32)	Ca (6.91)	F (4.84)	Cr (1.96)	K (1.10)	
Florentine green	Mg (9.96)	Si (7.39)	Fe (3.53)			
Green jasper	Si (14.52)	Fe (10.74)	Cr (1.04)			

Pb-based glazes were the most generally used glazes in Europe since 5–1st millennium BCE until about 15th century, therefore the second task was to investigate the detectability of pigments in their lead-based glaze mixtures using XRD analysis and FTIR spectroscopy. In order to verify the ability to detect pigments in their glaze mixtures of the above techniques, both analyses were performed on the model samples. The third task was to analyse morphological features of the fired ceramic glazes by optical and scanning electron microscopies.

3.1.2. XRD analysis

The XRD patterns of malachite and verdigris pigments are shown in Fig. 7. All diffraction peaks of pigment No. 1 (Table 1) correspond to a standard pattern of malachite $CuCO_3 \cdot Cu(OH)_2$ (PDF 72-0075) (see Fig. 7a). The formula of verdigris presented in the catalogue of Kremer Pigmente is given

as $Cu(CH_3COO)_2 \cdot [Cu(OH)_2]_3 \cdot 2H_2O$. However, XRD analysis data (Fig. 7b) confirmed that the purchased reagent is a copper acetate monohydrate $Cu(CH_3COO)_2 \cdot H_2O$ (PDF 27-0145). Both diffraction patterns contain weak peaks at 19.76° and 43.12° of 2θ for malachite and verdigris, respectively, of unidentified crystalline phases, however of insignificantly small concentrations.

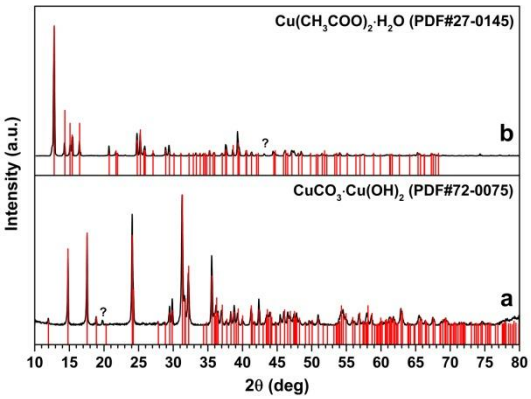

Figure 7. XRD patterns of commercial pigments malachite (a) and verdigris (b). Unidentified phases are marked as ?

XRD patterns of oxide pigments are given in Fig. 8. According to producers, cobalt green pigment should contain complicated mixture of Co, Ni, Al, Zn and Ti oxides, where spinel cobalt titanate Co_2TiO_4 is indicated as the main phase, and barium sulphate, chromium(III) oxide and titanium(IV) oxide are announced as secondary phases. However, EDX analysis revealed that Cr_2O_3 is not present in this mixture (see Table 2).

Moreover, XRD analysis showed that the main phase is rather nickel zinc titanium oxide $NiZnTiO_4$ (PDF 35-1372) than cobalt titanate Co_2TiO_4 (PDF 39-1410). Other determinated secondary phases were barium sulphate $BaSO_4$ (barite, PDF 24-1035) and nickel oxide NiO (bunsenite, PDF 47-1049) (Fig. 8a). Unfortunately, TiO_2 as a separate phase and crystalline phases containing aluminium were not determined. It is worth to mention that the XRD pattern of cobalt green pigment is very sophisticated, since the majority of peaks of the phases, except of $BaSO_4$, are overlapping. The XRD pattern of cobalt bottle green pigment corresponds exactly to the XRD pattern of cobalt chromium oxide $CoCr_2O_4$ (PDF 80-1668) (see Fig. 8b). However, cobalt bottle green pigment distinguishes more green tones than the pure $CoCr_2O_4$, which leads to assumption of presence of impurities. Nevertheless, EDX results differ from the composition stated by the producers (see Table 1), where presence of magnesium was detected instead

of declared titanium. Despite of that, the impurities are in undetectable quantities by the XRD analysis, yet enough to change to colour of the pigment. Finally, according to the XRD pattern of chrome oxide green (Fig. 8c), all peaks coincide to the pattern of chromium(III) oxide Cr_2O_3 (eskolaite, PDF 38-1479).

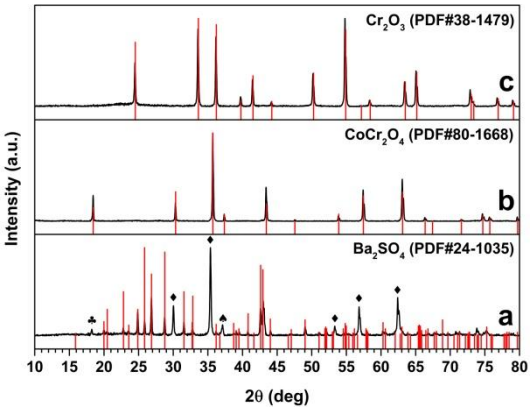

Figure 8. XRD patterns of green oxide pigments: cobalt green (a), cobalt bottle green (b), and chrome oxide green (c). The phases are marked: ♦ – $NiZnTiO_4$; ♣ – Co_2TiO_4; ♠ – NiO; vertical lines represent standard XRD pattern of $BaSO_4$

XRD patterns of the rest four green pigments (Egyptian green, Victoria green, Florentine green and green jasper) are presented in Fig. 9.

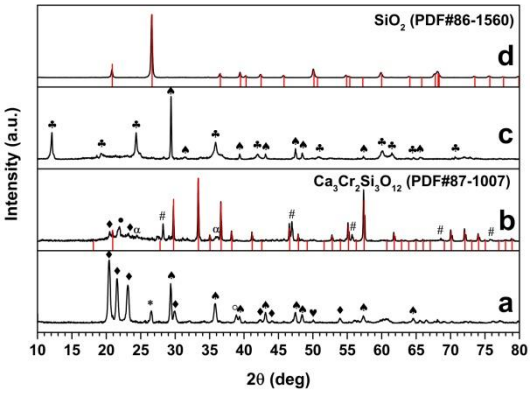

Figure 9. XRD patterns of silica containing pigments: Egyptian green (a), Victoria green (b), Florentine green (c), and green jasper (d). The phases are marked: ♠ – $CaCO_3$; ♦ – SiO_2 (tridymite); ♥ – Na_2CO_3; * – SiO_2 (quartz); o – CuO; # – CaF_2 (fluorite); α – Cr_2O_3; • – SiO_2 (cristabolite); ♣ – Mg–Fe–Si–O; vertical lines represent standard XRD pattern of $Ca_3Cr_2(SiO_4)_3$

The most complex pigment to identify was Egyptian green (see Fig. 9a). Egyptian green usually is obtained from Egyptian blue pigment $CaCuSi_4O_{10}$

(cuprorivaite) by heating it or its raw materials, such as siliceous sand, lime, copper compounds and flux (soda or other), above 1000 °C [107]. The XRD results revealed that this pigment contains calcite $CaCO_3$ (PDF 72-1652), tridymite SiO_2 (PDF 71-0197), copper(II) oxide CuO (PDF 74-1021), quartz SiO_2 (PDF 83-2465), and sodium carbonate Na_2CO_3 (PDF 86-0297). Presumably the XRD pattern of Egyptian green shows only starting materials for the green frit since no newly formed phase was determined. According to the data in catalogue of manufacturer, Victoria green pigment should be garnet calcium chromium silicate. Although the X-ray diffraction analysis (see Fig. 9b) confirmed the presence of $Ca_3Cr_2(SiO_4)_3$ (uvarovite, PDF 87-1007) as the main phase, it also showed the presence of calcium fluoride CaF_2 (PDF 35-0816), tridymite SiO_2 (PDF 71-0197), silica SiO_2 (cristabolite, PDF 77-1317), and chromium(III) oxide Cr_2O_3 (PDF 85-0730) as secondary phases. These results imply that Victoria green pigment contains primary materials of the synthesis in its mixture.

Unfortunately, even after XRD measurements the phase composition of green pigment Florentine green still remained unclear. The results revealed that Florentine green (see Fig. 9c) contains calcite $CaCO_3$ (PDF 81-2027) and magnesium iron silicate Mg–Fe–Si–O (PDF 22-0710). However, all diffraction peaks of green jasper (Fig. 9d) coincide only to silicon oxide SiO_2 (quartz, PDF 86-1560) and no phases of chromophore were identified. According to EDX results coinciding with literature, the chromophore should be iron [108, 109] and/or chromium [110] compounds.

The XRD patterns of prepared lead-based glaze mixtures containing different analogous pigments to historical green pigments are very similar, since the main detected phase in glaze mixtures is lead oxide Pb_3O_4 (minium, PDF 41-1493). Nevertheless, green pigment verdigris could be easily detected in the glaze mixture by XRD method (Fig. 10). The intense peak at $2\theta \approx 12.8°$ and a few weaker peaks at $2\theta \approx 24.7°$, 37.6°, and 42.5° could be easily attributed to copper(II) acetate monohydrate (PDF 27-0145). Besides, the weak peak of silicon oxide (quartz, PDF 86-1560) from the glaze mixture is observable at $2\theta \approx 20.8°$. Malachite (see Fig. 11a), both cobalt oxide-based pigments (Fig. 11b and c) and Victoria green (Fig. 11d) pigment in their glaze mixtures can be distinguished very roughly.

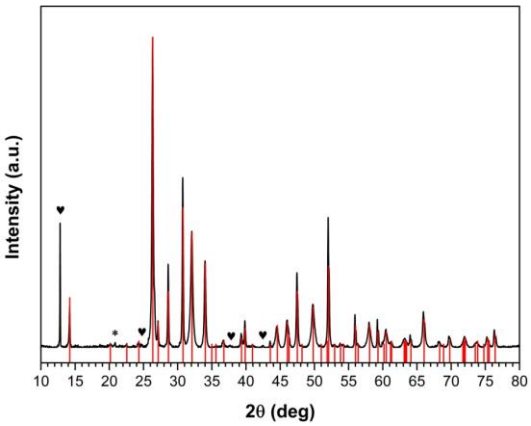

Figure 10. XRD pattern of glaze mixture containing the green pigment verdigris. The phases are marked: ♥ – $Cu(CH_3COO)_2 \cdot H_2O$; * – SiO_2 (quartz); vertical lines represent standard reference pattern of Pb_3O_4

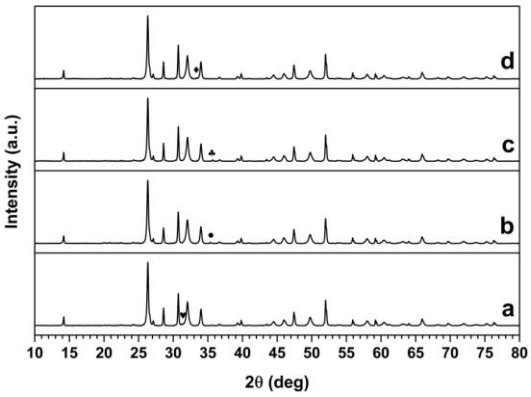

Figure 11. XRD patterns of glaze mixtures prepared with green pigments malachite (a), cobalt green (b), cobalt bottle green (c), and Victoria green (d). The phases are marked: ♥ – $Cu_2(OH)_2CO_3$; ● – $NiZnTiO_4$; ♣ – $CoCr_2O_4$; and ♦ – $Ca_3Cr_2(SiO_4)_3$

As it is seen from Fig. 11, all characteristic diffraction peaks of pigments are very weak. Nevertheless, these green pigments also could be determined by XRD method in their glaze mixtures.

Finally, no specific signals from investigated pigments were detected in the XRD patterns of glaze mixtures prepared with Cr_2O_3 (Fig. 12a), Egyptian green (Fig. 12b), Florentine green (Fig. 12c), and green jasper (Fig. 12d).

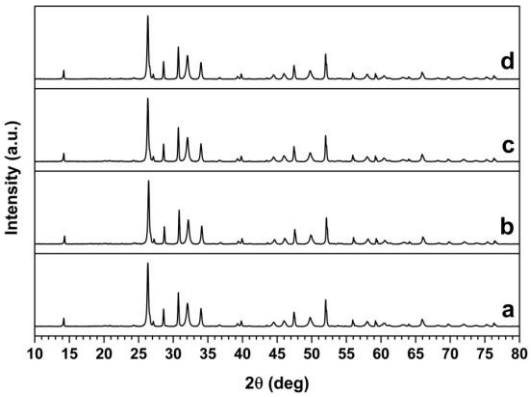

Figure 12. XRD patterns of glaze mixtures with green pigments chrome oxide green (a), Egyptian green (b), Florentine green (c), and green jasper (d)

All these XRD patterns are identical to the XRD patterns of individual lead-based glaze mixture without pigments. Consequently, chrome oxide green, Egyptian green, Florentine green and green jasper pigments could be hardly determined by XRD in their lead-based glaze mixtures, unless the concentration of pigment would be unusually very high.

3.1.3. FTIR spectroscopy

Additionally infrared spectroscopy was applied to test the possibility for the characterisation and determination of analogous to historical green pigments. Characterisation of individual pigments revealed that FTIR spectra of malachite and verdigris (see Fig. 13) contain absorption bands attributable to the carbon-oxygen vibration in double bond containing functional groups. Besides, the transmittance mode of both malachite and verdigris spectra shows the presence of bands of the O–H vibrations at 3402 and 3311 cm^{-1} for malachite (Fig. 13a) and ~3468, 3365 and 3266 cm^{-1} for verdigris (Fig. 13b) [111]. The absorption bands for malachite at 1490 and ~1386 cm^{-1} correspond to v_3 asymmetric stretching mode and v_1 symmetric stretching mode at 1096 cm^{-1} of CO_3^{2-} group [112]. For verdigris, the bands at ~1595 and 1418 cm^{-1} are due to the presence of COO^- group and correspond to the asymmetric stretching and symmetric stretching vibrations of the C–O bond in the acetate group, respectively [112]. The band for malachite at 1045 cm^{-1} coincides with δOH bending mode [111, 112]. Bending modes of C–H bond in verdigris are observed at 1048 and 1032 cm^{-1} [112]. For malachite two v_2 bending modes at ~870 and 817 cm^{-1} of CO_3^{2-} group are also visible [111].

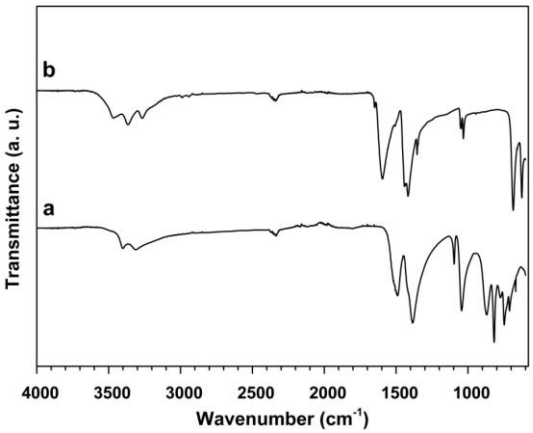

Figure 13. FTIR spectra of pigments malachite (a) and verdigris (b)

FTIR spectra of green oxide pigments are given in Fig. 14. All three spectra are very similar containing sharp peak at 668 cm^{-1}, which can be assigned to metal–oxygen (M–O) stretching vibrations [113].

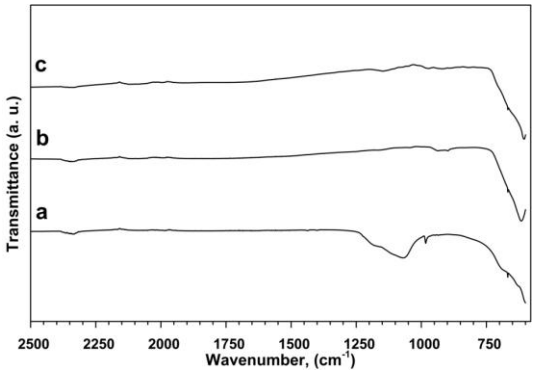

Figure 14. FTIR spectra of green oxide pigments: cobalt green (a), cobalt bottle green (b), and chrome oxide green (c)

This sharper and more intense band is also seen at the same wavenumber (668 cm^{-1}) in the FTIR spectra of green silica pigments (see Fig. 15). But in this case these bands along with intensive bands located in the region of ~1100–950 cm^{-1} could be attributed to Si–O vibrations [114].

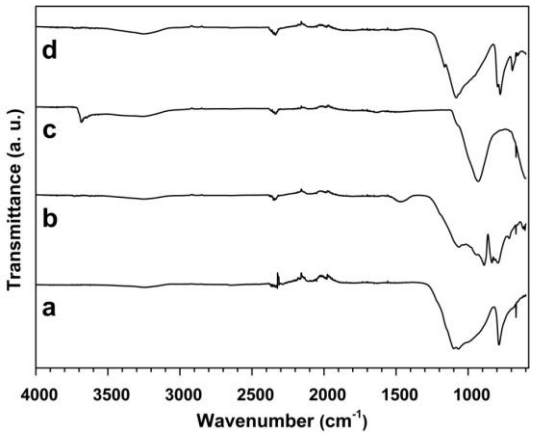

Figure 15. FTIR spectra of green silica pigments: Egyptian green (a), Victoria green (b), Florentine green (c), and green jasper (d)

FTIR results of characterisation of glaze mixtures revealed that the qualitative identification of the inorganic pigments in such range of wavenumbers is possible only for green pigments malachite (see Fig. 16a) and verdigris (Fig. 16b).

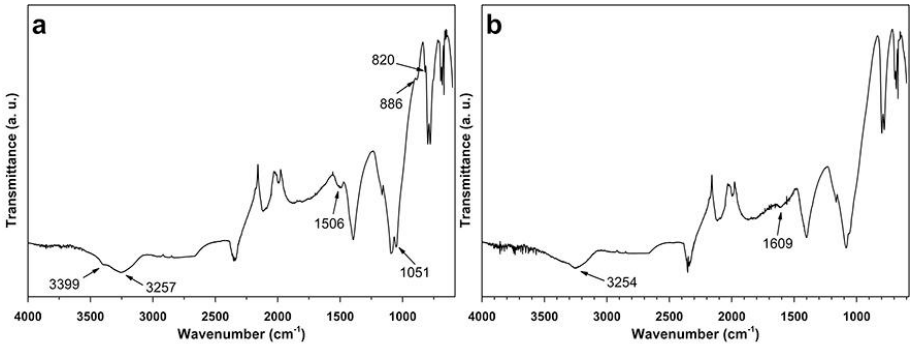

Figure 16. FTIR spectra of glaze mixtures with green pigments: malachite (a) and verdigris (b)

The FTIR spectra show that the characteristic vibrations are very well resolved. All vibration bands are slightly shifted to a higher wavenumber region. Week absorption peaks at ~1506 cm^{-1} and 886, 820 cm^{-1} for malachite in the glaze mixture coincide with an asymmetric stretching of $\nu_3CO_3^{2-}$ and bending modes of $\nu_2CO_3^{2-}$ vibrations, respectively. A week peak at 1051 cm^{-1} is ascribed to δOH and broad doublet at 3399 and ~3257 cm^{-1} is due to O–H stretching vibrations. A week absorption peak at ~1609 cm^{-1} in FTIR spectrum of glaze mixture with verdigris pigment corresponds to an asymmetric stretching vibration of the C–O bond in the acetate group and

broad band at ~3254 cm^{-1} corresponds to stretching mode in hydroxide group.

3.1.4. Morphological features of analogous to historical green pigments and their ceramic glazes

The morphological features of commercial pigments were investigated by scanning electron microscopy. The SEM micrographs revealed that particles of each pigment are differently shaped and of unequal size (from tens to hundreds microns). The representative SEM micrograph of cobalt bottle green pigment is given in Fig. 17.

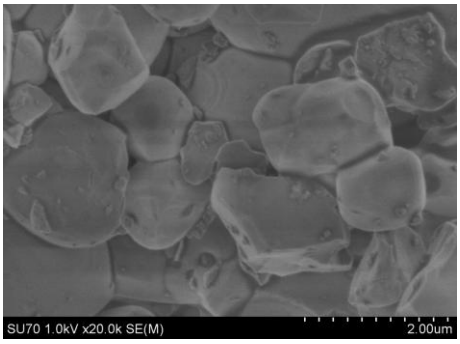

Figure 17. SEM micrograph of commercial green pigment cobalt bottle green

The prepared Pb-based ceramic glazes are not monochromic. Moreover, the colours of the glazes depend on the firing temperature. The digital photographs of the glazes are given in Fig. 18.

Investigation of the glazes through an optical microscope revealed that ceramic tiles are covered the glazes unequally. However, no texture of the ceramic itself was visible. The ceramic glazes with Egyptian, Victoria, Florentine greens and green jasper were similar to each other, having cracks and evenly distributed pigment on the surface, except the glaze with Victoria green (see Fig. 19). The glazes with malachite were similar to the glazes with verdigris. The glazes with cobalt green, cobalt bottle green and chrome oxide green were akin to each other. Furthermore, OM analysis revealed the main difference of the ceramic glazes prepared at different temperatures. Interestingly, the ceramic glazes fired at 900 °C contained smaller air bubbles compared to the glazes fired at 1000 °C.

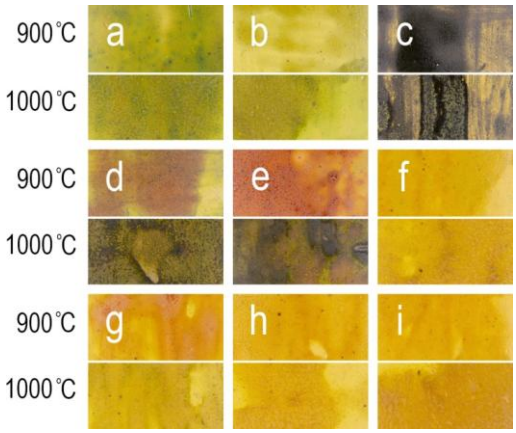

Figure 18. Digital photographs of Pb-based ceramic glazes with commercial pigments fired at different temperatures: a – malachite; b – verdigris; c – cobalt green; d – cobalt bottle green; e – chrome oxide green; f – Egyptian green; g – Victoria green; h – Florentine green; and i – green jasper

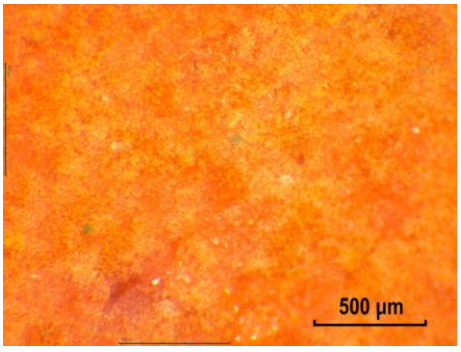

Figure 19. Image obtained by attached camera to optical microscope of Pb-based ceramic glaze with commercial Victoria green pigment fabricated at 1000 °C

Comparing the SEM images of the glazes obtained at different firing temperatures, the tendency of better externalised shape of the particles were observed for the samples obtained at higher temperature. The representative SEM images of the ceramic glazes prepared with commercial cobalt bottle green pigment are given in Fig. 20.

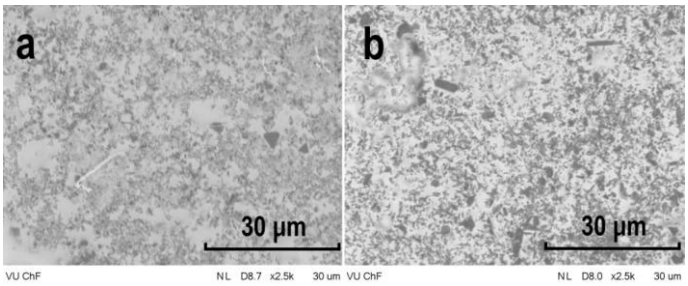

Figure 20. SEM micrographs of Pb-based ceramic glazes with cobalt bottle green commercial pigment, obtained at different firing temperatures: a – 900 °C; b – 1000 °C

For comparison, lead-free glazes were prepared at 1000 °C (see Fig. 21).

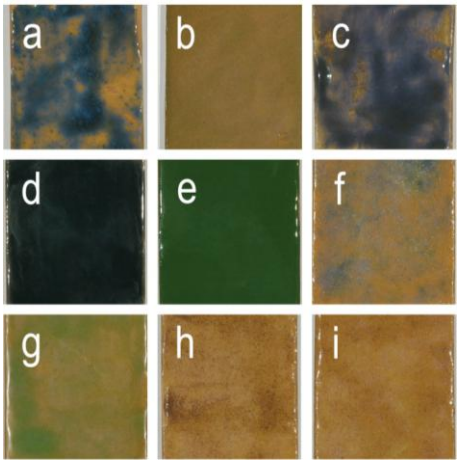

Figure 21. Digital photographs of Pb-free ceramic glazes with commercial pigments: a – malachite; b – verdigris; c – cobalt green; d – cobalt bottle green; e – chrome oxide green; f – Egyptian green; g – Victoria green; h – Florentine green; and i – green jasper

Almost all glazes covered the ceramic tiles unevenly and the colour of the tile could be seen through the transparent spots of glazes. It should be noted, that 5 wt% of the pigment was sufficient amount to colour the glaze evenly only in the case of cobalt bottle green and chrome oxide green. One could conclude that for the rest of the pigments there should be used bigger amount of the pigment to achieve uniform ceramic glazes. Moreover, green earths (Florentine green and green jasper) did not provide any colour for the glazes at all and only separate pigment particles could be seen.

OM analysis of the glazes revealed that the texture of the ceramic tiles could be seen through the transparent and colourless areas. The most

exclusive glazes were ones with the verdigris and Egyptian green pigments. Although the glaze with verdigris visually had slight presence of light green colour, the optical microscopy did not reveal any traces of pigment particles (see Fig. 22a). The base glaze with Egyptian green pigment (see Fig. 22b) revealed gas bubbles suspended in the glass. Such effect occurred most likely due to the decomposition of carbonates included in Egyptian green pigment mixture.

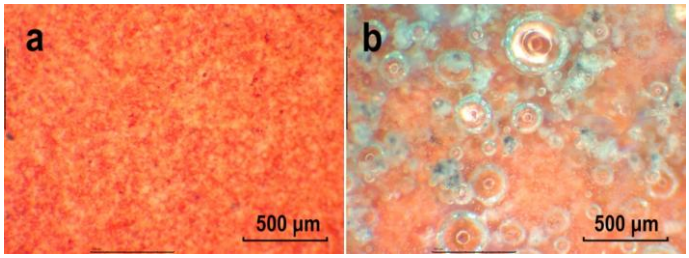

Figure 22. Images obtained by attached camera to optical microscope of Pb-free ceramic glazes with commercial pigments: a – verdigris; and b – Egyptian green

The SEM analysis confirmed the uneven distribution of the pigment particles for the most glazes. However, the cobalt bottle green pigment with well-resolved particles could be characterised as very well dispersed within the ceramic glaze (Fig. 23).

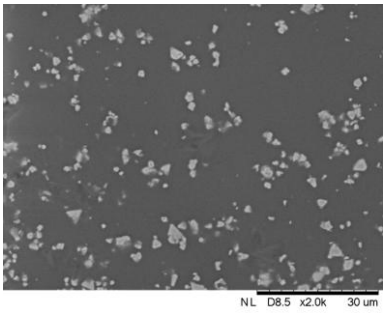

Figure 23. SEM micrograph of Pb-free ceramic glaze with pigment cobalt bottle green

As it was mentioned before, the materials with spinel structure is very attractive in pigmentary field. The nature of tetrahedral or octahedral cations and potential of different types of doping give diversity in colours and properties. Therefore, cobalt chromite with a spinel structure was chosen to be as a base structure for the syntheses of new green pigments.

3.2. Synthesis and characterisation of $Co_{1-x}M_xCr_2O_4$ pigments and glazes

Cobalt chromite based pigments $Co_{1-x}M_xCr_2O_4$ (M = Ni, Cu, and Zn) with different transition metal concentrations ($0 \leq x \leq 1$ with a step of 0.25) have been synthesised applying two aqueous synthesis approaches: sol-gel and sonochemical synthesis routes.

3.2.1. Synthesis by sol-gel method

XRD analysis.

X-ray diffraction patterns of Ni-substituted $Co_{1-x}Ni_xCr_2O_4$ powders obtained by sol-gel method at different temperatures are shown in Fig. 24. It is evident, that samples with a higher substitution ratio (x = 0.75 and 1) are not single phase compounds independent on the annealing temperature (Fig. 24a, b, c, and d).

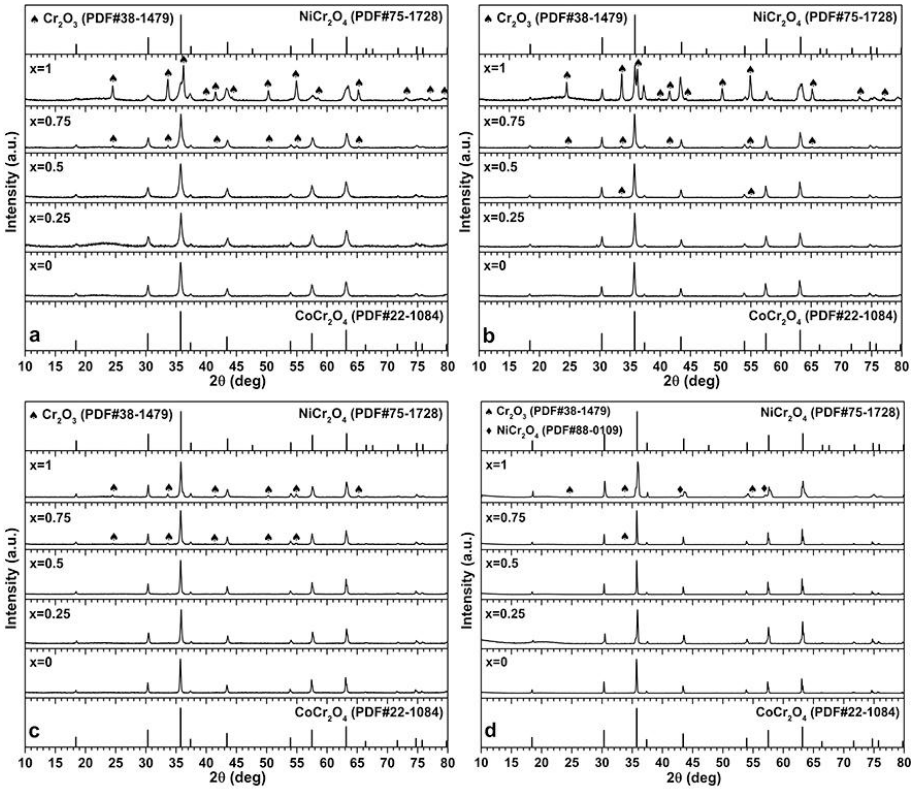

Figure 24. XRD patterns of sol-gel derived $Co_{1-x}Ni_xCr_2O_4$ (x = 0; 0.25; 0.5; 0.75; and 1) samples heated at 600 °C (a), 700 °C (b), 800 °C (c), and 1000 °C (d)

The formation of $Co_{1-x}Ni_xCr_2O_4$ solid solution is evident. The main phase of these samples is cubic $NiCr_2O_4$ (PDF 75-1728), whereas the formation of traces of secondary Cr_2O_3 (PDF 38-1479) phase depends on the substitution ratio x and the heating temperature. The less intensive characteristic peaks of Cr_2O_3 are seen in the XRD patterns of samples heated at higher temperatures. X-ray diffraction results demonstrate that substitution of cobalt by nickel in chromite proceeds by gradual transformation of cubic $CoCr_2O_4$ (PDF 22-1084) crystalline phase into cubic $NiCr_2O_4$ spinel phase. However, the powder with x = 1, heated at the highest temperature, contains additional tetragonal $NiCr_2O_4$ (PDF 88-0109) phase (see Fig. 24d). The coexistence of cubic and tetragonal phases of $NiCr_2O_4$ between 27 and 34 °C of ambient temperature was reported [115]. In addition, there is possibility of the tetragonal transformation to be caused by grinding the powder [116]. The fact that the majority of the powders are not single-phase is not critical, since in the pigmentary field the main goal is to achieve the proper parameters of the pigment for application in industry [29].

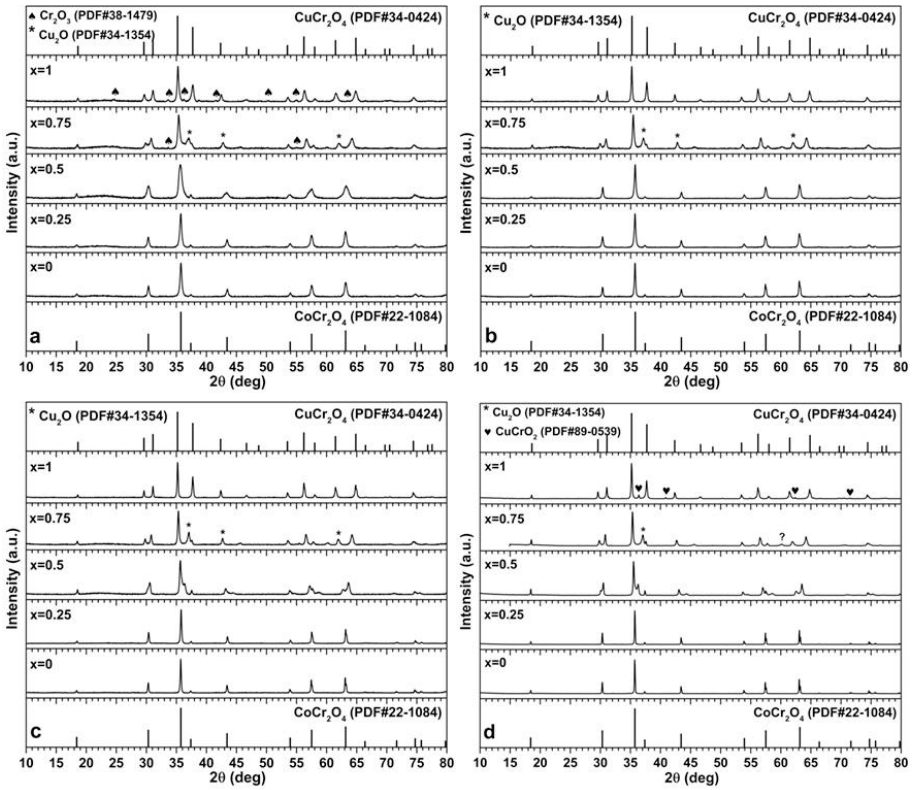

Figure 25. XRD patterns of sol-gel derived $Co_{1-x}Cu_xCr_2O_4$ (x = 0; 0.25; 0.5; 0.75; and 1) samples heated at 600 °C (a), 700 °C (b), 800 °C (c), and 1000 °C (d)

The X-ray diffraction results of Cu-substituted $Co_{1-x}Cu_xCr_2O_4$ powders (see Fig. 25) are similar to the results obtained for Ni-substituted ones. All four materials with x = 0.75 obtained at different temperatures contain $CuCr_2O_4$ (PDF 34-0424) as a primary phase and Cu_2O (PDF 34-1354) as a secondary phase. Furthermore, the lowest annealing temperature gives impurities for fully substituted sample as well. The powders with x = 0.75 and 1 heated at the temperature of 600 °C are mixtures of $CuCr_2O_4$, Cu_2O, and Cr_2O_3 crystalline phases (Fig. 25a). With increasing the temperature to 700 and 800 °C, fully substituted compounds were single phase tetragonal $CuCr_2O_4$ spinels. However, at the highest annealing temperature, additional phase of rhombohedral $CuCrO_2$ (PDF 89-0539) is also occurred. At the lower substitution ratios (0.25 and 0.5) the main detectable phase is cubic $CoCr_2O_4$. XRD results demonstrate that substitution of cobalt by copper in chromite proceeds by progressive transformation of $CoCr_2O_4$ cubic crystalline phase into the tetragonal spinel phase of $CuCr_2O_4$.

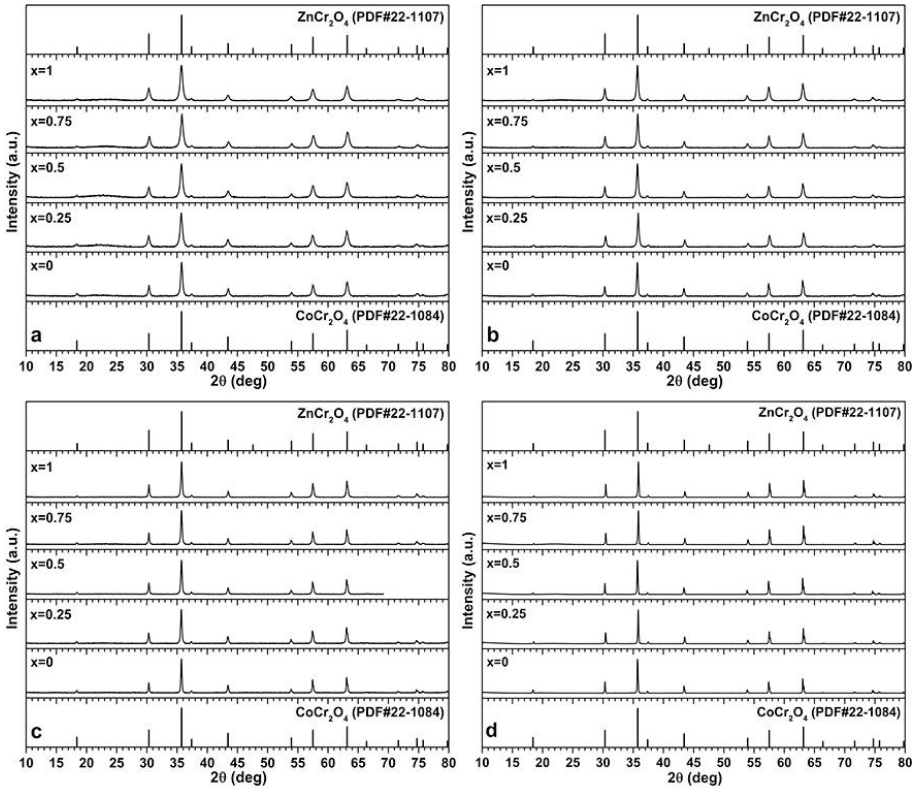

Figure 26. XRD patterns of sol-gel derived $Co_{1-x}Zn_xCr_2O_4$ (x = 0; 0.25; 0.5; 0.75; and 1) samples heated at 600 °C (a), 700 °C (b), 800 °C (c), and 1000 °C (d)

In case of Zn-substituted $Co_{1-x}Zn_xCr_2O_4$ compounds, all XRD patterns (see Fig. 26) showed the formation of single-phase compounds ($CoCr_2O_4$, when x = 0.25 and 0.5; $ZnCr_2O_4$ PDF 22-1107, when x = 0.75 and 1). The estimated crystallite size of $CoCr_2O_4$ samples was 28.0, 40.8, 48.92, and 48.94 nm obtained after the heat treatment at 600, 700, 800, and 1000 °C, respectively. For the $Co_{1-x}Ni_xCr_2O_4$ samples, the crystallite size varied from 21.3 to 27.2 nm, from 33.8 to 39.2 nm, from 39.7 to 44.5 nm, and from 30.6 to 65.3 nm for the samples obtained at 600, 700, 800, and 1000 °C, respectively. The crystallite size of $Co_{1-x}Cu_xCr_2O_4$ samples varied from 15.3 to 30.4 nm, from 33.8 to 44.2 nm, from 28.8 to 48.6 nm, and from 42.4 to 61.2 nm for the samples obtained at 600, 700, 800, and 1000 °C, respectively. In the case of $Co_{1-x}Zn_xCr_2O_4$ powders, the crystallite size changed from 20.4 to 23.3 nm, from 30.6 to 34.9 nm, from 39.1 to 40.8 nm, and from 57.5 to 61.3 nm for the samples heated at 600, 700, 800, and 1000 °C, respectively. As seen, the crystallite size increased less than or around 20 nm or less than 10 nm with increasing temperature from 600 to 700 °C, from 800 to 1000 °C or from 700 to 800 °C, respectively. Unfortunately, no correlation or linear dependence on the substitutional level for crystallite size was observed.

FTIR spectroscopy.

FTIR spectroscopy was used as additional tool for the structural characterisation of obtained powders. Spectra of pigments annealed at 1000 °C are given in Fig. 27. For all spectra, the band between 600–700 cm^{-1} corresponds to the stretching band of Cr–O in the octahedral system and the broad band around 500 cm^{-1} is assigned to the stretching bond of metal (Co and M (Ni, Cu, Zn))–O in the tetrahedral system [117]. Unfortunately, we were not able to identify additional bands at about 550 and 563 cm^{-1} for the Cu-doped powders (see Fig. 27b) with x = 0.75 and 1.0, respectively.

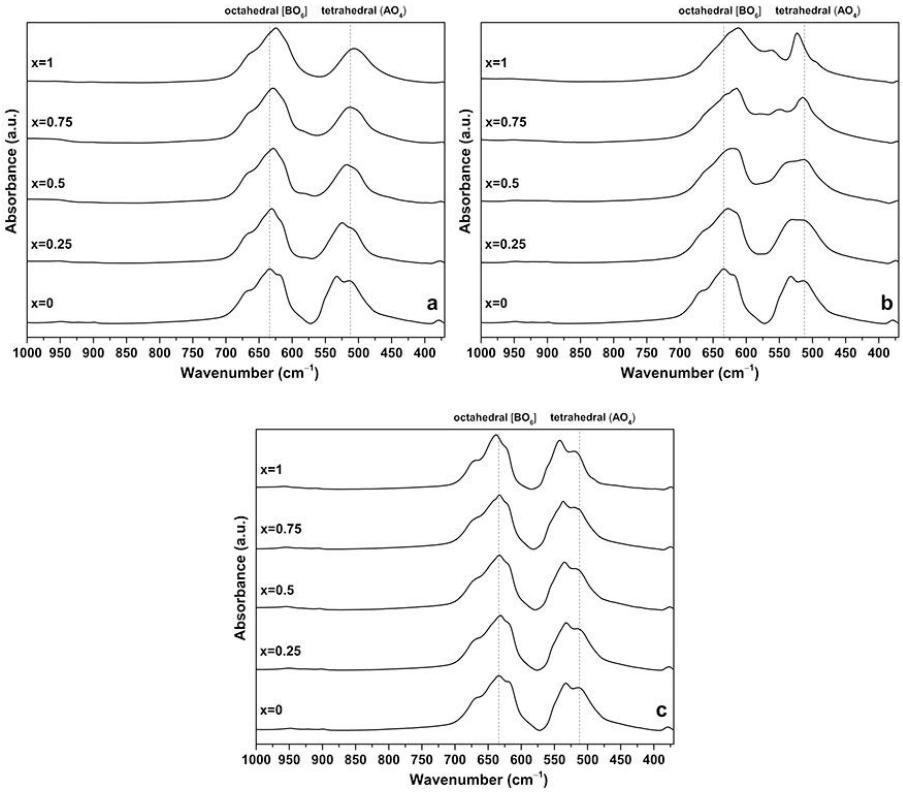

Figure 27. FTIR spectra of sol-gel derived $Co_{1-x}M_xCr_2O_4$ (x = 0; 0.25; 0.5; 0.75; and 1) samples annealed at 1000 °C, where M = Ni^{2+} (a); Cu^{2+} (b); and Zn^{2+} (c)

Raman spectroscopy.

Raman spectroscopy was performed on the samples annealed at 1000 °C (Fig. 28). According to literature [85], the typical Raman spectra of the pure cubic spinel consist of five fundamental bands ($A_{1g} + E_g + 3F_{2g}$). In our case, three main bands of $F_{2g}(1)$, E_g and A_{1g} modes are very well resolved for all samples. Formation of $NiCr_2O_4$ (see Fig. 28a) shifts Raman-active vibrations of $F_{2g}(1)$ mode to a lower frequency (~174 cm^{-1}) and reduces intensity of signal. The positions of E_g (497 cm^{-1}) and A_{1g} (655 cm^{-1}) modes are slightly shifted to higher frequencies.

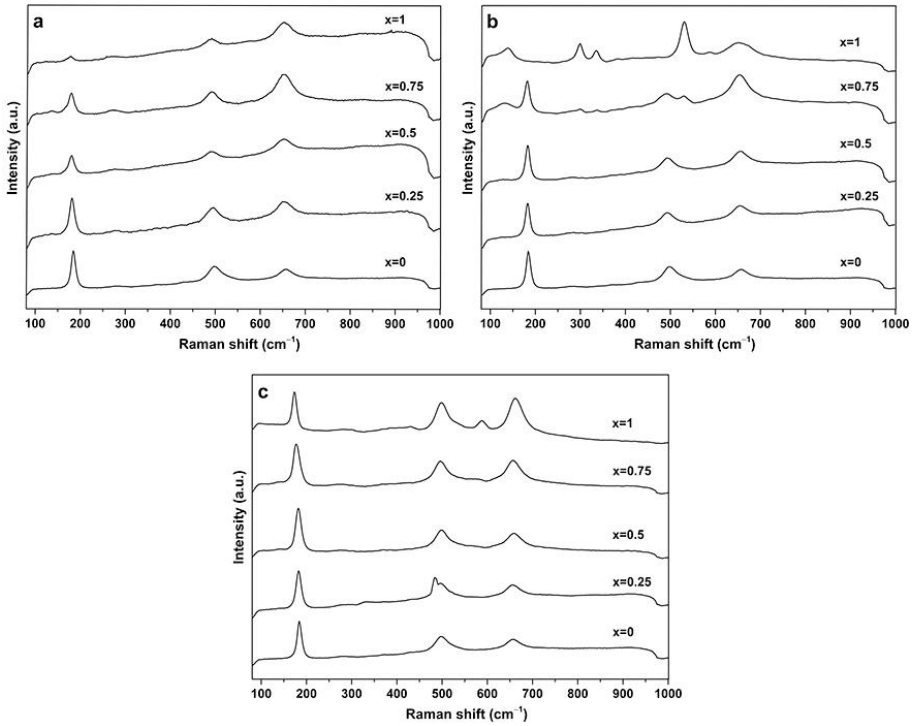

Figure 28. Raman spectra of sol-gel derived $Co_{1-x}M_xCr_2O_4$ (x = 0; 0.25; 0.5; 0.75; and 1) samples annealed at 1000 °C, where M = Ni^{2+} (a); Cu^{2+} (b); and Zn^{2+} (c)

In the case of Cu-doped samples (see Fig. 28b), only characteristic sharp band at about 180 cm^{-1} and broad bands at about 490 and 650 cm^{-1} (x = 0.25; 0.5; and 0.75) are well resolved and could be attributed to $F_{2g}(1)$, E_g and A_{1g} modes, respectively. However, additional bands at 298, 335 and 530 cm^{-1} are observed for the samples with the substitution ratios of 0.75 and 1.0. Unfortunately, we were not able to explain the appearance of these bands as well. Raman results of Zn-doped powders (see Fig. 28c) revealed typical spectrum of zinc chromium spinel (x = 1.0) with slight shift to a lower frequency. A sharp band at about 174 cm^{-1} and broader bands at about 498, 588 and 661 cm^{-1} could be assigned to $F_{2g}(1)$, $F_{2g}(2)$, $F_{2g}(3)$ and A_{1g} modes, respectively.

FTIR and Raman spectroscopic analyses confirmed the XRD results of formation of solid solutions having spinel crystal structure with additional crystalline phases.

ICP-OES analysis.

The ICP-OES analysis results of the $Co_{1-x}M_xCr_2O_4$ samples annealed at 1000 °C are given in Table 3.

Table 3. ICP-OES results of the $Co_{1-x}M_xCr_2O_4$ (x = 0; 0.25; 0.5; 0.75; and 1) powders annealed at 1000 °C

Theoretical ratio	Calculated ratio		
	Co : Ni : Cr	Co : Cu : Cr	Co : Zn : Cr
1 : 0 : 2	1 : 0.00 : 1.89	1 : 0.00 : 1.89	1 : 0.00 : 1.89
0.75 : 0.25 : 2	0.75 : 0.25 : 2.01	0.74 : 0.25 : 1.88	0.69 : 0.25 : 1.71
0.5 : 0.5 : 2	0.50 : 0.52 : 2.04	0.51 : 0.50 : 2.02	0.50 : 0.56 : 2.06
0.25 : 0.75 : 2	0.25 : 0.77 : 2.06	0.25 : 0.74 : 1.99	0.25 : 0.83 : 2.01
0 : 1 : 2	0.00 : 1.00 : 1.97	0.00 : 1.00 : 1.99	0.00 : 1.00 : 1.70

According to ICP-OES results, the experimental molar ratio is in a good agreement with theoretical formula.

Thermal analysis.

The thermal behaviour of sol-gel derived Co-M-Cr-O precursor gels was investigated for selected samples (x =0; 0.5; and 1). The thermal behaviour for all tested samples could be characterised in similar manner, therefore only TG/DTG analysis results of Ni-substituted precursor gels are given (see Fig. 29).

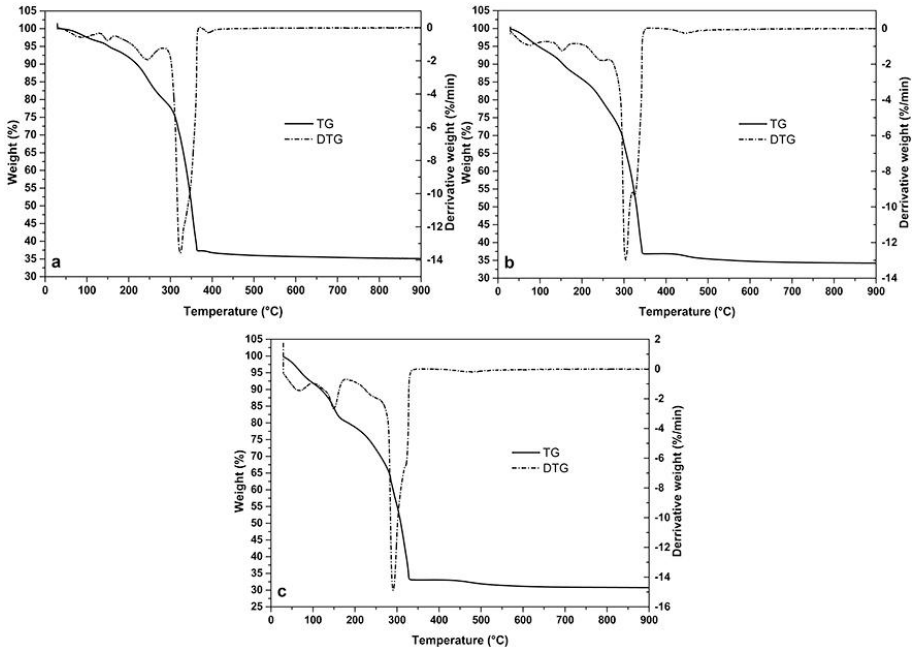

Figure 29. TG/DTG curves of sol-gel derived Co-Ni-Cr-O precursor gels, where x = 0 (a); x = 0.5 (b); and x = 1 (c)

The total weight loss for sol-gel derived precursor gels was about ~70 %. Three weight losses up to ~250 °C are observable in the TG curves for all samples, which correspond to dehydration and decomposition of nitrates and acetates. An abrupt weight loss (~13–14 %) at around 300 °C represents final decomposition of organic part of the gels, and further heat treatment of the gels results in the formation of mixed oxides at around 500 °C. Subsequent weight loss (~2 %) with further increase of the temperature is quite insignificant.

Optical properties.

The diffuse reflectance spectra of $M_xCr_2O_4$ (M = Co^{2+}, Ni^{2+}, Cu^{2+}, and Zn^{2+}) specimens heated at 600–800 °C are given in Fig. 30.

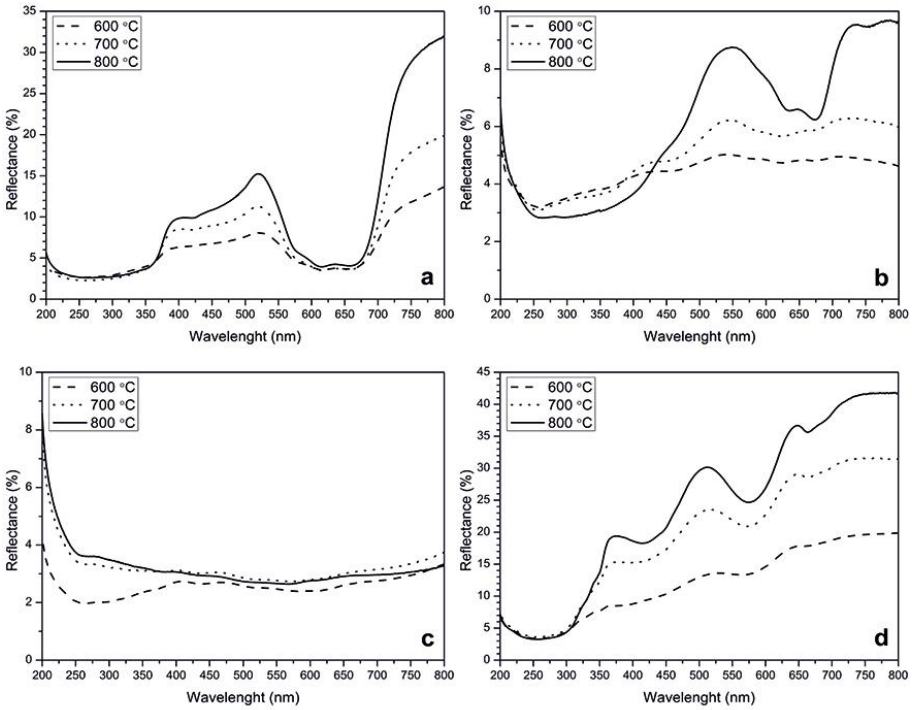

Figure 30. The diffuse reflectance spectra of sol-gel derived MCr_2O_4 powders obtained at various heating temperatures. M: (a) – Co, (b) – Ni, (c) – Cu, and (d) – Zn

It indicates that absorbance decreases with increasing the heating temperature in all cases. In the case of bluish-green $CoCr_2O_4$ sample, characteristic absorption bands of Cr^{3+} and Co^{2+} could be easily identified (Fig. 30a). The spectrum shows three bands of Cr^{3+} in octahedral coordination, peaked at around 270, 400 and 600 nm, that could be assigned

to $^4A_{2g} \rightarrow {}^4T_{1g}(P)$, $^4A_{2g} \rightarrow {}^4T_{1g}(F)$ and $^4A_{2g} \rightarrow {}^4T_{2g}(F)$ transitions, respectively [118, 119]. A broad and low intensity band between 400 and 500 nm is related to the blue absorption because of the spin-allowed transition of Cr^{3+} ion. Finally, the last absorption band, located between 580 and 680 nm, decomposes into three bands, which are characteristic for the presence of Co^{2+} ions (d^7 configuration) in tetrahedral coordination. These bands can be attributed to $^4A_2(F) \rightarrow {}^4T_1(P)$ transitions usually observed between 550 and 670 nm. Superpositions with $^4A_{2g} \rightarrow {}^4T_{2g}$ and $^4A_{2g} \rightarrow {}^2T_{1g}$ transitions of Cr^{3+} probably occurred in this range, observed at 580 and 660 nm, respectively [80, 118]. For the Ni-containing samples, which are the mixtures of $NiCr_2O_4$ and Cr_2O_3, the same characteristic absorption bands of Cr^{3+} in octahedral field at about 270 and 400 nm could be determined (Fig. 30b). However, the Cr_2O_3 impurity phase influences the intensity of absorption. The sample annealed at 800 °C having the lowest concentration of secondary phase gives the most intense charge transfer band. The reflectance curve of this pigment is the most characteristic for $NiCr_2O_4$ spinel. The absorption band observed at around 633 nm corresponds to $^3T_1(F) \rightarrow {}^3T_1(P)$ transition of Ni^{2+} ion in tetrahedral coordination. The absorption bands at around 680 and 750 nm could be attributed to $^3A_{2g}(F) \rightarrow {}^3T_{1g}(F)$ and $^3A_{2g}(F) \rightarrow {}^3T_{2g}(F)$ transitions of Ni^{2+} in octahedral coordination, respectively [118]. Nevertheless, the samples heat-treated at 600 and 700 °C showed very weak characteristic reflectance bands. The reflectance band at around 540 nm for all the samples stimulates the green colour in the human eyes visible region, therefore Ni-substituted pigments depending on the substitution level have various green shades [20]. Fig. 30c shows that $CuCr_2O_4$, having a nearly black hue, does not reflect the light in the visible region in contrast to the case of zinc chromite (Fig. 30d). In the latter case the main absorption bands at 420 and 575 nm are due to $^4A_{2g} \rightarrow {}^4T_{2g}$ and $A_{2g} \rightarrow {}^4T_{1g}(F)$ transitions of Cr^{3+} ions in octahedral position of the spinel crystal structure, respectively [89, 120]. Moreover, $^4A_{2g} \rightarrow {}^2T_{1g}$ and $^4A_{2g} \rightarrow {}^2E_g$ transitions between 650 and 680 nm for Cr^{3+} ions are also observable, since absorption bands of Co^{2+} ions with d^7 configuration is not overlapping them as in the case of $CoCr_2O_4$ [22].

3.2.2. Synthesis by sonochemical method

XRD analysis.

The XRD patterns of selected sonochemically derived specimens are shown in Fig. 31. The list of phase compositions of all samples is given in Table 4.

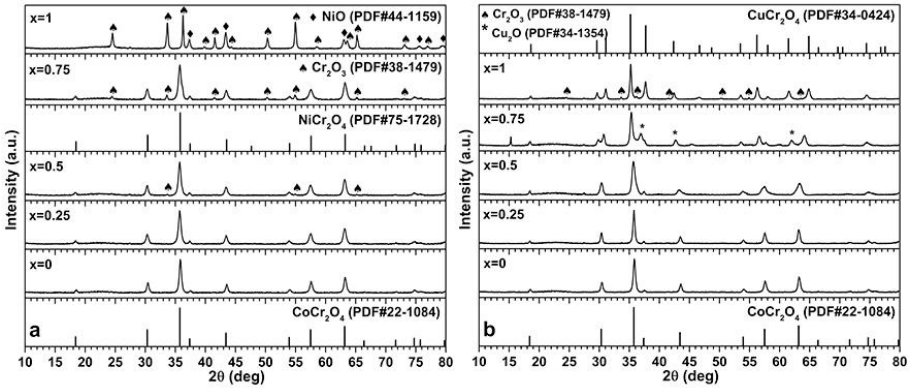

Figure 31. XRD patterns of sonochemically derived $Co_{1-x}Ni_xCr_2O_4$ (x = 0; 0.25; 0.5; 0.75; and 1) (a) and $Co_{1-x}Cu_xCr_2O_4$ (x = 0; 0.25; 0.5; 0.75; and 1) (b) samples heated at 700 °C

Table 4. Phase composition of pigments prepared by sonochemical synthesis method at different annealing temperatures

Sample name	Identified phases at different temperatures		
	600 °C	700 °C	800 °C
SN-Co0	$CoCr_2O_4$	$CoCr_2O_4$	$CoCr_2O_4$
SN-Ni0.25	$CoCr_2O_4$	$CoCr_2O_4$	$CoCr_2O_4$
SN-Ni0.5	$CoCr_2O_4$, Cr_2O_3	$CoCr_2O_4$, Cr_2O_3	$CoCr_2O_4$, Cr_2O_3
SN-Ni0.75	$NiCr_2O_4$, Cr_2O_3	$NiCr_2O_4$, Cr_2O_3	$NiCr_2O_4$, Cr_2O_3
SN-Ni1	NiO, Cr_2O_3	NiO, Cr_2O_3	$NiCr_2O_4$, Cr_2O_3
SN-Cu0.25	$CoCr_2O_4$	$CoCr_2O_4$	$CoCr_2O_4$
SN-Cu0.5	$CoCr_2O_4$	$CoCr_2O_4$	$CoCr_2O_4$
SN-Cu0.75	$CuCr_2O_4$, Cu_2O	$CuCr_2O_4$, Cu_2O	$CuCr_2O_4$, Cu_2O
SN-Cu1	$CuCr_2O_4$, Cr_2O_3	$CuCr_2O_4$, Cr_2O_3	$CuCr_2O_4$, Cr_2O_3
SN-Zn0.25	$CoCr_2O_4$	$CoCr_2O_4$	$CoCr_2O_4$
SN-Zn0.5	$CoCr_2O_4$	$CoCr_2O_4$	$CoCr_2O_4$
SN-Zn0.75	$ZnCr_2O_4$	$ZnCr_2O_4$	$ZnCr_2O_4$
SN-Zn1	$ZnCr_2O_4$	$ZnCr_2O_4$	$ZnCr_2O_4$

As seen, the spinel structure of nickel chromite was not obtained at the temperature of 600 and 700 °C (Fig. 31a) for fully substituted compounds. The obtained samples were the mixtures of NiO (PDF 44-1159) and Cr_2O_3 oxides. In addition, all samples with x = 0.5 and 0.75 contain Cr_2O_3 as a secondary phase independent on the heating temperature. The tendency of formation of $Co_{1-x}Cu_xCr_2O_4$ powders is the same as during the sol-gel processing. The samples with substitution of x = 0.75 are composed of spinel as primary phase and Cu_2O as secondary phase (Fig. 31b). Fully substituted

compounds synthesised at 700 and 800 °C, unlike in the case of sol-gel synthesis, are not monophasic and contain Cr_2O_3 as an impurity phase. Only Zn-substituted samples analogously to the pigments produced by sol-gel synthesis method are single phase compounds.

However, sonochemically synthesised samples are distinguished for lower crystallite size than the ones prepared by sol-gel method. The estimated crystallite size of $CoCr_2O_4$ powders was 14.8, 24.5, and 31.6 nm, for the samples heated at 600, 700, and 800 °C, respectively. In the case of $Co_{1-x}Ni_xCr_2O_4$ samples, crystallite size varied in the ranges of 11.9–20.6 nm, 18.1–27.3 nm, and 28.0–35.0 nm for the samples annealed at 600, 700, and 800 °C, respectively. The crystallite size of $Co_{1-x}Cu_xCr_2O_4$ samples changed in the ranges of 11.8–21.1 nm, 16.0–30.4 nm, and 19.5–36.0 nm for the samples obtained at 600, 700, and 800 °C, respectively. For the $Co_{1-x}Zn_xCr_2O_4$ powders, the crystallite size altered in the ranges of 13.6–15.5 nm, 20.4–23.9 nm, and 29.7–32.6 nm for the samples heated at 600, 700, and 800 °C, respectively.

As it was mention before, for comparison a coprecipitation reaction was performed to obtain $Co_{1-x}M_xCr_2O_4$ ($M = Ni^{2+}$, Cu^{2+}, and Zn^{2+}; x = 0 and 0.5) powders, since ammonia caused spontaneous precipitation. The identified phases are summarised in Table 5.

Table 5. Phase composition of $Co_{1-x}M_xCr_2O_4$ pigments prepared by coprecipitation synthesis method (x = 0 and 0.5) at different annealing temperatures

Sample name	Identified phases at different temperatures		
	600 °C	700 °C	800 °C
PR-Co0	$CoCr_2O_4$	$CoCr_2O_4$	$CoCr_2O_4$
PR-Ni0.5	$CoCr_2O_4$, Cr_2O_3	$CoCr_2O_4$, Cr_2O_3	$NiCr_2O_4$, Cr_2O_3
PR-Cu0.5	$CuCr_2O_4$	$CuCr_2O_4$	$CuCr_2O_4$, $CoCr_2O_4$, $CoCo_2O_4$, ?
PR-Zn0.5	$CoCr_2O_4$	$CoCr_2O_4$	$CoCr_2O_4$

As it was expected, all non-substituted samples and Zn-doped ones obtained at different temperatures were single phase compounds. Similar to sonochemically derived $Co_{0.5}Ni_{0.5}Cr_2O_4$ powders, PR-Ni0.5 powders prepared at 600 and 700 °C were the mixtures of cubic cobalt chromite and chromium oxide phases. However, the primary phase at the highest temperature changed into cubic $NiCr_2O_4$. The intensity of characteristic peaks of secondary Cr_2O_3 phase decreased with the increasing of annealing temperature. Surprisingly, the determined crystalline phase of Cu-substituted samples at lower heating temperatures was cubic $CuCr_2O_4$ (PDF 26-0509). Nevertheless, the sample, obtained at the highest temperature contained even

four crystalline phases: cubic $CuCr_2O_4$ (PDF 26-0509) as a main phase, and cubic $CoCr_2O_4$ (PDF 35-1321), $CoCo_2O_4$ (PDF 80-1538), and an unidentified phase as impurities.

Estimated crystallite sizes of pigments were very similar to ones obtained sonochemically. Depending on the temperature the crystallite size varied from 16.1 to 31.6 nm, from 12.2 to 27.2 nm, from 12.5 to 27.1 nm, and from 11.9 to 27.2 nm for $CoCr_2O_4$, Ni-, Cu-, and Zn-doped samples, respectively.

Thermal analysis.

The thermal behaviour of the precursors obtained by sonochemical and coprecipitation synthesis methods was investigated for the selected samples (for both methods x = 0 and 0.5). The TG/DTG curves of Ni-substituted precursors are given in Fig. 32.

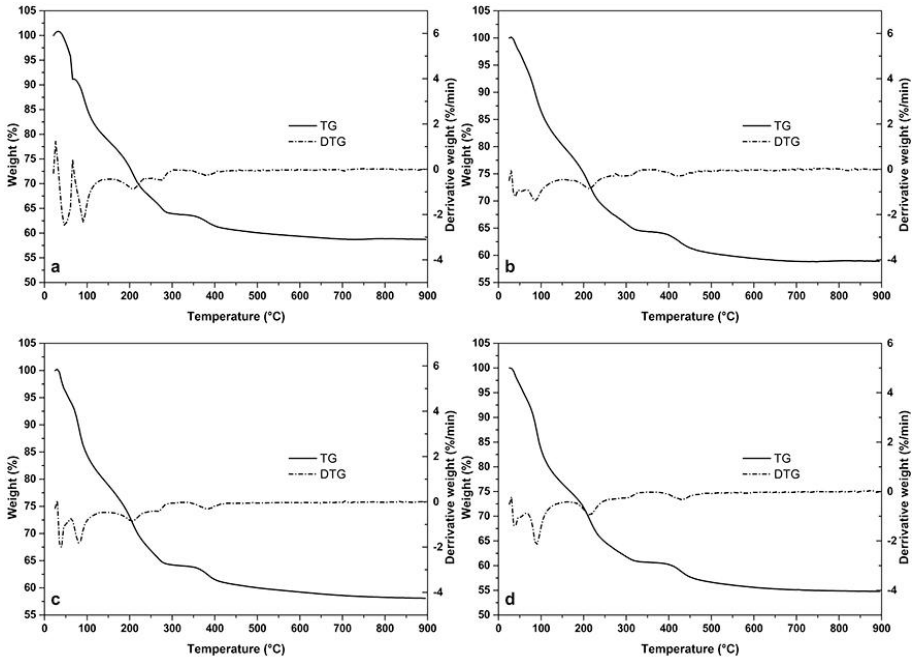

Figure 32. TG/DTG curves of Co-Ni-Cr-O precursors, obtained by sonochemical (a, b) and coprecipitation (c, d) synthesis methods. x = 0 (a, c) and x = 0.5 (b, d)

It is obvious, that TG/DTG curves of precursors obtained by sonochemical and coprecipitation synthesis methods are similar; however, drastically differ from the ones prepared by sol-gel method. The TG curves presented in Fig. 32 can be characterised in sloping manner and with lower weight loss (up to ~50 %). The dehydration and decomposition of

hydroxides occurs up to 150 °C and later the decomposition of nitrates and acetates takes place.

UV-Vis spectroscopy.

The UV-Vis diffuse reflectance results of pigments synthesised by sonochemical synthesis method given in Fig. 33 are very much alike to previously discussed results of sol-gel-obtained pigments.

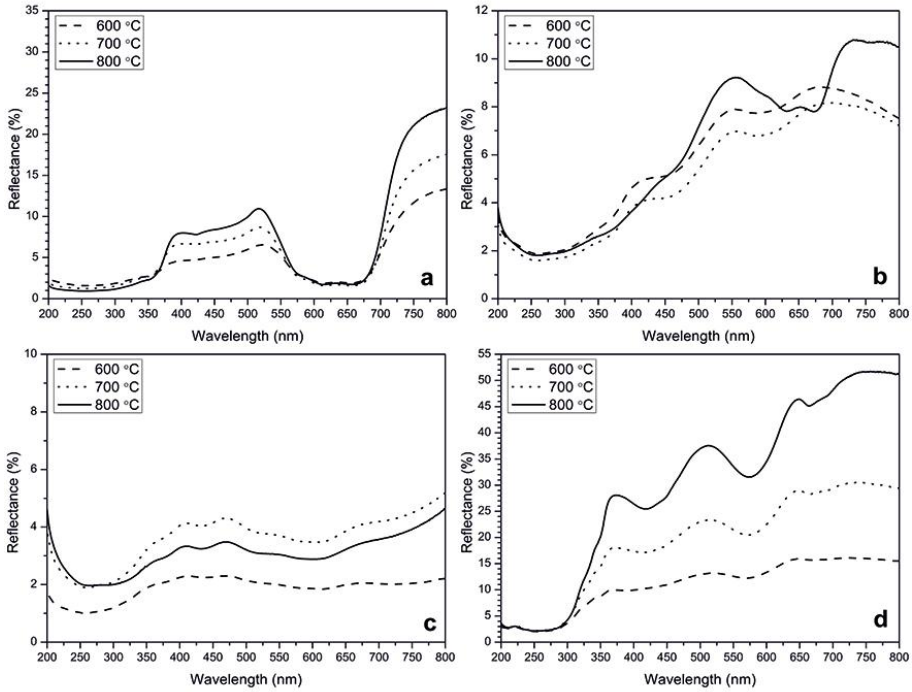

Figure 33. The diffuse reflectance spectra of sonochemically synthesised MCr_2O_4 samples at various heating temperatures, where the cation M^{2+} is: (a) – Co, (b) – Ni, (c) – Cu, and (d) – Zn

The main significant differences are in the cases of Ni- and Cu-containing samples (Fig. 33b and c), respectively. Ni-substituted samples calcined at 600 and 700 °C are the mixtures of NiO and Cr_2O_3, which may cause similar intensity of reflectance with samples heated at 800 °C (mixture of $NiCr_2O_4$ and Cr_2O_3 phases). All spectra of Cu-substituted pigments contain bands below 600 nm, which could be attributed to the secondary Cr_2O_3 phase. Almost no differences in the reflectance spectra of sol-gel and sonochemically obtained Co and Zn pigments were observed. The reflectance bands of sonochemically derived $CoCr_2O_4$ and $ZnCr_2O_4$ powders

are typical for these compounds and are nearly identical to the spectra of sol-gel powders.

3.2.3. Morphological and colourimetric characterisation of pigments and their corresponding glazes

According to the XRD results, the powders prepared by sol-gel method are more homogeneous than the ones obtained by sonochemical synthesis method. The phase composition, however, is very similar. Nevertheless, the morphology of synthesised pigments differs significantly.

Morphology.

SEM micrographs of sol-gel derived $CuCr_2O_4$ samples heated at 600–800 °C are shown in Fig. 34. As seen in Fig. 34a and b, the agglomerated plate-like crystals 200–400 nm in size covered with smaller particles have formed at lower temperatures (600–700 °C). However, the formation of fine particles with narrow size distribution (150–200 nm) at 800 °C is evident (Fig. 34c).

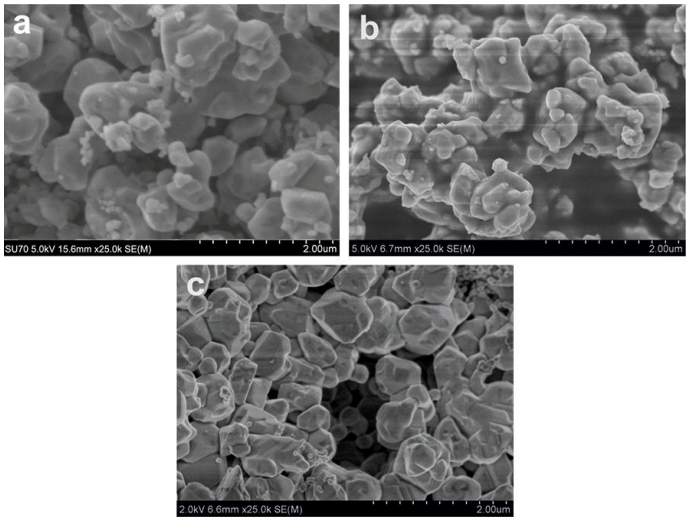

Figure 34. SEM micrographs of sol-gel derived $CuCr_2O_4$ samples heated at 600 °C (a), 700 °C (b), and 800 °C (c)

SEM micrographs of sonochemically derived $CuCr_2O_4$ samples heated at 600–800 °C are presented in Fig. 35. The chromite particles obtained at different temperatures showed almost identical morphology. The micrographs of $CuCr_2O_4$ samples fabricated at 600 and 700 °C show solids composed of spherically shaped particles with narrow particle size

distribution. The majority of particles have formed in nanometer size (less than 100 nm). The particles of $CuCr_2O_4$ samples heated at 800 °C are also agglomerated and show variation in size from 100 to 200 nm (Fig. 35c).

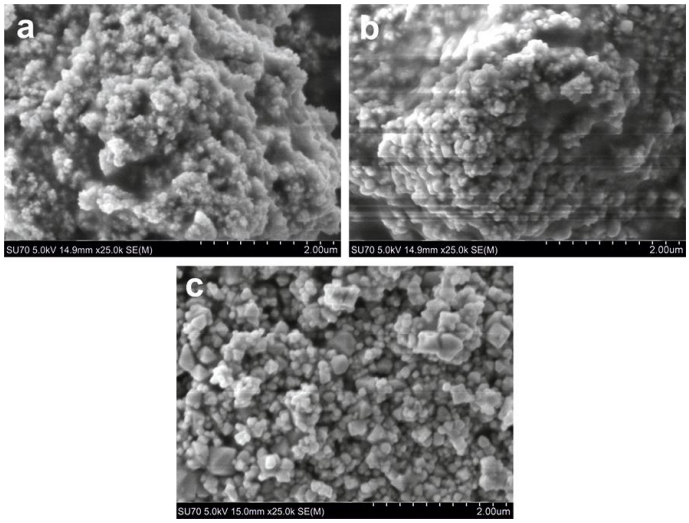

Figure 35. SEM micrographs of sonochemically derived $CuCr_2O_4$ samples heated at 600 °C (a), 700 °C (b), and 800 °C (c)

The size and shape of chromite particles depend not only on the used synthesis method, but also on the nature of the octahedral cation A^{2+}. Fig. 36 represents SEM images of sol-gel derived $CoCr_2O_4$, $NiCr_2O_4$, and $ZnCr_2O_4$ chromites heated at 800 °C. Surprisingly, the SEM micrographs of $CuCr_2O_4$, $CoCr_2O_4$, $NiCr_2O_4$, and $ZnCr_2O_4$ at 800 °C show different morphological features. Very small nano-sized spherical particles of $CoCr_2O_4$ have formed. However, differently shaped and bigger (150–200 nm) $NiCr_2O_4$ particles were obtained showing high degree of agglomeration. On the other hand, the microporous $ZnCr_2O_4$ solids have formed during the same sol-gel processing.

Fig. 37 represents SEM images of sonochemically derived $CoCr_2O_4$, $NiCr_2O_4$, and $ZnCr_2O_4$ chromites heated at 800 °C.

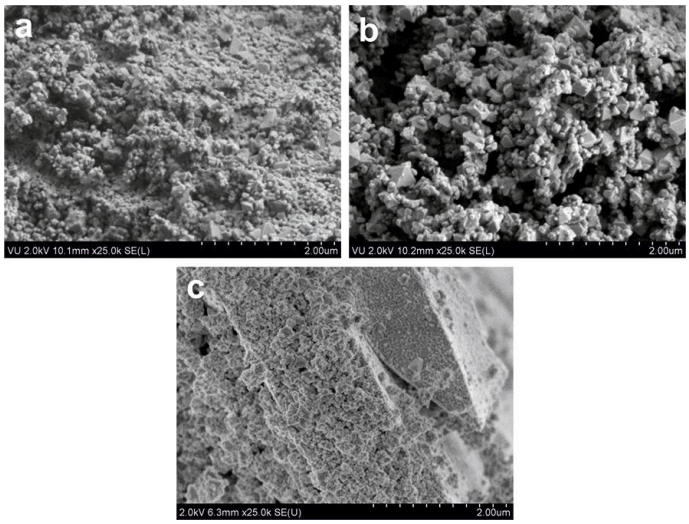

Figure 36. SEM micrographs of sol-gel derived pigments heated at 800 °C: (a) – $CoCr_2O_4$, (b) – $NiCr_2O_4$, and (c) – $ZnCr_2O_4$

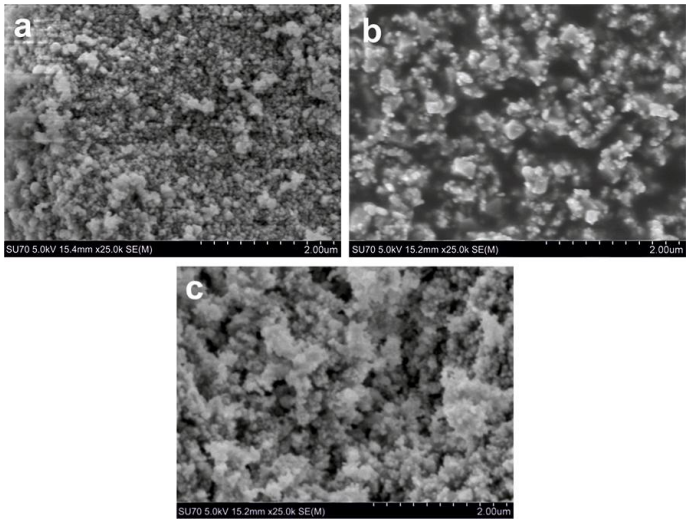

Figure 37. SEM micrographs of sonochemically derived pigments heated at 800 °C: (a) – $CoCr_2O_4$, (b) – $NiCr_2O_4$, and (c) – $ZnCr_2O_4$

As seen, the surface morphology of $NiCr_2O_4$ specimen is very similar to $CuCr_2O_4$ one, while SEM images of $CoCr_2O_4$ and $ZnCr_2O_4$ samples reveal slightly different microstructure. The obtained powders mostly consist of irregular shape sub-micron particles ranging from 110 nm to 0.5 μm in size. However, a few larger agglomerates having porous microstructure have formed as well. Unfortunately, all samples could not be characterised as

uniform in size and shape; any powder contains particles of slightly different form and size.

As it was mentioned before, sol-gel derived pigments annealed at 1000 °C were used to prepare both Pb-based and Pb-free ceramic glazes. Comparing the SEM images of the Pb-based glazes with distinct amount of the pigment (see Fig. 38), one could see that there were no big differences in morphology between more and less concentrated glazes.

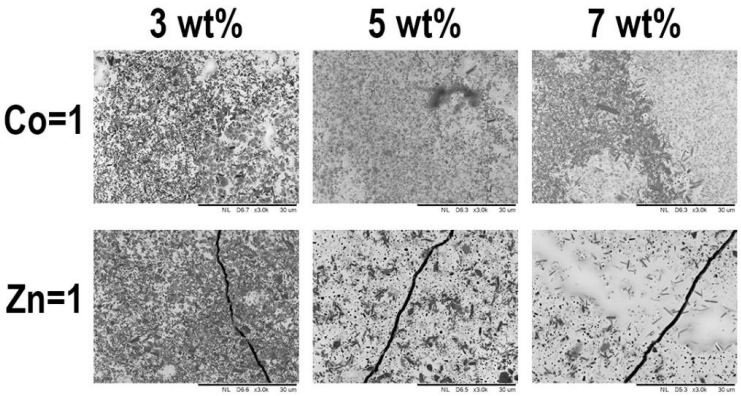

Figure 38. SEM micrographs of the Pb-based glazes with different amounts of $CoCr_2O_4$ and $ZnCr_2O_4$ pigments

The morphology of all prepared Pb-free glazes was very similar. The representative SEM micrograph of ceramic glaze with $ZnCr_2O_4$ pigment is given in Fig. 39.

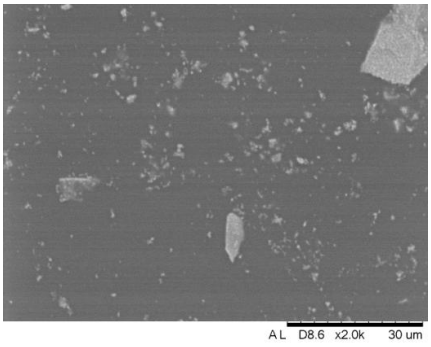

Figure 39. SEM micrograph of base (Pb-free) ceramic glaze with $ZnCr_2O_4$ pigment

Colourimetry.

The general tendency of increasing the lightness (L^*) with increasing of the heating temperature is obvious for the $CoCr_2O_4$ samples (Table 6).

Table 6. CIELab colourimetric parameters of sol-gel and sonochemically synthesised at different temperatures $CoCr_2O_4$ pigments

Sample	*L**	*a**	*b**	Sample	*L**	*a**	*b**
SG-Co0-600	43.43	-6.03	-3.08	**SN-Co0-600**	39.39	-5.43	-2.70
SG-Co0-700	46.70	-10.01	-4.74	**SN-Co0-700**	43.91	-10.50	-6.19
SG-Co0-800	48.23	-12.88	-4.17	**SN-Co0-800**	49.39	-16.07	-8.37

According to the UV-Vis diffuse reflectance results, all these samples are characterised by negative values of colourimetric parameters *a** and *b**, corresponding to the bluish green colour. The much higher negative values of parameter *a** than parameter *b** could be caused by superposition transitions of Cr^{3+} ion in UV-Vis diffuse reflectance spectra [80]. Interestingly, the higher heating temperature was used, the deeper and lighter green and blue hues were obtained.

The negative *a** values were determined for Ni-substituted $Co_{1-x}Ni_xCr_2O_4$ samples synthesised by both sol-gel and sonochemically methods (see Table 7). The parameter *b** showed a tendency to increase with increasing amount of Ni, giving warm green colours for the pigments. The progressive doping by Ni^{2+} ion, however, provides scattered results of parameter *L**. Nevertheless, the samples obtained at higher temperatures having the same substitution level are lighter. This can be also clearly seen from the photographs of pigments presented in Fig. 40.

Table 7. CIELab colourimetric parameters of sol-gel and sonochemically synthesised at different temperatures $Co_{1-x}Ni_xCr_2O_4$ (x = 0.25; 0.5; 0.75; and 1) pigments

Sample	*L**	*a**	*b**	Sample	*L**	*a**	*b**
SG-Ni0.25-600	42.03	-4.68	-2.03	**SN-Ni0.25-600**	38.67	-3.89	-2.37
SG-Ni0.5-600	42.89	-4.87	-1.05	**SN-Ni0.5-600**	40.26	-4.13	-1.42
SG-Ni0.75-600	43.23	-3.41	0.75	**SN-Ni0.75-600**	41.06	-2.55	-0.05
SG-Ni1-600	41.60	-1.09	0.13	**SN-Ni1-600**	43.71	-0.77	3.04
SG-Ni0.25-700	46.44	-8.49	-2.78	**SN-Ni0.25-700**	42.44	-7.79	-5.02
SG-Ni0.5-700	47.04	-8.90	-0.23	**SN-Ni0.5-700**	44.51	-7.63	-2.66
SG-Ni0.75-700	45.23	-4.78	1.52	**SN-Ni0.75-700**	42.63	-3.60	-0.24
SG-Ni1-700	43.95	-1.51	1.90	**SN-Ni1-700**	44.61	-0.69	4.00
SG-Ni0.25-800	49.15	-12.55	-3.48	**SN-Ni0.25-800**	48.57	-13.63	-5.88
SG-Ni0.5-800	49.57	-12.11	0.29	**SN-Ni0.5-800**	48.49	-10.28	-1.20
SG-Ni0.75-800	47.36	-6.67	2.28	**SN-Ni0.75-800**	46.51	-6.41	0.95
SG-Ni1-800	46.84	-4.00	5.60	**SN-Ni1-800**	47.28	-2.79	6.08

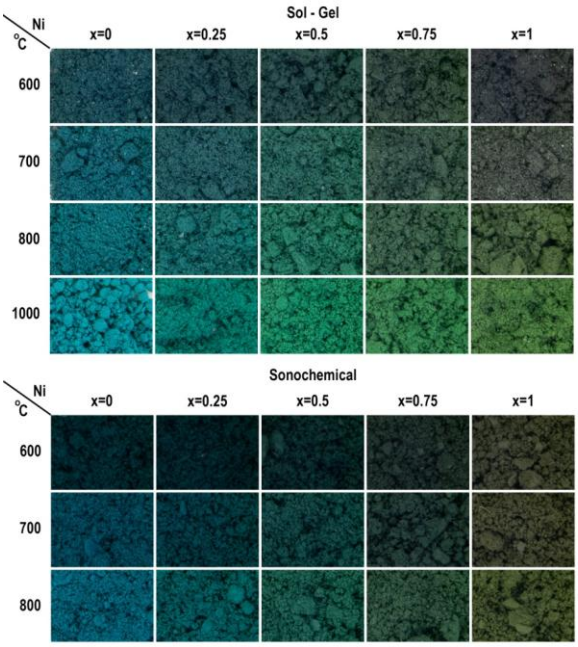

Figure 40. Photographs of $Co_{1-x}Ni_xCr_2O_4$ pigments produced by sol-gel and sonochemical synthesis methods and heated at various temperatures

The darkest samples are black Cu-doped $Co_{1-x}Cu_xCr_2O_4$ powders (Fig. 41). For both synthesis methods blue shades are stronger than green shades (Table 8), which is also noticeable with the naked eye for x = 0.25 and 0.5. In agreement with the diffuse reflectance spectra, sonochemically synthesised pigments (when x = 1 at 600 and 700 °C, and x = 0.25; 0.5; 0.75; and 1 at 800 °C) are slightly lighter than sol-gel derived pigments.

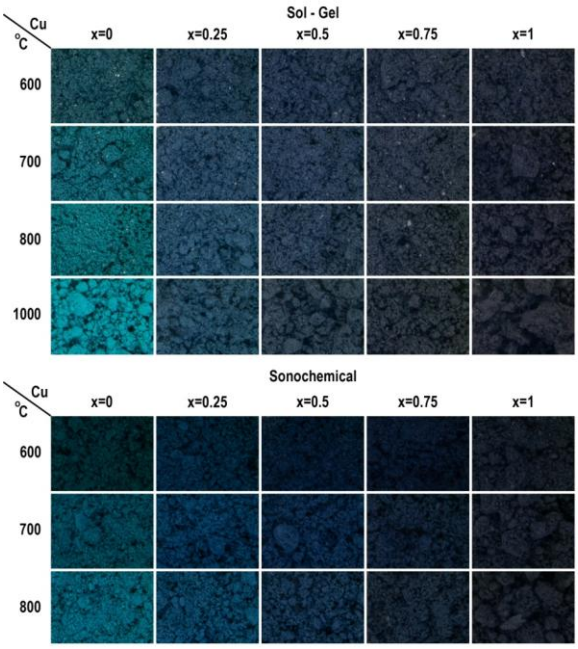

Figure 41. Photographs of $Co_{1-x}Cu_xCr_2O_4$ pigments produced by sol-gel and sonochemical synthesis methods and heated at various temperatures

Table 8. CIELab colourimetric parameters of sol-gel and sonochemically synthesised at different temperatures $Co_{1-x}Cu_xCr_2O_4$ (x = 0.25; 0.5; 0.75; and 1) pigments

Sample	*L**	*a**	*b**	Sample	*L**	*a**	*b**
SG-Cu0.25-600	41.53	-2.98	-4.36	**SN-Cu0.25-600**	39.63	-3.25	-5.18
SG-Cu0.5-600	41.12	-1.79	-4.09	**SN-Cu0.5-600**	38.33	-1.41	-4.34
SG-Cu0.75-600	40.45	-1.06	-3.02	**SN-Cu0.75-600**	38.37	-0.89	-3.77
SG-Cu1-600	39.22	-0.25	-1.82	**SN-Cu1-600**	39.92	-0.55	-2.12
SG-Cu0.25-700	42.95	-5.18	-6.65	**SN-Cu0.25-700**	42.69	-4.61	-8.12
SG-Cu0.5-700	41.97	-3.67	-5.55	**SN-Cu0.5-700**	41.01	-2.10	-6.00
SG-Cu0.75-700	40.57	-1.60	-3.16	**SN-Cu0.75-700**	40.29	-1.33	-4.07
SG-Cu1-700	38.57	-0.39	-1.93	**SN-Cu1-700**	40.37	-0.44	-2.21
SG-Cu0.25-800	44.03	-6.27	-7.69	**SN-Cu0.25-800**	46.01	-5.75	-8.33
SG-Cu0.5-800	42.26	-3.46	-4.66	**SN-Cu0.5-800**	43.47	-2.86	-5.98
SG-Cu0.75-800	40.48	-1.41	-2.59	**SN-Cu0.75-800**	41.44	-1.52	-3.35
SG-Cu1-800	38.89	-0.29	-1.60	**SN-Cu1-800**	40.16	-0.29	-1.85

The most evident changes of colours can be achieved by the progressive substitution of Co^{2+} ions by Zn^{2+} (Fig. 42). The colourimetric parameters of $Co_{1-x}Zn_xCr_2O_4$ pigments obtained by both synthesis methods are summarised in Table 9. The gradual substitution results in an increase of the lightness *L**,

reaching the maximum value of 61.71 for the sol-gel and 68.13 for sonochemically synthesised (both heated at 800 °C) pigments, which is in a good agreement with the UV-Vis reflectance spectra. The increase of coordinate *b** value confirms the intensification of the yellow hue. Up to x = 0.75, the various green colours of the samples are evident in agreement with negative values of parameter *a**. However, at the highest content of Zn^{2+} ion (x = 1), the pigments turn to yellowish green and bluish shade is not so evident anymore. Moreover, powder series, obtained at the highest heating temperature, are the lightest ones for all types of A^{2+} ion substitution.

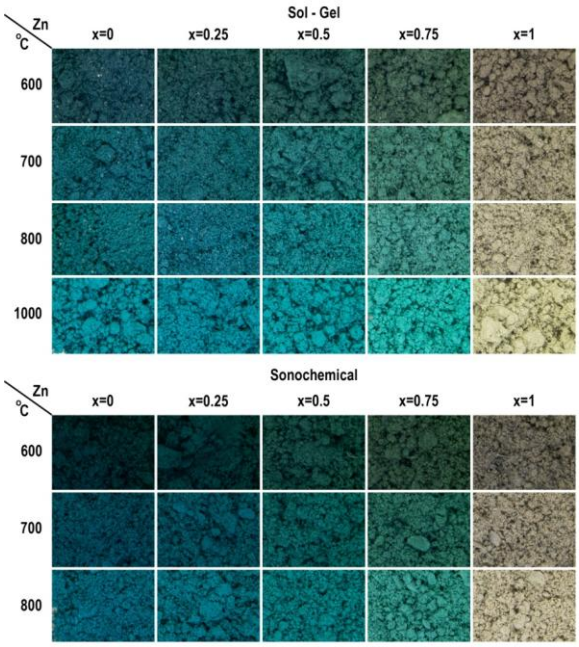

Figure 42. Photographs of $Co_{1-x}Zn_xCr_2O_4$ pigments produced by sol-gel and sonochemical synthesis methods and heated at various temperatures

Table 9. CIELab colourimetric parameters of sol-gel and sonochemically synthesised at different temperatures $Co_{1-x}Zn_xCr_2O_4$ (x = 0.25; 0.5; 0.75; and 1) pigments

Sample	*L**	*a**	*b**	Sample	*L**	*a**	*b**
SG-Zn0.25-600	43.61	-6.67	-1.68	**SN-Zn0.25-600**	40.74	-6.03	-2.37
SG-Zn0.5-600	44.71	-6.85	-0.63	**SN-Zn0.5-600**	43.16	-6.74	-0.97
SG-Zn0.75-600	45.31	-5.10	1.16	**SN-Zn0.75-600**	43.91	-5.16	0.50
SG-Zn1-600	48.74	0.20	3.24	**SN-Zn1-600**	48.84	-0.49	0.99
SG-Zn0.25-700	47.24	-10.16	-4.17	**SN-Zn0.25-700**	45.45	-10.68	-5.23
SG-Zn0.5-700	49.05	-11.34	-3.56	**SN-Zn0.5-700**	47.38	-11.56	-3.67
SG-Zn0.75-700	51.05	-9.60	-0.42	**SN-Zn0.75-700**	47.15	-10.04	-4.07
SG-Zn1-700	56.59	-1.09	3.97	**SN-Zn1-700**	57.63	1.07	1.97
SG-Zn0.25-800	49.28	-12.30	-5.37	**SN-Zn0.25-800**	52.04	-17.05	7.81
SG-Zn0.5-800	52.41	-14.83	-4.79	**SN-Zn0.5-800**	54.49	-17.81	-6.29
SG-Zn0.75-800	55.18	-13.37	-1.95	**SN-Zn0.75-800**	57.35	-16.10	-3.08
SG-Zn1-800	61.71	-2.27	4.63	**SN-Zn1-800**	68.13	-1.98	4.58

Pb-based ceramic glazes were prepared using different amount of the pigments. For comparison, the colourimetric results only for the glazes fabricated with fully substituted pigments are given. Unfortunately, the colourimetric analysis of the glazes was not very precise. The obtained glazes, depending on the concentration of the pigment, were not monochromatic. The patchiness of the surfaces led to incorrect results, since the measurements are taken not from the whole surface (see Table 10).

Table 10. CIELab colourimetric parameters of Pb-based ceramic glazes with different amounts of sol-gel derived MCr_2O_4 (M = Co^{2+}, Ni^{2+}, Cu^{2+}, and Zn^{2+}) pigments

Pigment		*L**	*a**	*b**
Formula	wt%			
	3	38.17	1.79	6.49
$CoCr_2O_4$	5	37.36	0.79	5.60
	7	35.18	–0.31	–0.49
	3	37.30	3.74	4.67
$NiCr_2O_4$	5	35.60	2.34	1.22
	7	35.07	1.21	–0.46
	3	36.99	1.92	5.64
$CuCr_2O_4$	5	36.64	0.59	0.94
	7	34.09	0.04	–0.68
	3	40.94	10.94	10.06
$ZnCr_2O_4$	5	38.80	7.49	4.49
	7	39.85	8.81	6.11

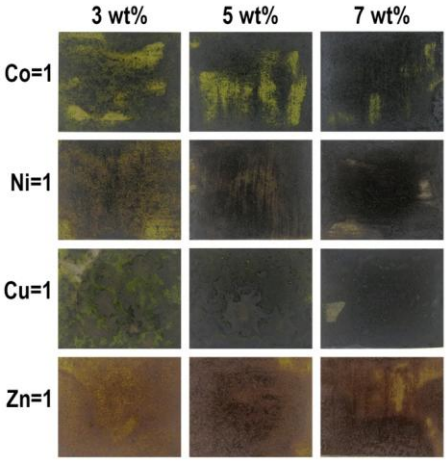

Figure 43. Digital photographs of Pb-based ceramic glazes with different amount of sol-gel derived MCr_2O_4 (M = Co^{2+}, Ni^{2+}, Cu^{2+}, and Zn^{2+}) pigments

According to the results, the dominant colour for all the samples is medium dark shade of brown or grey, although visually glazes have more green colour (see Fig. 43).

The chromatic coordinates of selected samples of lead-free ceramic glazes are given in Table 11.

Table 11. CIELab colourimetric parameters of Pb-free ceramic glazes with sol-gel derived MCr_2O_4 (M = Co^{2+}, Ni^{2+}, Cu^{2+}, and Zn^{2+}) pigments

Sample	*L**	*a**	*b**
$CoCr_2O_4$	42.29	–0.76	–2.25
$NiCr_2O_4$	33.42	–4.63	1.04
$CuCr_2O_4$	38.15	2.90	–1.92
$ZnCr_2O_4$	50.34	–1.18	6.31

The given results showed that parameter *a** for all ceramic glazes, except the one with $CuCr_2O_4$ pigment, had negative values giving greenish hue. However, the obtained ceramic glazes were non-monochromic as well (see Fig. 44), leading to contradictory results. On the other hand, the patchiness of the glazes might be considered as useful artistic feature.

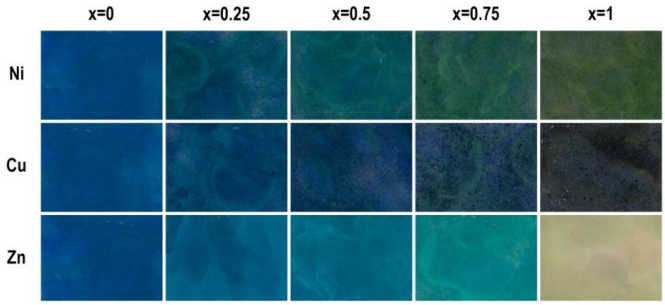

Figure 44. Photographs of Pb-free ceramic glazes with sol-gel derived $Co_{1-x}M_xCr_2O_4$ (x = 0.25; 0.5; 0.75; and 1) pigments

3.3. Sol-gel synthesis and characterisation of $CoCr_{2-x}Ln_xO_4$ pigments and glazes

In this part of dissertation $CoCr_{2-x}Ln_xO_4$ (Ln = Tm^{3+} and Yb^{3+}) pigments with different substitutional level of lanthanide (x = 0–0.5) were synthesised. The phase composition, crystallite size, morphological features and colour parameters of new compositions were investigated.

XRD analysis.

X-ray diffraction patterns of Tm-substituted $CoCr_{2-x}Tm_xO_4$ (x = 0.1–0.5) powdered samples, depending on the substitution ratio and heating temperature, are given in Fig. 45.

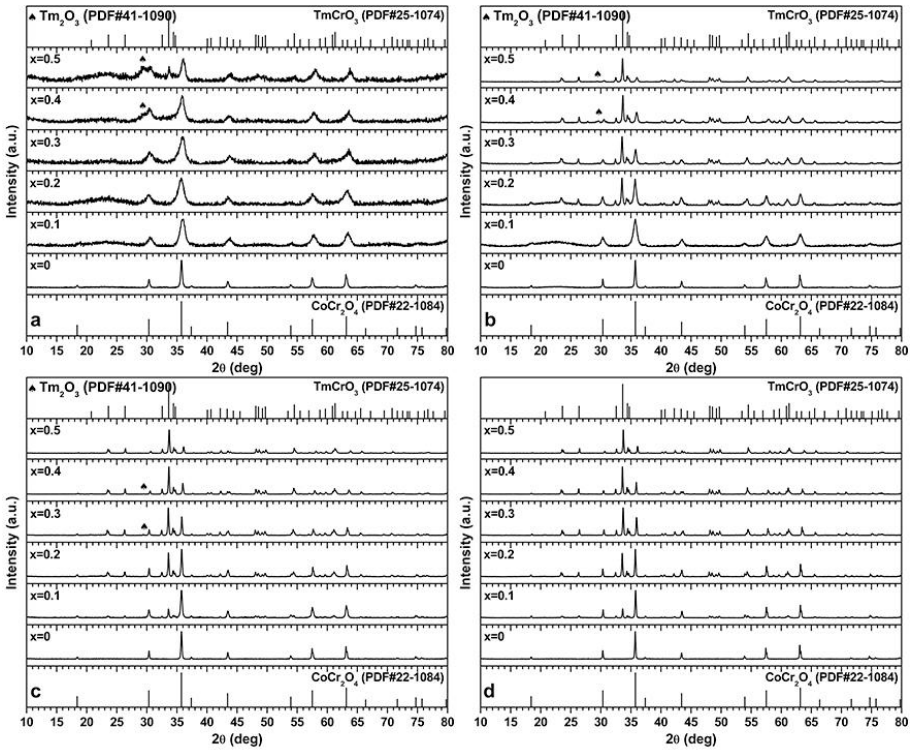

Figure 45. XRD patterns of $CoCr_{2-x}Tm_xO_4$ powders (x = 0–0.5) calcined at 700 °C (a) and annealed at 800 °C (b), 900 °C (c), and 1000 °C (d)

Phase composition analysis revealed that the chromium substitution by thulium in the spinel crystal structure is problematic. The formation of perovskite thulium chromite $TmCrO_3$ (PDF 25-1074, orthorhombic *P*bnm) phase along with spinel $CoCr_2O_4$ (PDF 22-1084, cubic $Fd\bar{3}m$ space group) phase was detected in all of the cases. However, the spinel as the main crystalline phase has formed in powders obtained at 700 °C (see Fig. 45a) and with the lowest substitutional amount by thulium ($x \leq 0.2$) at higher temperatures (see Fig. 45b–d). The perovskite was predominant phase in the samples with $x > 0.2$ for the samples, obtained at 800–1000 °C. Moreover, several samples obtained at 700–900 °C contained additional Tm_2O_3 phase (PDF 41-1090, cubic I*a*3).

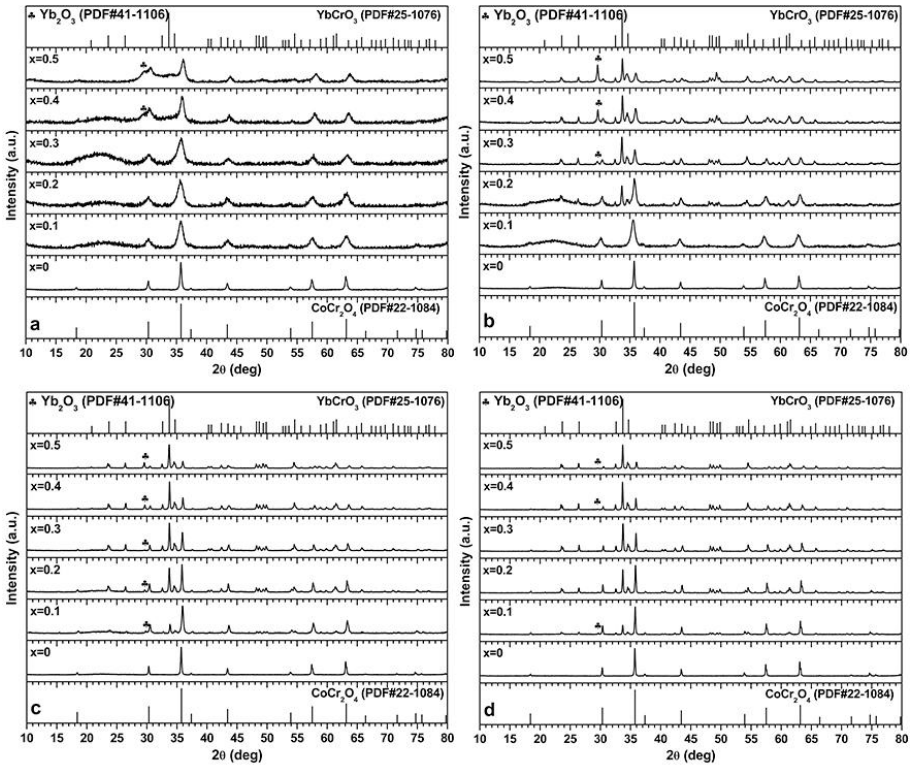

Figure 46. XRD patterns of $CoCr_{2-x}Yb_xO_4$ powders (x = 0–0.5) calcined at 700 °C (a) and annealed at 800 °C (b), 900 °C (c), and 1000 °C (d)

The similar situation was observed during the synthesis of ytterbium-substituted samples. The XRD patterns of $CoCr_{2-x}Yb_xO_4$ (x = 0.1–0.5) specimens are shown in Fig. 46. Together with spinel $CoCr_2O_4$ and perovskite ytterbium chromite $YbCrO_3$ (PDF 25-1076, orthorhombic *P*bnm) crystalline phases, however, the different amounts of Yb_2O_3 phase (PDF 41-1106, cubic I*a*3) was also observed in some cases depending on the heating temperature. Again, in the samples with lower substitutional level ($x \leq 0.2$) annealed at 800–1000 °C (see Fig. 46b–d) and in the samples heated at the lowest temperature (see Fig. 46a) the dominant phase was cobalt chromium spinel, and the main phase of perovskite ytterbium chromite was in the samples when $x > 0.2$ (Fig. 46b–d). The increase of intensity of reflections attributable to the perovskite phase and the decrease of spinel phase with the increasing amount of lanthanide ions was well distinguished for all syntheses.

Interestingly, the gradual slight shifting of the spinel phase reflections to higher angles is observed with the increasing amount of lanthanide in both $CoCr_{2-x}Tm_xO_4$ and $CoCr_{2-x}Yb_xO_4$ series of compounds. For the Tm- and Yb-

substituted samples (when x = 0.5) obtained at 1000 °C the most intense peak shifts over 0.39 and 0.28 2θ degrees, respectively. The estimated crystallite size for the samples obtained at the highest temperature varied in the range of 51.5–61.5 nm and 37.7–57.6 nm for Tm-substituted and Yb-substituted samples, respectively (see Table 12).

Table 12. The lattice constants and estimated crystallite sizes of the spinel phase in $CoCr_{2-x}Tm_xO_4$ and $CoCr_{2-x}Yb_xO_4$ samples

Amount of Tm (x)	*a* (Å) (±0.0003)	Crystallite size (nm)	Amount of Yb (x)	*a* (Å) (±0.0003)	Crystallite size (nm)
0	8.3206	51.49	0	8.3209	51.49
0.1	8.3086	51.53	0.1	8.3105	54.39
0.2	8.3006	54.37	0.2	8.2940	57.64
0.3	8.2814	51.64	0.3	8.2815	37.72
0.4	8.2588	57.68	0.4	8.2620	54.48
0.5	8.2370	61.45	0.5	8.2392	51.67

The cell parameters of these powders decreased with the increasing the amount of lanthanide ions confirming the existence of lanthanide ions, at least very negligible amount, in the spinel phase. For the same samples, the crystallite size of perovskite phase ranged from 50.3 to 56.1 nm ($TmCrO_3$) and from 50.3 to 56.2 nm ($YbCrO_3$). These results are presented in Table 13. Unfortunately, no correlation or linear dependence of crystallite size on the substitutional level for was observed.

Since the lanthanide ion substitution in $CoCr_{2-x}Ln_xO_4$ at high concentrations of substituents is problematic, additional sol-gel syntheses of $CoCr_{2-x}Tm_xO_4$ and $CoCr_{2-x}Yb_xO_4$ with lower amount of lanthanides (x = 0.01; 0.02; 0.03; 0.04 and 0.05) were performed. The XRD patterns revealed that $CoCr_{2-x}Tm_xO_4$ samples with the main crystalline spinel phase were obtained (see Fig. 47). However, insignificant amount of Cr_2O_3 was observed in the samples with x = 0.03, obtained at 700–900 °C. Moreover, minor amount of thulium perovskite phase has formed for the compositions with x = 0.05 heated at 900 and 1000 °C (Fig. 47c and d).

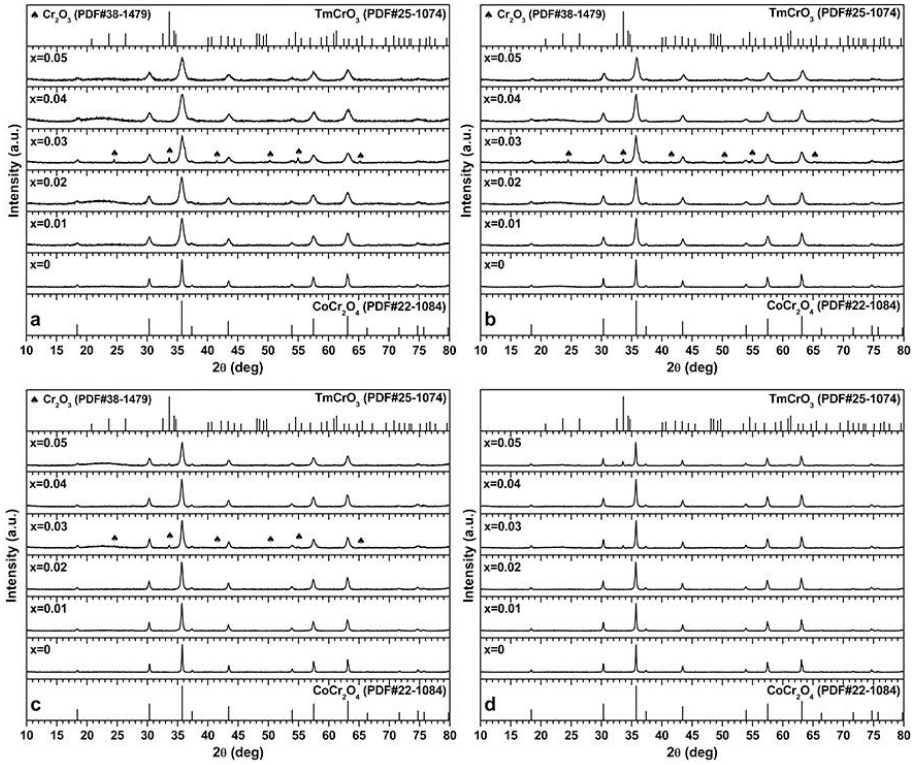

Figure 47. XRD patterns of $CoCr_{2-x}Tm_xO_4$ powders (x = 0–0.05) calcined at 700 °C (a) and annealed at 800 °C (b), 900 °C (c), and 1000 °C (d)

XRD patterns of $CoCr_{2-x}Yb_xO_4$ samples having lower amount of ytterbium are shown in Fig. 48. As seen, the XRD results confirmed the formation of the spinel as the main crystalline phase for all the compositions. Again, minor amount of ytterbium chromite as side phase has formed only at higher concentration of Yb for the samples annealed at 900 and 1000 °C (Fig. 48c and d). Furthermore, the impurity of ytterbium oxide was not detected in all cases.

Table 13. The lattice constants and estimated crystallite sizes of the perovskite phase in $CoCr_{2-x}Tm_xO_4$ and $CoCr_{2-x}Yb_xO_4$ samples

Amount of	Lattice constant (Å)			Crystallite	Amount of	Lattice constant (Å)			Crystallite
Tm (x)	*a* (±0.0003)	*b* (±0.0003)	*c* (±0.0004)	size (nm)	Yb (x)	*a* (±0.0003)	*b* (±0.0003)	*c* (±0.0005)	size (nm)
0.1	5.2024	5.4932	7.4903	56.12	0.1	5.1881	5.4880	7.4746	50.26
0.2	5.2031	5.4962	7.4904	52.96	0.2	5.1820	5.4856	7.4670	53.06
0.3	5.1978	5.4916	7.4814	53.05	0.3	5.1801	5.4859	7.4649	53.08
0.4	5.1920	5.4877	7.4732	56.10	0.4	5.1758	5.4833	7.4573	56.16
0.5	5.1880	5.4835	7.4662	50.27	0.5	5.1704	5.4790	7.4483	56.18

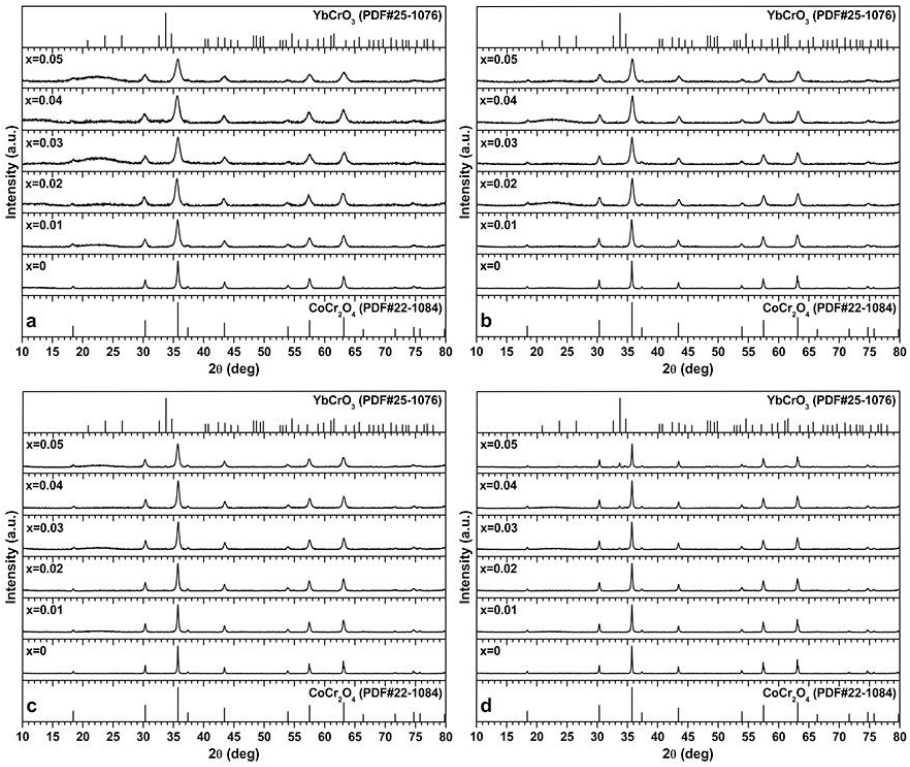

Figure 48. XRD patterns of $CoCr_{2-x}Yb_xO_4$ powders (x = 0–0.05) calcined at 700 °C (a) and annealed at 800 °C (b), 900 °C (c), and 1000 °C (d)

The estimated crystallite size of the main spinel phase for all compositions (x = 0–0.05) obtained at 1000 °C ranged nonlinearly from 32.61 to 51.51 nm in Tm-substituted samples and from 37.62 to 54.35 nm in Yb-substituted samples.

XPS analysis.

The XPS measurements were performed to investigate the oxidation states of cobalt, by studying the Co2p core level peaks of the six Tm- and Yb-substituted $CoCr_{2-x}Ln_xO_4$ samples with x = 0.1, 0.3 and 0.5. The Co2p XPS spectra are presented in Fig. 49.

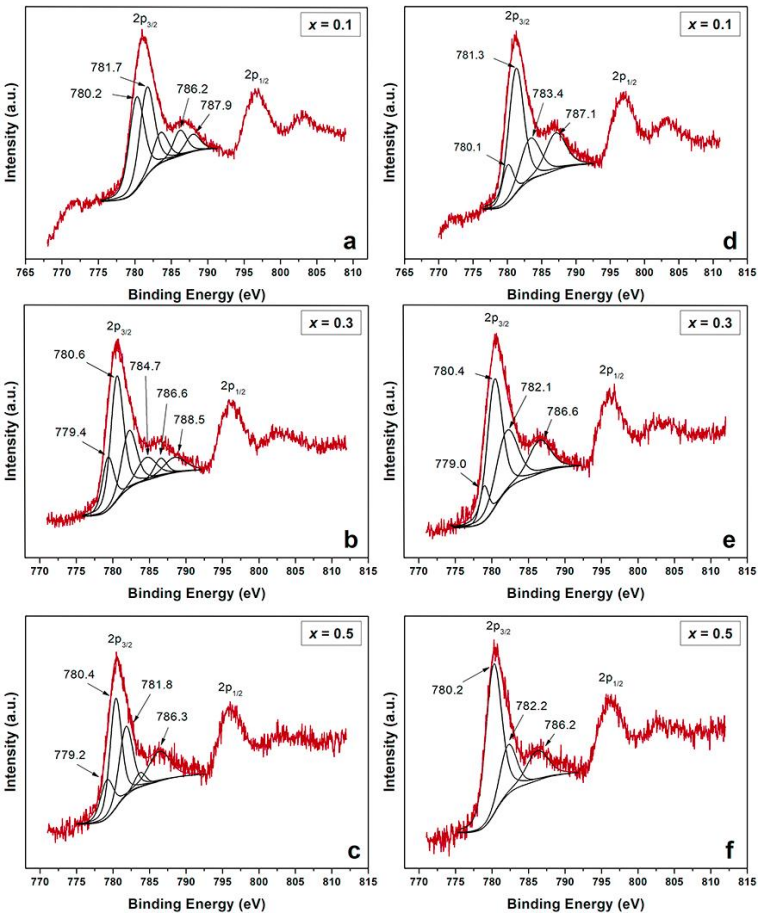

Figure 49. XPS Co2p core level spectra of $CoCr_{2-x}Tm_xO_4$ (a–c) and $CoCr_{2-x}Yb_xO_4$ (d–f) samples sintered at 700 °C

The peak at binding energy BE = 780.0–780.6 eV could be attributed to CoO and at BE = 781.3–782.2 eV to $Co(OH)_2$ [121] in all cases. According to the literature, the peak at around 779.4 eV may be attributed to Co^{3+} cations [80, 122]. Namely, these peaks were observed for the Tm-substituted samples with high amount of thulium at 779.4 eV (x = 0.3; Fig. 49b) and at 779.2 eV (x = 0.5; Fig. 49c). Therefore, the partial intercalation of Co^{3+} ion into position of Cr^{3+} at octahedral sites could be confirmed [80]. The assumption of formation of lanthanide-containing $CoCo_2O_4$ phase during the synthesis of $CoCr_{2-x}Ln_xO_4$ (x = 0.1–0.5) powders was refused with reference to Rietveld refinement calculations. However, XPS analysis showed that Co(II) is the main oxidation state of cobalt in these mixed-metal oxides. The XPS spectra of Yb-substituted $CoCr_{2-x}Yb_xO_4$ samples (Fig. 49d–f) did not reveal peaks of trivalent cobalt, which could annotate the XRD results.

Morphological and colourimetric characterisation.

The morphology of the sintered pigments and their corresponding glazes was investigated by SEM method. The SEM micrographs of $CoCr_{2-x}Tm_xO_4$ and $CoCr_{2-x}Yb_xO_4$ pigments are shown in Fig. 50.

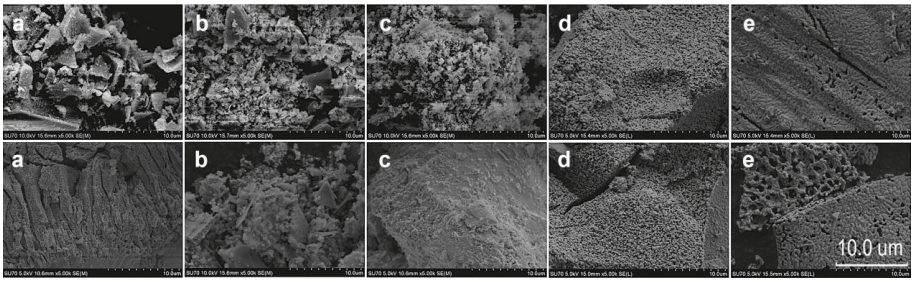

Figure 50. SEM micrographs of sol-gel derived $CoCr_{2-x}Tm_xO_4$ (top) and $CoCr_{2-x}Yb_xO_4$ (bottom) pigments with different substitution ratio of lanthanide: a) x = 0; b) x = 0.01; c) x = 0.05; d) x = 0.1 and e) x = 0.5

At the low lanthanide substitutional level the surface of synthesised pigments is composed of irregularly shaped particles which are highly agglomerated. However, with increasing the amount of Tm and Yb the spherically shaped particles with uniform size distribution have formed. Moreover, the SEM micrographs of the samples revealed porous microstructure of the samples. The representative SEM micrographs of the ceramic glazes obtained using sol-gel derived pigments $CoCr_{2-x}Tm_xO_4$ and $CoCr_{2-x}Yb_xO_4$ with x = 0.5 are presented in Fig. 51.

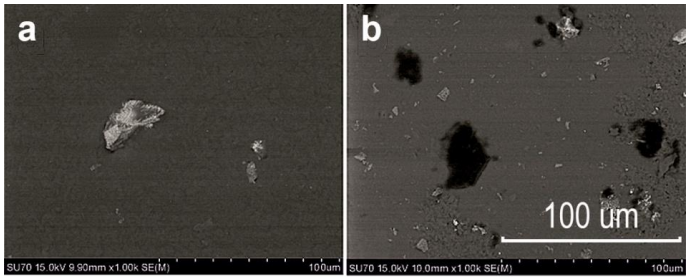

Figure 51. SEM micrographs of the glazes prepared using $CoCr_{1.5}Tm_{0.5}O_4$ (a) and $CoCr_{1.5}Yb_{0.5}O_4$ (b) pigments

It is clearly seen, that the pigment powders in the ceramic glazes are well dispersed over ceramic tiles. No cracks, caves or other physical defects could be observed on the surface of ceramic glazes.

The colourimetric parameters of the pigments $CoCr_{2-x}Ln_xO_4$ (x = 0; 0.01; 0.03; 0.05; 0.1; 0.3 and 0.5) obtained at 1000 °C are summarised in Table 14.

Table 14. CIELab colourimetric parameters of $CoCr_{2-x}Tm_xO_4$ and $CoCr_{2-x}Yb_xO_4$ powders prepared at 1000 °C

Amount of Tm (x)	*L**	*a**	*b**	Amount of Yb (x)	*L**	*a**	*b**
0	52.38	-21.01	-9.03	0	52.42	-21.28	-9.36
0.01	49.97	-14.97	-5.97	0.01	50.25	-16.14	-6.33
0.03	49.31	-15.04	-5.08	0.03	48.65	-13.17	-3.19
0.05	48.47	-12.56	-3.39	0.05	47.31	-4.83	3.15
0.1	44.25	-5.48	0.63	0.1	44.55	-6.58	0.67
0.3	41.86	-0.98	0.73	0.3	43.14	-0.59	-0.11
0.5	42.45	-0.02	-0.29	0.5	43.55	-0.03	-0.42

It is evident that the lightness (*L**) of the pigments is gradually dropping with increasing the Ln^{3+} content, while the progressive increase for parameters *a** and *b** is also observed. Similar values of the parameters *a** and *b** for the pigments with the highest substitutional levels provide brownish tone.

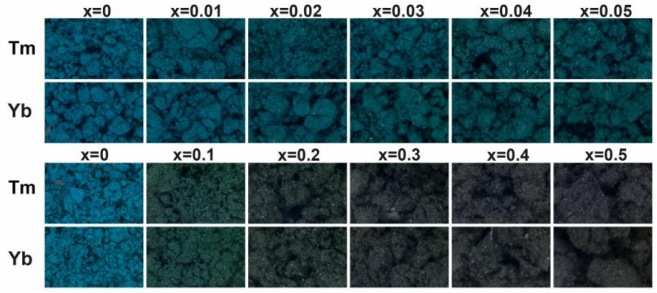

Figure 52. Digital photographs of $CoCr_{2-x}Tm_xO_4$ and $CoCr_{2-x}Yb_xO_4$ pigments obtained at 1000 °C

Fig. 52 displays the colours of the pigments obtained at 1000 °C with all compositions. As it can be seen, the colours of the pigments with lower amount of lanthanides (x = 0–0.05) are very much alike to each other, confirming the CIELab results. The greenest pigments from the higher composition powders are x = 0.1 substituted ones, and the rest of the pigments have gradual brown tone.

The colourimetric parameters of the glazes prepared using sol-gel derived $CoCr_{2-x}Ln_xO_4$ (x = 0; 0.01; 0.03; 0.05; 0.1; 0.3; and 0.5) pigments are presented in Table 15.

Table 15. CIELab colourimetric parameters of the glazes obtained using $CoCr_{2-x}Tm_xO_4$ and $CoCr_{2-x}Yb_xO_4$ pigments

Amount of Tm (x)	*L**	*a**	*b**	Amount of Yb (x)	*L**	*a**	*b**
0	37.06	-16.33	-10.23	0	34.38	-14.12	-10.27
0.01	34.74	-12.51	-8.23	0.01	34.36	-11.80	-8.69
0.03	33.21	-12.29	-8.14	0.03	33.34	-11.78	-8.06
0.05	34.65	-12.44	-7.27	0.05	34.75	-12.24	-7.27
0.1	30.98	-7.54	-4.49	0.1	31.03	-6.34	-5.29
0.3	29.13	-2.06	-1.49	0.3	30.02	-2.29	0.18
0.5	29.87	-0.92	-0.02	0.5	29.58	-1.27	1.36

Obviously, the obtained results reveal analogous behaviour. The *L** values of the both type of glazes, when x = 0.05 are aberrant due to the preparation of glazes, when the milky film of the components of the base glaze was formed onto the top of the ceramic glaze. The colourimetric parameters *a** and *b** of the glazes prepared with smaller content of lanthanides differ little from the parameters of the glazes prepared without lanthanide. Thus, the variation in lanthanide and its concentration for the ceramic glazes having different shade of bluish-green colours could be obtained. The significant distinctions are observed in the cases of the ceramic glazes with higher amount of Tm and Yb, giving brownish green colour. These results are well visible in Fig. 53.

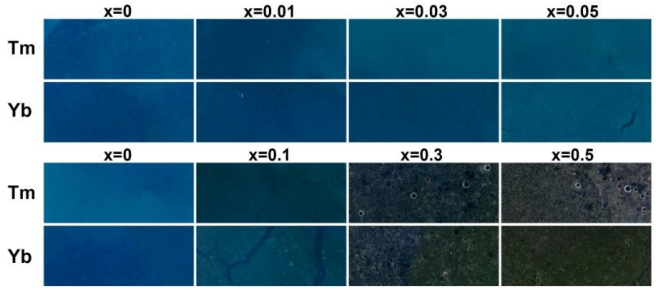

Figure 53. Digital photographs of representative ceramic glazes prepared using sol-gel derived $CoCr_{2-x}Tm_xO_4$ and $CoCr_{2-x}Yb_xO_4$ pigments

Apparently, the colourimetric appearance of both the pigments and the ceramic glazes correlates well with the XRD results while the dominant spinel phase gives bluish-green colour and the dominant orthochromite phase leads to dark green colour.

3.4. Sol-gel synthesis and characterisation of $CoCr_{2-x}Ga_xO_4$ pigments and glazes

In the last part of dissertation $CoCr_{2-x}Ga_xO_4$ pigments with different substitution ratio of gallium (x = 0; 0.5; 1; 1.5; and 2) were synthesised using the same synthetic approach. The phase composition, crystallite size, morphological features, and colour parameters of new compositions were investigated.

XRD analysis.

X-ray diffraction patterns of Ga-doped $CoCr_{2-x}Ga_xO_4$ (x = 0–2 with a step of 0.5) samples, depending on the substitution ratio and heating temperature, are given in Fig. 54.

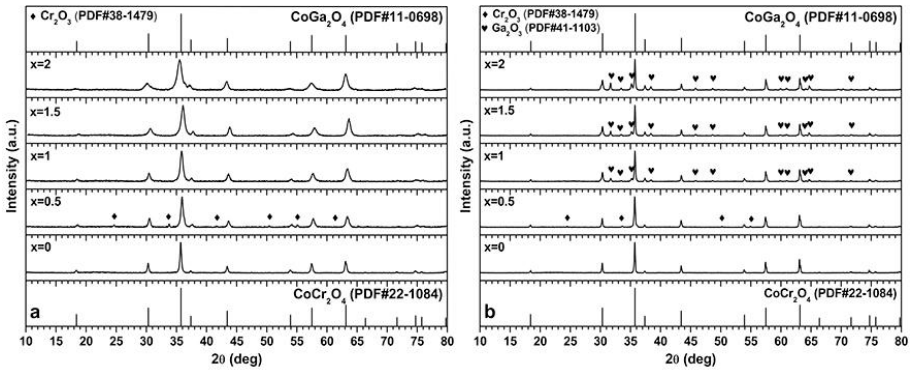

Figure 54. XRD patterns of $CoCr_{2-x}Ga_xO_4$ powders (x = 0–2) calcined at 700 °C (a) and annealed at 1000 °C (b)

The main crystalline phase of the synthesis products obtained at 700 °C was solid solution of cubic $CoCr_2O_4$ (PDF 22-1084) and $CoGa_2O_4$ (PDF 11-0698) spinels. However, additional Cr_2O_3 phase (PDF 38-1479) was observed for the sample with x = 0.5. Phase composition analysis revealed that chromium substitution by gallium was not successful at higher temperature. Interestingly, XRD patterns of the samples with x = 1–2 annealed at 1000 °C showed minor amount of Ga_2O_3 crystalline phase (PDF 41-1103) (see Fig. 54b), which was not observed in the samples, heated at 700 °C.

The estimated crystallite size of the spinel phase for all compositions ranged from 11.4 to 32.6 nm and from 46.6 to 54.4 nm for the samples obtained at 700 and 1000 °C, respectively. The crystallite size decreased linearly with the increase of substitution ratio.

Morphological and colourimetric characterisation.

The SEM micrographs of selected pigment samples (x = 0.5 and 2) obtained at deferent heating temperatures are given in Fig. 55.

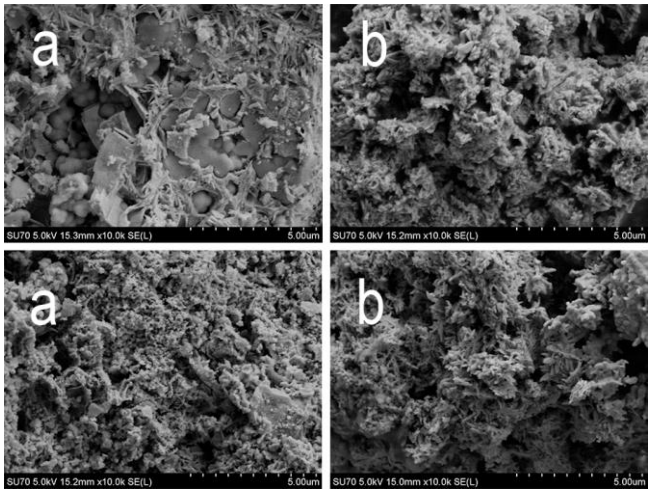

Figure 55. SEM micrographs of sol-gel derived $CoCr_{2-x}Ga_xO_4$ pigments, when x = 0.5 (a) and x = 2 (b), obtained at 700 °C (top) and 1000 °C (bottom)

At the low heating temperature the surface of synthesised pigments is composed of irregularly shaped particles which are highly agglomerated independently on the substitutional level. The particles with the lowest substitution ratio (Fig. 55a) are composed of particles with irregular shape. The particles of the sample annealed at 1000 °C with the highest substitution ratio (Fig. 55b, bottom) are needle-like plates. Nevertheless, agglomeration of the particles is very high and no separate particles could be clearly distinguished. The representative SEM micrograph and digital picture of optical microscopy of the ceramic glaze obtained using sol-gel derived fully substituted $CoGa_2O_4$ pigment is presented in Fig. 56.

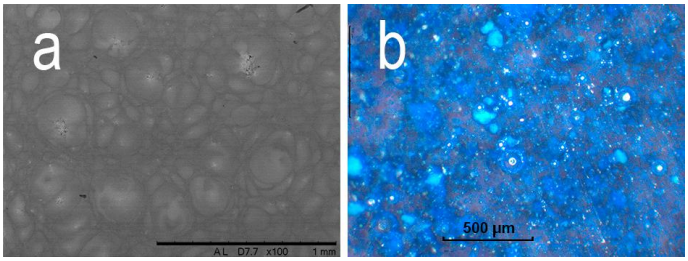

Figure 56. Images of the glaze prepared using $CoGa_2O_4$, obtained by: (a) – SEM and (b) – OM

SEM investigation revealed well dispersion of the pigments over ceramic tiles. However, no separate particles are visible in the $CoGa_2O_4$ glaze (Fig. 56a). Optical microscopy confirmed the presence of pigment particles within the glaze and negligible formation of gas bubbles. No cracks, caves or other physical defects could be observed on the surface of ceramic glazes.

The colourimetric parameters of the pigments obtained at 1000 °C and corresponding glazes are summarised in Table 16.

Table 16. CIELab colourimetric parameters of the $CoCr_{2-x}Ga_xO_4$ pigments obtained at 1000 °C and corresponding glazes

Amount of	Pigment			Glaze		
Ga (x)	*L**	*a**	*b**	*L**	*a**	*b**
0	47.69	–8.31	–3.89	33.47	-10.92	-10.36
0.5	50.25	-12.39	-7.56	30.86	-7.59	-4.41
1	48.48	-8.49	-5.60	31.53	-4.01	-4.16
1.5	52.48	-11.83	-8.36	30.74	-4.32	–6.84
2	54.44	-9.48	–14.07	27.69	3.67	–9.35

As it was presumed, the most divergent results of the CIELab measurements are of the pigment and glaze samples when x = 0.5. The impurity of Cr_2O_3 gives greener hue to mentioned specimens, reasoning the most negative values of parameter *a**, comparing to the results of other samples with x = 1–2. The general tendency of increase of lightness parameter *L** for the pigments and decrease for the glazes with increase of substitution ratio is well observed. Moreover, for the pigments the values of parameter *b** are increasing negatively with the increase of gallium concentration, implying the enhancement of blue hue. On the contrary, for the glazes the values of parameter *a** convert into positive values, meaning the enhancement of red hue.

Corresponding to the CIELab results, the pigments give diversity in colours from bluish green to light blue (Fig. 57).

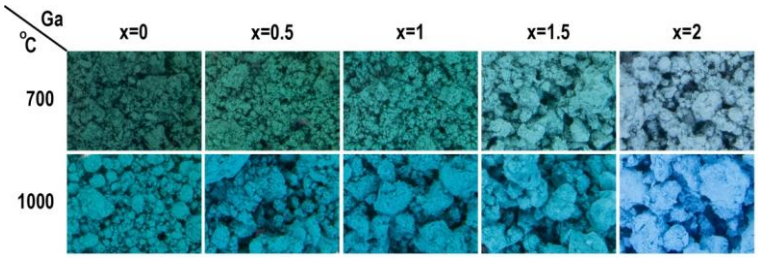

Figure 57. Digital photographs of Ga-doped cobalt chromite pigments obtained at different heating temperatures

It is obvious that the pigments annealed at 1000 °C distinguish brighter colours. The confirmation of the CIELab results of ceramic glazes is given in Fig. 58.

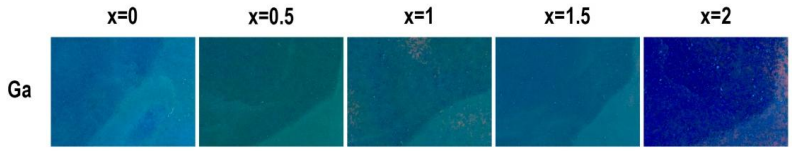

Figure 58. Digital photographs of the ceramic glazes prepared with Ga-doped pigments

The outstanding glazes are obtained with different substitutional level of gallium. As it was expected, the glaze with $CoCr_{1.5}Ga_{0.5}O_4$ pigment possess green hue due to the additional phase of chromium(III) oxide phase. However, the most unexpected results, concerning the colours of the pigments, were with the fully substituted pigmented glaze, which turned out to be violetish blue.

CONCLUSIONS

1. According to XRD analysis results, the chemical composition of three purchased pigments (malachite, cobalt bottle green and chrome oxide green) corresponded to the given in the Kremer Pigmente catalogue. However, the chemical composition of the rest six pigments (verdigris, Victoria, cobalt, Egyptian, and Florentine greens and green jasper) differs from nominal one.
2. It was demonstrated that only verdigris could be easily determined by XRD analysis in its glaze mixture. Malachite, cobalt green, cobalt bottle green, chrome oxide green and Victoria green could be hardly distinguished whereas Egyptian green, Florentine green and green jasper would be completely undetectable. Moreover, it was demonstrated that FTIR analysis of green pigments in glaze mixtures in the range of 4000–600 cm^{-1} is possible only for pigments containing carboxylate or carbonate functional groups (malachite and verdigris).
3. The single-phase cobalt-chromium spinels $CoCr_2O_4$ and $Co_{1-x}Zn_xCr_2O_4$ (x = 0–1 with a step of 0.25) were successfully synthesised using sol-gel and sonochemical synthesis methods in the temperature range of 600–1000 °C. However, the phase compositions of Ni- and Cu-substituted chromites ($Co_{1-x}Ni_xCr_2O_4$ and $Co_{1-x}Cu_xCr_2O_4$) were found to be the mixtures of spinel-type and simple oxide crystalline phases at higher substitution ratios of 0.75 and 1.
4. The colour of the pigments depended on the origin of the octahedral cation A^{2+}. The increase of Ni^{2+} content led to warm green colour. The Zn^{2+} enrichment in tetrahedral ligand field gave the variety of green shades form bluish green to yellowish green. Only Cu-doped pigments exhibited less different hues and were dark, nearly black. No main differences of the colours between pigments, produced by the sol-gel and sonochemical synthesis methods were detected.
5. Pb-based ceramic glazes coloured with sol-gel derived pigments displayed dark brownish green, nearly black colours for Co-, Ni, and Cu-substituted pigments. Glazes with Zn-substituted pigments appeared in more brown hues. Pb-free ceramic glazes, on the other hand, displayed bluish green hues and colours corresponding to the colours of the pigments.
6. The XRD analysis of sol-gel derived $CoCr_{2-x}Ln_xO_4$ (Ln = Tm^{3+} and Yb^{3+}) pigments with different substitutional level of lanthanide (x = 0–0.5) revealed that powders with higher concentration of lanthanide (x = 0.05–0.5) were mixtures of spinel and perovskite crystalline phases.
7. The colours of obtained $CoCr_{2-x}Ln_xO_4$ pigments and their corresponding ceramic glazes varied depending on the dominant phase: prevailing spinel

phase gave bluish-green colour, and the main perovskite phase gave dark brown hue.

8. The main crystalline phase of the synthesis products in the system of $CoCr_{2-x}Ga_xO_4$ obtained at 700 °C was solid solution of cubic $CoCr_2O_4$ and $CoGa_2O_4$ spinels. However, additional Cr_2O_3 phase was observed for the sample with x = 0.5. Interestingly, XRD patterns of the samples with x = 1–2 annealed at 1000 °C showed minor amount of Ga_2O_3 crystalline phase, which was not observed in the samples, heated at 700 °C.

9. The colours of obtained $CoCr_{2-x}Ga_xO_4$ pigments and their corresponding ceramic glazes were unexpected. The substitution of Cr^{3+} by Ga^{3+} ion led to the gradual light blueness of the pigment. The impurity of Cr_2O_3 in the sample with the lowest substitution ratio gave the green hue to both the pigment and corresponding ceramic glaze. Surprisingly, the ceramic glaze prepared using fully substituted $CoGa_2O_4$ pigment turned out to possess violetish blue colour.

10. SEM analysis revealed that the surface of all synthesised materials was composed of highly agglomerated particles.

LIST OF PUBLICATIONS

Articals in journals

1. **Grazenaite E.**, Jasulaitiene J., Ramanauskas R., Kareiva A. *Sol–gel synthesis, characterization and application of lanthanide-doped cobalt chromites ($CoCr_{2-x}Ln_xO_4$; Ln = Tm^{3+} and Yb^{3+})*. Journal of the European Ceramic Society. 2018, 38: 3361-3368.
2. **Grazenaite E.**, Pinkas J., Beganskiene A., Kareiva A. *Sol–gel and sonochemically derived transition metal (Co, Ni, Cu, and Zn) chromites as pigments: A comparative study*. Ceramics International. 2016, 42: 9402-9412.
3. **Grazenaite E.**, Kiuberis J., Beganskiene A., Senvaitiene J., Kareiva A. *XRD and FTIR characterisation of historical green pigments and their lead-based glazes*. Chemija. 2014, 25 (4): 199-205.

Published contributions to academic conference

1. **Grazenaite E.**, Kareiva A. *Cobalt chromite based pigments as colorants for ceramic glazes: The influence of the substitution type* // There is no future without the past: Science on the interface of 19^{th}-20^{th} centuries. The international conference dedicated to the 215^{th} birth anniversary of Ignacy Domeyko. Vilnius, Lithuania, 28-30 Jul 2017, pp. 78-79.
2. **Grazenaite E.**, Kareiva A. *Galium doped cobalt chromites as ceramic pigments* // Functional materials and Nanotechnologies 2017: international conference. Tartu, Estonia, 24-27 Apr 2017, p. 91.
3. **Grazenaite E.**, Kareiva A. *Sol-gel synthesis of cobalt chromite powders doped with lanthanides* // Advanced materials and technologies: the 18^{th} international conference-school. Palanga, Lithuania, 27-31 Aug 2016, p. 102.
4. **Grazenaite E.**, Kareiva A. *Commercial and sol-gel derived cobalt chromites as ceramic pigments: a comparative study* // Chemistry and chemical technology 2016: international conference of Lithuanian Society of Chemistry. Vilnius, Lithuania, 28-29 Apr 2016, p. 227.
5. **Grazenaite E.** *Thermal behaviour of the precursors for transition metal (Co, Ni, Cu and Zn) chromites synthesized via aqueous coprecipitation, sol-gel and sonochemical synthesis routes* // Nanochemistry and nanomaterials 2015: 2^{nd} international conference of chemists: the international conference. Vilnius, Lithuania, 22-24 Oct 2015, p. 24.
6. **Grazenaite E.**, Beganskiene A., Pinkas J., Kareiva A. *Synthesis, characterisation and application of novel green pigments $Co_{(1-x)}M_xCr_2O_4$*

(M = Cu, Zn, Ni) // Advanced materials and technologies 2015: the international conference, Palanga, Lithuania, 27-31 Aug 2015, p 76.

7. **Grazenaite E.**, Pinkas J., Roupcova P., Losos Z., Kareiva A. *Synthesis and characterisation of* $Co_{1-x}M_xCr_2O_4$ *as green pigments* // Chemistry and chemical technology 2015: international conference of Lithuanian Chemical Society, dedicated to Professor Vitas Daukšas on his 80th birth anniversary, Vilnius, Lithuania, 23 Jan 2015, pp 83-85.

8. **Grazenaite E.**, Senvaitiene S., Kiuberis J., Kareiva A. *Characterization of green historical pigments and glazes using FTIR and XRD analysis methods* // Chemistry and chemical technology 2014: the international conference, Kaunas, Lithuania, 25 Apr 2014.

Publications not included in the thesis

1. Golubevas R., Zarkov A., **Grazenaite E.**, Alinauskas L., Garskaite E., Kareiva A. *Preparation and characterization of the inorganic-organic (bioglass-poly(methyl methacrylate)) composite for bone tissue engineering* // Advanced materials and technologies: book of abstracts of the 18th international conference-school. Palanga, Lithuania, 27-31 Aug 2016, p. 103.

2. Stankeviciute Z., Grigoraviciute-Puroniene I., **Grazenaite E.**, Alinauskas L., Garskaite E., Kareiva A. *Synthesis of β-tricalcium phosphate powders with controlled crystallinity* // Nanostructured hybrid materials: protective and functional coatings, surface treatment, bioceramics, biocomposites and membranes: HINT workshop. Vilnius, Lithuania, 14-16 Mar 2016, p. 42.

3. Zarkov A., Vegelyte V., Alinauskas L., Stankeviciute Z., **Grazenaite E.**, Prichodko A., Grigoraviciute-Puroniene I., Opuchovic O., Tautkus S., Skaudzius R., Garskaite E., Beganskiene A., Kareiva A. *Sol-gel processing route to calcium hydroxyapatite bioceramics: repeatability issues* // Nanostructured hybrid materials: protective and functional coatings, surface treatment, bioceramics, biocomposites and membranes: HINT workshop. Vilnius, Lithuania, 14-16 Mar 2016, p. 14.

ACKNOWLEDGEMENTS

Finally, I came to the part where I can express my gratitude to all the people, who guided and helped me throughout this long scientific journey.

First and foremost, I would like to sincerely thank my research supervisors, prof. (HP) dr. Aldona Beganskienė and especially prof. habil. dr. Aivaras Kareiva, for all the knowledge, guidance and comprehension during these past years. I am also very grateful to my scientific consultant prof. RNDr. Jiří Pinkas for all the useful advices and exciting acquaintanceship with sonochemistry. Thank you very much for the given opportunity to work in your laboratory.

I am especially thankful to all the specialists from Masaryk University and Central European Institute of Technology (CEITEC), who provided me with a great help during my internship in Czech Republic. Thank you, ing. PhD Pavla Roupcova, for your uncountable XRD measurements. I am grateful to assoc. prof. RNDr. Zdeněk Losos for the instructions and advices with Raman measurements, mgr. Lucie Šimoníková for the challenging ICP-OES measurements and finally mgr. PhD Zdeněk Moravec for the prompt TG/DTG measurements. And special thanks goes to the entire prof. J. Pinkas' research group. Dear friends, you helped me a lot both with my research and my everyday surroundings and made me feel welcomed and honoured during my whole stay in Brno. You hold a special part of my heart.

I want to express my gratitude to Gediminas Kreiza and Karolis Kazlauskas from the Institute of Applied Research, Vilnius University, for their assistance in CIELab measurements. Special thanks goes to PhD Vitalija Jasulaitienė from the Centre for Physical Sciences and Technology for performing XPS measurements and her help interpreting of obtained results.

I would like to thank assoc. prof. dr. Ramūnas Skaudžius for the valuable introduction to Rietveld refinement using FullProf software. Dr. Olga Opuchovič, many thanks to you for TG/DTG measurements and for always being ready to help me with any questions I had. I am thankful to former intern PhD student Sung-Wei Yang from National Taipei University of Technology and former specialist Danas Sakalauskas for taking SEM microghraphs of my samples. Danas Sakalauskas together with PhD student Tomas Murauskas deserved gratitude for the help with FTIR measurements. I also appreciate the assistance with DR-UV measurements provided by prof. dr. Simas Šakirzanovas.

I would like to express my appreciation to Education Exchanges Support Foundation for providing the funding for the internship and CEITEC CZ.1.05/1.1.00/02.0068 for the financial assistance.

My dear colleagues and friends from the Institute of Chemistry, Faculty of Chemistry and Geosciences, thank you all for the support and encouragement over past these years. I am deeply grateful to you all, especially to dr. Justina Gaidukevič, dr. Eva Raudonytė, dr. Lina Pavasarytė and Aurelija Smalenskaitė.

I really appreciate the comprehension, encouragement and constant motivation, provided by my colleagues from Centre of Cultural Heritage and my dear old long time not seen friends. Thank you all for your tolerance and patience!

Last but not least, the biggest thanks goes to my family. Thank you for your love, patience and versatile support. The genuine appreciation goes to my beloved father for the help adjusting the thesis images.

Thank you all, dear people!

REFERENCES

[1] L. Bloomfield, Colour in Glazes, A & C Black, London, 2012.
[2] I.S. Ahmed, H.A. Dessouki, A.A. Ali, Synthesis and characterization of new nano-particles as blue ceramic pigment, Spectroc. Acta Pt. A-Molec. Biomolec. Spectr. 71(2) (2008) 616-620.
[3] M. Llusar, A. Fores, J.A. Badenes, J. Calbo, M.A. Tena, G. Monros, Colour analysis of some cobalt-based blue pigments, J Eur Ceram Soc 21(8) (2001) 1121-1130.
[4] Parmelee CW, E.D. Lynch, Ceramic glazes, 2nd ed., Industrial Publications, Chicago, 1951.
[5] M. Bouchard, A. Gambardella, Raman microscopy study of synthetic cobalt blue spinels used in the field of art, J Raman Spectrosc 41(11) (2010) 1477-1485.
[6] S.R. Prim, A. García, R. Galindo, S. Cerro, M. Llusar, M.V. Folgueras, G. Monrós, Pink ceramic pigments based on chromium doped $M(Al_{2-x}Cr_x)O_4$, M = Mg, Zn, normal spinel, Ceram Int 39(6) (2013) 6981-6989.
[7] M. Dondi, C. Zanelli, M. Ardit, G. Cruciani, L. Mantovani, M. Tribaudino, G.B. Andreozzi, Ni-free, black ceramic pigments based on Co—Cr—Fe—Mn spinels: A reappraisal of crystal structure, colour and technological behaviour, Ceram Int 39(8) (2013) 9533-9547.
[8] J. Gilabert, M.D. Palacios, M.J. Orts, S. Mestre, Solution combustion synthesis of $(Ni,Fe)Cr_2O_4$ pigments: Effect of post-synthesis thermal treatments, Ceram Int 43(15) (2017) 12789-12798.
[9] O.O. Vasil'kov, O.P. Barinova, S.V. Kirsanova, N.A. Marnautov, A.B. Elfimov, Ceramic Black Pigments Based on Chromium-Nickel Spinel $NiCr_2O_4$, Glass and Ceramics 74(7-8) (2017) 236-239.
[10] J. Cai, M. Lu, K. Guan, W. Li, F. He, P. Chen, C. Peng, P. Rao, J. Wu, Effect of ZnO/MgO ratio on the crystallization and optical properties of spinel opaque glazes, J Am Ceram Soc 101(4) (2018) 1754-1764.
[11] Y. Tang, C. Wu, Y. Song, Y. Zheng, K. Zhao, Effects of colouration mechanism and stability of $CoAl_2O_4$ ceramic pigments sintered on substrates, Ceram Int 44(1) (2018) 1019-1025.
[12] J. Cai, M. Lv, K. Guan, Q. Sun, C. Peng, J. Wu, Y. Liu, Development of spinel opaque glazes for ceramic tiles, J Eur Ceram Soc 38(1) (2018) 297-302.
[13] J. Senvaitienė, Kultūros objektų charakterizavimas ir cheminių konservavimo procesų įtakos jų degradacijai tyrimas, Vilnius University, Vilnius, 2006, p. 105.

[14] D. Jonynaitė, Kobalto neorganinių pigmentų istorinių analogų tyrimas ir naujų sintezė zolių-gelių metodu, Vilnius University, Vilnius, 2011, p. 115.
[15] A. Abel, 24 - The history of dyes and pigments: From natural dyes to high performance pigments A2 - Best, J., Colour Design: Theories and Applications (Second Edition), Woodhead Publishing 2017, pp. 557-587.
[16] J.R. Barnett, S. Miller, E. Pearce, Colour and art: A brief history of pigments, Opt Laser Technol 38(4–6) (2006) 445-453.
[17] J. Bagdzevičienė, J. Kruopaitė, Pigmentai ir dažikliai restauruojant kultūros vertybes, Savastis, Vilnius, 2005.
[18] N. Eastaugh, W. V., Chaplin T., S. R., Pigment Compendium: A Dictionary and Optical Microscopy of Historical Pigments, Butterworth-Heinemann, Oxford, 2008.
[19] X. Wang, B. Mu, A. Hui, Q. Wang, A. Wang, Low-cost bismuth yellow hybrid pigments derived from attapulgite, Dyes Pigm 149 (2018) 521-530.
[20] Q.F. Geng, X. Zhao, X.H. Gao, S.R. Yang, G. Liu, Combustion Synthesis and Characterization of Spinel $NiCr_2O_4$, Chinese J Inorg Chem 28(9) (2012) 1979-1984.
[21] P. Ma, Q. Geng, X. Gao, S. Yang, G. Liu, Solution combustion of spinel CuMn2O4 ceramic pigments for thickness sensitive spectrally selective (TSSS) paint coatings, Ceram Int 42(10) (2016) 11966-11973.
[22] H.R. Hedayati, A.A. Sabbagh Alvani, H. Sameie, R. Salimi, S. Moosakhani, F. Tabatabaee, A. Amiri Zarandi, Synthesis and characterization of $Co_{1-x}Zn_xCr_{2-y}Al_yO_4$ as a near-infrared reflective color tunable nano-pigment, Dyes Pigm 113 (2015) 588-595.
[23] W. Liu, T. Du, Q. Ru, S. Zuo, X. Yang, C. Yao, Y. Kong, Facile synthesis and characterization of 2D kaolin/$CoAl_2O_4$: A novel inorganic pigment with high near-infrared reflectance for thermal insulation, Appl Clay Sci 153 (2018) 239-245.
[24] L. Yuan, A. Han, M. Ye, X. Chen, C. Ding, L. Yao, Synthesis and characterization of novel nontoxic $BiFe_{1-x}Al_xO_3$/mica-titania pigments with high NIR reflectance, Ceram Int 43(18) (2017) 16488-16494.
[25] L.K.C. de Souza, J.R. Zamian, G.N. da Rocha Filho, L.E.B. Soledade, I.M.G. dos Santos, A.G. Souza, T. Scheller, R.S. Angélica, C.E.F. da Costa, Blue pigments based on $Co_xZn_{1-x}Al_2O_4$ spinels synthesized by the polymeric precursor method, Dyes Pigm 81(3) (2009) 187-192.
[26] A. Garcia, M. Llusar, J. Calbo, M.A. Tena, G. Monros, Low-toxicity red ceramic pigments for porcelainised stoneware from lanthanide-cerianite solid solutions, Green Chem 3(5) (2001) 238-242.
[27] H. Yuan, J. Zhang, R. Yu, Q. Su, Preparation of ternary rare earth sulfide $La_xCe_{2-x}S_3$ as red pigment, J Rare Earth 31(3) (2013) 327-330.

[28] V.S. Vishnu, M.L. Reddy, Near-infrared reflecting inorganic pigments based on molybdenum and praseodymium doped yttrium cerate: Synthesis, characterization and optical properties, Sol Energ Mat Sol C 95(9) (2011) 2685-2692.
[29] O. Opuchovic, G. Kreiza, J. Senvaitiene, K. Kazlauskas, A. Beganskiene, A. Kareiva, Sol-gel synthesis, characterization and application of selected sub-microsized lanthanide (Ce, Pr, Nd, Tb) ferrites, Dyes Pigm 118 (2015) 176-182.
[30] R.C. Olegario, E.C.F. de Souza, J.F.M. Borges, J.B.M. da Cunha, A.V.C. de Andrade, S.R.M. Antunes, A.C. Antunes, Synthesis and characterization of Fe^{3+} doped cerium-praseodymium oxide pigments, Dyes Pigm 97(1) (2013) 113-117.
[31] V. De la Luz, M. Prades, H. Beltran, E. Cordoncillo, Environmental-friendly yellow pigment based on Tb and M (M = Ca or Ba) co-doped Y_2O_3, J Eur Ceram Soc 33(15-16) (2013) 3359-3368.
[32] K.J. Sreeram, R. Srinivasan, J. Meena Devi, B. Unni Nair, T. Ramasami, Cerium molybdenum oxides for environmentally benign pigments, Dyes Pigm 75(3) (2007) 687-692.
[33] P. Lunakova, M. Trojan, J. Luxova, J. Trojan, $BaSn_{1-x}Tb_xO_3$: A new yellow pigment based on a perovskite structure, Dyes Pigm 96(1) (2013) 264-268.
[34] G. George, The structural and optical studies of titanium doped rare earth pigments and coloring applications, Dyes Pigm 112 (2015) 81-85.
[35] S. Jose, M.L. Reddy, Lanthanum-strontium copper silicates as intense blue inorganic pigments with high near-infrared reflectance, Dyes Pigm 98(3) (2013) 540-546.
[36] A. Beganskiene, R. Raudonis, A. Kareiva, Sol-gel preparation and characterization of novel mixed-metal cobaltates-aluminates, Chemical Engineering Communications 200(2) (2013) 305-315.
[37] S.W. Kim, Y. Saito, T. Hasegawa, K. Toda, K. Uematsu, M. Sato, Development of a novel nontoxic vivid violet inorganic pigment - Mn^{3+}-doped $LaAlGe_2O_7$, Dyes Pigm 136 (2017) 243-247.
[38] P.M. Pimentel, S.V.M. Lima, A.F. Costa, M.S.C. Câmara, J.D.C. Carregosa, R.M.P.B. Oliveira, Gelatin synthesis and color properties of (La, Pr, Nd) lanthanide aluminates, Ceram Int 43(8) (2017) 6592-6596.
[39] G. George, L.S. Kumari, V.S. Vishnu, S. Ananthakumar, M.L.P. Reddy, Synthesis and characterization of environmentally benign calcium-doped $Pr_2MO_2O_9$ pigments: Applications in coloring of plastics, J Solid State Chem 181(3) (2008) 487-492.

[40] P.P. Rao, M.L.P. Reddy, $(TiO_2)_{(1)}(CeO_2)_{(1-x)}(RE_2O_3)_{(x)}$ - novel environmental secure pigments, Dyes Pigm 73(3) (2007) 292-297.
[41] G. Daly, Developing Glazes, The American Ceramic Society, Ohio, 2013.
[42] N. Liu, Y. Yang, Y. Wang, W. Hu, X. Jiang, M. Ren, M. Yang, C. Wang, Nondestructive characterization of ancient faience beads unearthed from Ya'er cemetery in Xinjiang, Early Iron Age China, Ceram Int 43(13) (2017) 10460-10467.
[43] Z. Bahrani, Mesopotamia: Ancient Art and Architecture, Thames & Hudson, London, 2017.
[44] P. Shi, F. Wang, J. Zhu, B. Zhang, T. Zhao, Y. Wang, Y. Qin, Study on the Five dynasty sky-green glaze from Yaozhou kiln and its coloring mechanism, Ceram Int 43(3) (2017) 2943-2949.
[45] J.-Y. Kim, H. No, A.Y. Jeon, U. Kim, J.-H. Pee, W.-S. Cho, K.J. Kim, C.M. Kim, C.S. Kim, Mössbauer spectroscopic and chromaticity analysis on colorative mechanism of celadon glaze, Ceram Int 37(8) (2011) 3389-3395.
[46] A. Aguilar-Elguézabal, M. Román-Aguirre, L. De la Torre-Sáenz, P. Pizá-Ruiz, M. Bocanegra-Bernal, Synthesis of $CoAl_2O_4/Al_2O_3$ nanoparticles for ceramic blue pigments, Ceram Int 43(17) (2017) 15254-15257.
[47] Z. Pan, Y. Wang, H. Huang, Z. Ling, Y. Dai, S. Ke, Recent development on preparation of ceramic inks in ink-jet printing, Ceram Int 41(10, Part A) (2015) 12515-12528.
[48] J. Wu, K. Li, X. Xu, J. Yu, X. Li, J. Tian, In situ synthesis of spherical $CdS_{1-x}Se_x$ red pigment used for ceramic ink-jet printing, Mater Chem Phys 203 (2018) 193-201.
[49] M. Jovaní, M. Domingo, T.R. Machado, E. Longo, H. Beltrán-Mir, E. Cordoncillo, Pigments based on Cr and Sb doped TiO_2 prepared by microemulsion-mediated solvothermal synthesis for inkjet printing on ceramics, Dyes Pigm 116 (2015) 106-113.
[50] P.M.T. Cavalcante, M. Dondi, G. Guarini, M. Raimondo, G. Baldi, Colour performance of ceramic nano-pigments, Dyes Pigm 80(2) (2009) 226-232.
[51] M. Jovaní, M. Fortuño-Morte, H. Beltrán-Mir, E. Cordoncillo, Environmental-friendly red-orange ceramic pigment based on Pr and Fe co-doped $Y_2Zr_2O_7$, J Eur Ceram Soc 38(4) (2018) 2210-2217.
[52] M. Jovaní, A. Sanz, H. Beltrán-Mir, E. Cordoncillo, New red-shade environmental-friendly multifunctional pigment based on Tb and Fe doped $Y_2Zr_2O_7$ for ceramic applications and cool roof coatings, Dyes Pigm 133 (2016) 33-40.

[53] O. Opuchovic, G. Kreiza, J. Senvaitiene, K. Kazlauskas, A. Beganskiene, A. Kareiva, Sol-gel synthesis, characterization and application of selected sub-microsized lanthanide (Ce, Pr, Nd, Tb) ferrites, Dyes Pigm 118 (2015) 176-182.
[54] G. Tian, W. Wang, D. Wang, Q. Wang, A. Wang, Novel environment friendly inorganic red pigments based on attapulgite, Powder Technology 315 (2017) 60-67.
[55] E. Tóth, T.G. Weiszburg, T. Jeffries, C.T. Williams, A. Bartha, É. Bertalan, I. Cora, Submicroscopic accessory minerals overprinting clay mineral REE patterns (celadonite–glauconite group examples), Chemical Geology 269(3) (2010) 312-328.
[56] L.M. Moretto, E.F. Orsega, G.A. Mazzocchin, Spectroscopic methods for the analysis of celadonite and glauconite in Roman green wall paintings, J Cult Herit 12(4) (2011) 384-391.
[57] G.D. Hatton, A.J. Shortland, M.S. Tite, The production technology of Egyptian blue and green frits from second millennium BC Egypt and Mesopotamia, Journal of Archaeological Science 35(6) (2008) 1591-1604.
[58] P. Colomban, The Destructive/Non-Destructive Identification of Enameled Pottery, Glass Artifacts and Associated Pigments—A Brief Overview, Arts 2(3) (2013) 77.
[59] L. Verger, O. Dargaud, M. Chassé, N. Trcera, G. Rousse, L. Cormier, Synthesis, properties and uses of chromium-based pigments from the Manufacture de Sèvres, J Cult Herit 30 (2018) 26-33.
[60] D. Esteves, W. Hajjaji, M.P. Seabra, J.A. Labrincha, Use of industrial wastes in the formulation of olivine green pigments, J Eur Ceram Soc 30(15) (2010) 3079-3085.
[61] T. Dimitrov, S. Kozhukharov, N. Velinov, Synthesis of pigments of $Fe_2O_3 \cdot SiO_2$ system, with Ca, Mg, or Co oxide additions, Bol Soc Esp Ceram V 56(2) (2017) 55-63.
[62] F. Andreola, L. Barbieri, F. Bondioli, M. Cannio, A.M. Ferrari, I. Lancellotti, Synthesis of chromium containing pigments from chromium galvanic sludges, Journal of Hazardous Materials 156(1) (2008) 466-471.
[63] H. Onoda, K. Sugimoto, Synthesis of novel green phosphate pigments in imitation of natural ores, Journal of Asian Ceramic Societies 5(2) (2017) 123-126.
[64] S. Jose, A. Prakash, S. Laha, S. Natarajan, M.L. Reddy, Green colored nano-pigments derived from Y_2BaCuO_5: NIR reflective coatings, Dyes Pigm 107 (2014) 118-126.

[65] T. Masui, N. Takeuchi, H. Nakado, N. Imanaka, Novel environment-friendly green pigments based on rare earth cuprate, Dyes Pigm 113 (2015) 336-340.
[66] W. Hajjaji, C. Zanelli, M.P. Seabra, M. Dondi, J.A. Labrincha, Cr-doped titanite pigment based on industrial rejects, Chemical Engineering Journal 158(2) (2010) 167-172.
[67] J. Gilabert, M.P. Gómez-Tena, V. Sanz, S. Mestre, Effect of secondary thermal treatment on crystallinity of spinel-type $Co(Cr,Al)_2O_4$ pigments synthesized by solution combustion route, J Non-Cryst Solids (2018).
[68] M. Llusar, T. Bermejo, J.E. Primo, C. Gargori, V. Esteve, G. Monrós, Karrooite green pigments doped with Co and Zn: Synthesis, color properties and stability in ceramic glazes, Ceram Int 43(12) (2017) 9133-9144.
[69] J. Zou, W. Zheng, TiO_2@$CoTiO_3$ complex green pigments with low cobalt content and tunable color properties, Ceram Int 42(7) (2016) 8198-8205.
[70] K.E. Sickafus, J.M. Wills, N.W. Grimes, Structure of spinel, J Am Ceram Soc 82(12) (1999) 3279-3292.
[71] D.H. Taffa, R. Dillert, A.C. Ulpe, K.C.L. Bauerfeind, T. Bredow, D.W. Bahnemann, M. Wark, Photoelectrochemical and theoretical investigations of spinel type ferrites ($M_xFe_{3-x}O_4$) for water splitting: a mini-review, SPIE, 2016, p. 25.
[72] Z.W. Wang, P. Lazor, S.K. Saxena, G. Artioli, High-pressure Raman spectroscopic study of spinel ($ZnCr_2O_4$), J Solid State Chem 165(1) (2002) 165-170.
[73] C. Rath, P. Mohanty, A. Banerjee, Magnetic properties of nanoparticles of cobalt chromite, J Magn Magn Mater 323(12) (2011) 1698-1702.
[74] S.S. Acharyya, S. Ghosh, S. Adak, D. Tripathi, R. Bal, Fabrication of $CuCr_2O_4$ spinel nanoparticles: A potential catalyst for the selective oxidation of cycloalkanes via activation of C_{sp3}-H bond, Catal Commun 59 (2015) 145-150.
[75] A.E. Giannakas, A.K. Ladavos, G.S. Armatas, P.J. Pomonis, Surface properties, textural features and catalytic performance for NO plus CO abatement of spinels MAl_2O_4 (M = Mg, Co and Zn) developed by reverse and bicontinuous microemulsion method, Appl Surf Sci 253(16) (2007) 6969-6979.
[76] S.A. Hosseini, A. Niaei, D. Salari, M.C. Alvarez-Galvan, J.L.G. Fierro, Study of correlation between activity and structural properties of Cu-(Cr, Mn and $Co)_2$ nano mixed oxides in VOC combustion, Ceram Int 40(4) (2014) 6157-6163.

[77] S.S. Manoharan, K.C. Patil, Combustion Synthesis of Metal Chromite Powders, J Am Ceram Soc 75(4) (1992) 1012-1015.
[78] S.K. Durrani, S.Z. Hussain, K. Saeed, Y. Khan, M. Arif, N. Ahmed, Hydrothermal synthesis and characterization of nanosized transition metal chromite spinels, Turk J Chem 36(1) (2012) 111-120.
[79] G. Marquez, V. Sagredo, C. Marquina, T.E. Torres, M.R. Ibarra, G.F. Goya, Magnetic Properties of $CoFe_{0.5}Cr_{1.5}O_4$ Nanoparticles, Rev Mex Fis 58(2) (2012) 138-141.
[80] S.A. Eliziário, J.M. de Andrade, S.J.G. Lima, C.A. Paskocimas, L.E.B. Soledade, P. Hammer, E. Longo, A.G. Souza, I.M.G. Santos, Black and green pigments based on chromium–cobalt spinels, Mater Chem Phys 129(1–2) (2011) 619-624.
[81] Z. Congmian, Z. XiaoZhe, W. Wengang, G. Wenzhe, P. Ankit, X. Xiaoshan, S. Jian, M. Li, H. Denglu, Nanostructural origin of semiconductivity and large magnetoresistance in epitaxial $NiCo_2O_4/Al_2O_3$ thin films, Journal of Physics D: Applied Physics 51(14) (2018) 145308.
[82] Q.F. Geng, X. Zhao, X.H. Gao, S.R. Yang, G. Liu, Low-temperature combustion synthesis of $CuCr_2O_4$ spinel powder for spectrally selective paints, J Sol-Gel Sci Techn 61(1) (2012) 281-288.
[83] H.-g. Zhang, W.-h. Wang, E.-k. Liu, X.-d. Tang, G.-j. Li, H.-w. Zhang, G.-h. Wu, Compensation effect and magnetostriction in $CoCr_{2-x}Fe_xO_4$, Phys Status Solidi B 250(7) (2013) 1287-1292.
[84] M. Ptak, M. Maczka, A. Gagor, A. Pikul, L. Macalik, J. Hanuza, Temperature-dependent XRD, IR, magnetic, SEM and TEM studies of Jahn-Teller distorted $NiCr_2O_4$ powders, J Solid State Chem 201 (2013) 270-279.
[85] D. Zakutna, A. Repko, I. Matulkova, D. Niznansky, A. Ardu, C. Cannas, A. Mantlikova, J. Vejpravova, Hydrothermal synthesis, characterization, and magnetic properties of cobalt chromite nanoparticles, J Nanopart Res 16(2) (2014) 2251.
[86] S. Li, G. Zhao, H. Bi, Z. Huang, H. Lai, R. Gai, Y. Du, Synthesis and anomalous magnetic properties of $CoCr_2O_4$ nanocrystallites with lattice distortion, J Magn Magn Mater 305(2) (2006) 448-451.
[87] E. Mohammad, K. Ahmad Reza, Synthesis of Cobalt Chromite Nanoparticles by Thermolysis of Mixed Cr^{3+} and Co^{2+} Chelates of 2-Mercaptopyridin N-Oxide, Nano-Micro Lett 4(2) (2012) 083-089.
[88] Z.Q. Zhu, X.D. Cheng, W.P. Ye, J. Min, Synthesis of $NiCr_2O_4$ spinel coatings with high emissivity by plasma spraying, Int J Min Met Mater 19(3) (2012) 266-270.
[89] D. Gingasu, I. Mindru, L. Patron, D.C. Culita, J.M. Calderon-Moreno, L. Diamandescu, M. Feder, O. Oprea, Precursor method—A

nonconventional route for the synthesis of $ZnCr_2O_4$ spinel, J Phys Chem Solids 74(9) (2013) 1295-1302.
[90] D.P. Dutta, J. Manjanna, A.K. Tyagi, Magnetic properties of sonochemically synthesized $CoCr_2O_4$ nanoparticles, J Appl Phys 106(4) (2009).
[91] W.Z. Lv, Q. Qiu, F. Wang, S.H. Wei, B. Liu, Z.K. Luo, Sonochemical synthesis of cobalt aluminate nanoparticles under various preparation parameters, Ultrason Sonochem 17(5) (2010) 793-801.
[92] W.P. Huang, H. Li, B.L. Zhu, Y.F. Feng, S.R. Wang, S.M. Zhang, Selective hydrogenation of furfural to furfuryl alcohol over catalysts prepared via sonochemistry, Ultrason Sonochem 14(1) (2007) 67-74.
[93] N. Dupont, A. Kaddouri, P. Gelin, Physicochemical and catalytic properties of sol gel-prepared copper-chromium oxides, J Sol-Gel Sci Techn 58(1) (2011) 302-306.
[94] D. Jasaitis, D. Beganskiene, J. Senvaitiene, A. Kareiva, R. Ramanauskas, R. Juskenas, A. Selskis, Sol-gel synthesis and characterization of cobalt chromium spinel $CoCr_2O_4$, Chemija 22(2) (2011) 125-130.
[95] J. Barman, S. Ravi, Study of exchange bias behavior in $Ni(Cr_{1-x}Fe_x)_{(2)}O_4$, Solid State Commun 201 (2015) 59-63.
[96] H.T. Cui, M. Zayat, D. Levy, Sol-gel synthesis of nanoscaled spinels using propylene oxide as a gelation agent, J Sol-Gel Sci Techn 35(3) (2005) 175-181.
[97] M. Kakihana, Invited review: “Sol-gel” preparation of high temperature superconducting oxides, J Sol-Gel Sci Techn 6(1) (1996) 7–55.
[98] M. Zayat, D. Levy, Blue $CoAl_2O_4$ Particles Prepared by the Sol−Gel and Citrate−Gel Methods, Chem Mater 12(9) (2000) 2763-2769.
[99] T. Coradin, J. Livage, Sol–Gel Synthesis of Solids, Encyclopedia of Inorganic and Bioinorganic Chemistry, John Wiley & Sons2006.
[100] R. Gupta, K. Kumar, Bioactive materials for biomedical applications using sol–gel technology, Biomed Mater 3(3) (2008) 034005.
[101] C.J. Brinker, G.W. Scherer, Sol-Gel Science: The Physics and Chemistry of Sol-Gel Processing, Academic Press, Inc., San Diego, 1990.
[102] L.L. Hench, J.K. West, The sol-gel process, Chemical Reviews 90(1) (1990) 33-72.
[103] S. Asgharzadehahmadi, A.A. Abdul Raman, R. Parthasarathy, B. Sajjadi, Sonochemical reactors: Review on features, advantages and limitations, Renewable and Sustainable Energy Reviews 63 (2016) 302-314.
[104] K.S. Suslick, T. Hyeon, M. Fang, A.A. Cichowlas, Sonochemical synthesis of nanostructured catalysts, Mater Sci Eng A 204(1) (1995) 186-192.

[105] F. Shahangi Shirazi, K. Akhbari, Sonochemical procedures; the main synthetic method for synthesis of coinage metal ion supramolecular polymer nano structures, Ultrason Sonochem 31 (2016) 51-61.
[106] D. Jonynaite, J. Senvaitiene, J. Kiuberis, A. Kareiva, R. Juskenas, R. Ramanauskas, XRD characterization of cobalt-based historical pigments and glazes, Chemija 20(1) (2009) 10-18.
[107] G.A. Mazzocchin, D. Rudello, C. Bragato, F. Agnoli, A short note on Egyptian blue, J Cult Herit 5(1) (2004) 129-133.
[108] A. Rafalska-Lasocha, Z. Kaszowska, W. Lasocha, R. Dziembaj, X-ray powder diffraction investigation of green earth pigments, Powder Diffr 25(1) (2010) 38-45.
[109] D. Hradil, T. Grygar, M. Hruskova, P. Bezdicka, K. Lang, O. Schneeweiss, M. Chvatal, Green earth pigment from the Kadan region, Czech Republic: Use of rare Fe-RICH smectite, Clay Clay Miner 52(6) (2004) 767-778.
[110] M. Inês Teixeira, L.V.E. Caldas, Dosimetric characteristics of jasper samples for high dose dosimetry, Appl Radiat Isotopes 70(7) (2012) 1417-1419.
[111] R.L. Frost, D.L. Wain, W.N. Martens, B.J. Reddy, Vibrational spectroscopy of selected minerals of the rosasite group, Spectrochim Acta A 66(4–5) (2007) 1068-1074.
[112] D. Buti, F. Rosi, B.G. Brunetti, C. Miliani, In-situ identification of copper-based green pigments on paintings and manuscripts by reflection FTIR, Anal Bioanal Chem 405(8) (2013) 2699-711.
[113] B. Nandapure, S. Kondawar, M. Salunkhe, A. Nandapure, Nanostructure cobalt oxide reinforced conductive and magnetic polyaniline nanocomposites, J Compos Mater 47(5) (2013) 559-567.
[114] V. Stubican, R. Roy, Isomorphous substitution and infra-red spectra of the layer lattice silicates, Am Mineral 46(1-2) (1961) 32-51.
[115] P.J. Wojtowicz, Theoretical Model for Tetragonal-to-Cubic Phase Transformations in Transition Metal Spinels, Physical Review 116(1) (1959) 32-45.
[116] B.D. Hosterman, Raman Spectroscopic Study of Solid Solution Spinel Oxides, Physics and Astronomy, University of Nevada, Las Vegas, 2011, p. 155.
[117] S.A. Hosseini, M.C. Alvarez-Galvan, J.L.G. Fierro, A. Niaei, D. Salari, MCr_2O_4 (M = Co, Cu, and Zn) nanospinels for 2-propanol combustion: Correlation of structural properties with catalytic performance and stability, Ceram Int 39(8) (2013) 9253-9261.

[118] N. N. Greenwood, A. Earnshaw, Chemistry of the Elements, 2nd ed., Butterworth-Heinemann, Oxford, 1997.
[119] G. Blasse, B.C. Grabmaier, Luminescent Materials, Springer-Verlag, Berlin, 1994.
[120] S. Naz, S.K. Durrani, M. Mehmood, M. Nadeem, Hydrothermal synthesis, structural and impedance studies of nanocrystalline zinc chromite spinel oxide material, J Saudi Chem Soc.
[121] S. Surviliene, V. Jasulaitiene, A. Cesuniene, A. Lisowska-Oleksiak, The use of XPS for study of the surface layers of Cr-Co alloy electrodeposited from Cr(III) formate-urea baths, Solid State Ionics 179(1-6) (2008) 222-227.
[122] L. Lukashuk, K. Fottinger, E. Kolar, C. Rameshan, D. Teschner, M. Havecker, A. Knop-Gericke, N. Yigit, H. Li, E. McDermott, M. Stoger-Pollach, G. Rupprechter, Operando XAS and NAP-XPS studies of preferential CO oxidation on Co_3O_4 and CeO_2-Co_3O_4 catalysts, J Catal 344 (2016) 1-15.

UŽRAŠAMS

Vilnius University Press
Universiteto st. 1, LT-01513 Vilnius
E-mail info@leidykla.vu.lt,
www.leidykla.vu.lt
Printed 20 copies